DEVELOPMENT OF DRUG-LOADED MICROBUBBLES FOR *IN-VITRO* APPLICATIONS IN CELL BIOLOGY

A Thesis Submitted to
the Graduate School of Engineering and Sciences of
İzmir Institute of Technology
In Partial Fulfillment of the Requirements for the Degree of

MASTER OF SCIENCE

in Biotechnology

by
Sema COŞKUN

January, 2017
İzmir

We approve the thesis of **Sema COŞKUN**

Examining Committee Members:

_____

Assoc. Prof. Dr. Ekrem ÖZDEMİR

Department of Chemical Engineering, İzmir Institute of Technology

_____

Assoc. Prof. Dr. Zekiye SULTAN ALTUN

Department of Basic Oncology, Dokuz Eylül University

_____

Prof. Dr. Mehmet POLAT

Department of Chemical Engineering, İzmir Institute of Technology

_____

Prof. Dr. Safiye AKTAŞ

Department of Basic Oncology, Dokuz Eylül University

_____

Prof. Dr. Selahattin YILMAZ

Department of Chemical Engineering, İzmir Institute of Technology

31 January 2017

_____   _____

Assoc. Prof. Dr. Ekrem ÖZDEMİR   **Assoc. Prof. Dr. Zekiye S. ALTUN**
Supervisor, Department of   Co-Supervisor, Department of
Chemical Engineering   Basic Oncology
İzmir Institute of Technology   Dokuz Eylül University

_____   _____

Assoc. Prof. Dr. Engin ÖZÇİVİCİ   **Prof. Dr. Aysun SOFUOĞLU**
Head of Department of   Dean of the Graduate School of
Biotechnology and Bioengineering   Engineering and Sciences

ACKNOWLEDGEMENTS

ABSTRACT

DEVELOPMENT OF DRUG-LOADED MICROBUBBLES FOR *IN-VITRO* APPLICATIONS IN CANCER CELL BIOLOGY

Doxorubicin (DOX) is one of the drugs for cancer therapy. When DOX is used in solution, it affects not only the cancer cells but also the healthy cells. In order to eliminate possible side effects, DOX was encapsulated within liposomes and applied for the cancer therapy. Because the circulation time for liposomes is longer in the body, they accumulate in capillaries, especially at the finger tips and at the toe of the foot called the hand-and-foot syndrome. Here, we proposed to couple the liposomes containing DOX with the microbubbles as the ultrasound contrast agent and deliver the drug to the area of interest. Therefore, DOX was loaded within the liposomes and characterized for their DOX contents. The DOX containing liposomes were conjugated with microbubbles through the avidin-biotin chemistry. It was found that the loaded-DOX content within the liposomes was Langmuir-type. The loaded DOX content increased at lower DOX concentrations and leveled off at higher DOX concentrations. The Langmuir constants can be used in designing DOX loading experiments. The DOX containing liposomes were coupled with the microbubbles and found an optimum of 7.0 for the avidin/biotin mole ratio on the microbubbles. At the optimum avidin/biotin ratio, the conjugated lipo-DOX amount was 3×10^{-8} μg-DOX/MB. It was concluded that the DOX molecules can be loaded within the liposomes and easily conjugated with the microbubbles and employed in cancer treatments.

ÖZET

KANSER HÜCRE BİYOLOJİSİNDE *IN-VITRO* UYGULAMALAR İÇİN İLAÇ YÜKLÜ MİKROKÖPÜKÇÜKLERİN GELİŞTİRİLMESİ

Doksorubisin (DOX), kanser tedavisinde kullanılan ilaçlardan bir tanesidir. DOX çözelti olarak kullanıldığı zaman sadece kanser hücrelerini değil aynı zamanda sağlıklı hücrelere de zarar verir. DOX'un olası zararlı yan etkilerini ortadan kaldırmak için DOX lipozomların içerisine hapsedilir ve kanser tedavisinde kullanılır. Lipozomların vücut içerisinde dolaşım süresi uzun olduğu için lipozomlar kılcal damarlarda toplanır. Özellikle parmak uçlarında ve ayak parmaklarında toplandığı için el-ayak sendromu olarak adlandırılan bir hastalığa sebep olur. Bu problemden yola çıkarak DOX içeren lipozomların ultrason kontrast ajanı olan mikroköpükçüklerle birleştirilmesi ve ilgili bölgeye ilacın salınımının yapılması tasarlandı. Bu sebeple DOX, lipozomların içerisine yüklendi ve DOX içeriği karakterize edildi. Daha sonra DOX yüklü lipozomlar, avidin-biyotin kimyası kullanılarak mikroköpükçükler ile birleştirildi. Lipozomların içerisine yüklenmiş olan DOX miktarının Langmuir tipi bir bağıntıya uyduğu bulundu. Yüklenmiş olan DOX, düşük DOX konsantrasyonlarında artış gösterirken yüksek DOX konsantrasyonlarında bir sabitlenme gösterdi. Benzer sonuçlar farklı lipozom konsantrasyonlarında da gözlendi. Langmuir sabitlerinin DOX yükleme deneylerinin tasarımında kullanılabileceği düşünüldü. DOX yüklü lipozomlar, mikroköpükçüklerle birleştirildi ve bu birleşimde avidin/biyotin mol oranının optimum 7.0 olduğu bulundu. Optimum avidin/biyotin oranında mikroköpükçüklerle birleştirilmiş DOX yüklü lipozomlar (lipo-dox) 3×10^{-8}µg-DOX/MB olarak bulundu. Sonuç olarak, DOX molekülleri lipozomların içerisine başarılı bir şekilde yüklendi, kolayca mikroköpükçüklerle birleştirildi ve kanser tedavisinde kullanılmak üzere hazırlanmış oldu.

TABLE OF CONTENTS

LIST OF FIGURES

LIST OF TABLES

CHAPTER 1

INTRODUCTION

Modern medical sciences have developed "smart drugs for targeted therapy". These drugs targeted the cancer cells with high success rates and extended the lifetime without severe side effects. Targeted smart drugs are produced by using liposomes which are biocompatible and displaying similarities with biological membranes. The side effects of anti-cancer agents are therefore reduced by the liposome technology. Encapsulation of cytotoxic drugs into the liposomes has prevented their metabolic degradation and increased the curative effect.[1] For pharmaceutical production, doxorubicin hydrochloride (DOX-HCl) has generally been used to treat breast cancer. DOX-HCl is an anthracycline antibiotic and amphipathic molecule. However, DOX is toxic and causes cardiac damage if its amount used is higher than 550 mg/m^2. Also, when DOX is used in its free form, it does not only affect the cancer cells but also the healthy cells. In order to decrease the side effects of the free drugs, liposomes were used to encapsulate the drugs for a new drug design. [2, 3]

Liposomes have been used to trap and deliver drugs for the treatment of diseases. However, because the lifetime of a liposomal drug is longer in the body, it accumulates in the capillaries especially on the tips of fingers and toes. Therefore, it is called hand and foot syndrome. It was proposed that if the liposomes were conjugated with the microbubbles and targeted to the cancer cells, they can be directly delivered to the area of interest with the limited harm to the body. The accumulation of drugs can also be monitored by oscillating the microbubbles as the ultrasound contrast agent under ultrasound. Therefore, it was aimed in this thesis to load DOX within liposomes, conjugate them with microbubbles, and characterize them for cancer treatments.

CHAPTER 2

LITERATURE SURVEY

2.1. Cancer and Treatment

Cancer is a community health problem in all over the world. The most common cancer types are lung, colon, breast, prostate, stomach, and liver.[4] Cancer statistics show that the incidence of cancer types depends on the gender. Lung and prostate cancers are the most common cancer types in men and breast cancer is the most common cancer type in women. Cancer is simply a disease which is defined as uncontrolled cell proliferation, loss of apoptosis (programmed cell death), metastasis, and angiogenesis.[5] There are ten hallmarks about cancer cells such as replicative immortality, genome instability, evading growth suppression, sustained proliferation, resist cellular death, altered metabolism, avoiding immune destruction, tumor-promoting inflammation, angiogenesis, and activation of invasion and metastasis.[6]

The term "cancer" comes from Greek as "karkinos" which is synonym for "crab". The Greek physicians Hippocrates and Galen resembled some tumors to a crab with swollen veins along the skin. Later, this term evolved to the Latin term "cancer" which corresponds to crab. Cancer is also referred to as tumor and sometimes neoplasm.[7] Cancers can be divided sub-groups according to their origin of tissue.[5] There are four main types of cancers: Carcinoma arises in epithelial tissue that is found in the internal and external lining of the body. Adenocarcinomas are the most common form of cancer, and they develop in an organ or gland such as prostate cancer, breast cancer, and liver cancer. Squamous cell carcinomas are a malignant tumor, and they develop in the squamous epithelium of organs which are skin, bladder, esophagus, and lung. Sarcoma arises from connective tissue that is found in bones, tendons, cartilage, muscle, and fat. This form of cancer accounts for less than 10% of all cancers. Leukemia is a blood cancer that originates in the bone marrow. Lymphoma develops in the lymph system which is a vital part of the immune system.[8]

A normal cell divides only when a chemical signal stimulates it. These signals are interpreted in the nucleus. When the chemical signals stimulate the cells, they reproduce their genetic information and divide into two identical daughter cells. This process is called mitosis. These signals also stop dividing the cell to prevent occurring many cells. But, in cancer cells, the sick cells do not receive the chemical signals and continue dividing for an uncontrolled growth. A cancer cell is similar to a normal cell in regulation of cell proliferation, cell survival, and cellular communication. In a normal cell, any DNA replication error ends up in programmed cell death or apoptosis. But, in a cancer cells, a similar DNA replication error may be insensitive to the sick cells which can further divide and pass on the daughter cells. This mutation causes the differentiations of the genome of the cancer cells because they never undergo programmed cell death. That is, one of the reasons why cancer patients become resistant to treatments due to the tumor cell heterogeneity.[9] During cancer development, the formation of new blood cells is called angiogenesis, which supplies the necessary nutrients and oxygen to the tumor cells.[10] Angiogenesis also provides a pathway for direct communication between tumor cells and blood stream. This event causes the metastasis by moving the tumor cells from their primary place to a different organ via lymph or blood. In angiogenesis, tumor cells evade from extracellular matrix (ECM), enter into the blood stream (intravasation), escape from the immune system, travel along the organism, and leak from a vessel (extravasation) into a different location of the body. As a result of this journey, metastasis took place.[11, 12]

The physiological properties such as pH, ionic strength, and temperature are important for tissues. For example, the pH of tumor tissues is more acidic than the normal tissues in a wide variety of cancer types. The intracellular pH (pH_i) is nearly the same and varies within ±0.1-0.2 pH units or less within normal and tumor tissues.[13] The change in extracellular pH (pH_e) is more than +0.2 pH units in normal tissues and from -0.2 to 0.6 units in the tumor tissues. A cancer cell has higher pH_i and lower pH_e than a normal cell as shown in Figure 2.1. The breast tumor in acute acidosis has a pH_i of 7.4 and pH_e of 6.8, in chronic acidosis, a pH_i of 7.2 and a pH_e of 6.7 while the normal breast duct has a pH_i of 7.2 and a pH_e of 7.4.[14]
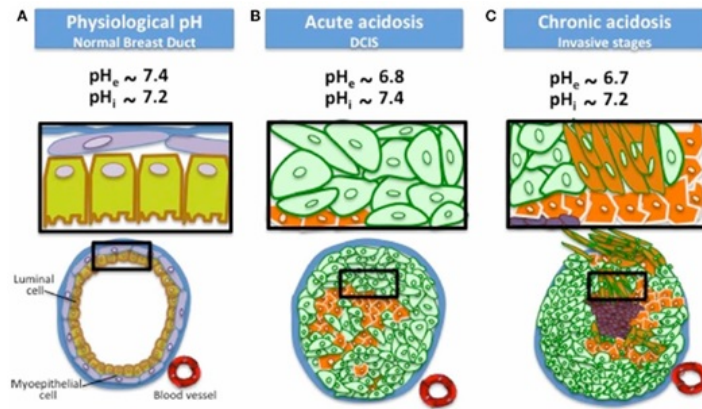
Figure 2.1. The pH differences between normal and tumor tissues of breast.[14]

There are many types of cancer treatment such as surgery, radiation, hormonal therapy, chemotherapy, targeted therapy, and immunotherapy. Surgery and radiation are common for all cancer types. A tumor is removed by surgery or killed by radiation. Radiation working principle is based on killing dividing cells via DNA damage which leads to cell death.[15] Chemotherapy is a time dependent technique compared to surgery and radiation in cancer therapy. The human body composes of chemicals or hormones which regulate metabolic activities in cells and organs what to do. These hormones can also activate cancer for growth. However, in chemotherapy, drugs are designed for cells not to divide since cancer cells tend to divide more rapidly. There are some side effects in chemotherapy such as hair loss, risk of infection, nausea and diarrhea as the white blood cells fight with infection.[16] The chemotherapy agents could be metals (platinum agents like cisplatin, carboplatin, oxaliplatin), the antimetabolites (5-fluorouracil, capecitabine, gemcitabine, pemetrexed), alkylators (cyclophosphamide), antibiotics (doxorubicin), and topoisomerase inhibitors (etoposide, irinotecan). Another approach in cell division is the microtubules inhibition. The microtubules were prevented from aggregation by the vinca alkaloids like vinorelbine, vinblastine, and vincristine. Another approach is to use taxanes such as docetaxel, paclitaxel and cabazitaxel to prevent the microtubules disassembly. Therefore, the cells are prohibited for cell division and undergo programmed cell death when these drugs interfere with microtubule function.[17] Also, immunotherapy uses medicines to induce the patient's immune system to identify and kill the cancer cells more effectively.[18]

Targeted therapy inhibits mutated or overexpressed proteins to prevent cancer growing. Thus, the treatment is special for the cancer cells without causing side effects

as seen in chemotherapy and hormonal therapy. Some targeted therapy treatments and their drugs are shown in Table 2. 1.[19] Targeted cancer therapy is a new approach for cancer treatment, and it has been designed for new treatments and drugs as specifically targeted to the cancer cells. The mechanism of targeted therapy is based on the targeting the cancer cells avoiding normal cells, which causes the cancer cells to die. Targeted therapies are specific for individual cancers, and so the different targeted therapies are used for cancer treatments such as artificial DNA nanostructures, nano-particle drug carriers, nanogels and others.[20] Artificial DNA nanostructures are designed with DNA molecules using DNA technology and DNA origami methods. Their structures are the same with normal DNA, but they do not carry genetic information. Targeted drug delivery possesses the drug encapsulation and releases the drugs by interacting with the desired stimulus.[21] Nanoparticles are tiny particles, and there are polymer coats around them. This polymer enables to release the drugs thereby controls diffusion or erosion from the core across the polymeric membrane or matrix. The solubility and diffusivity of a drug are the determining factors for the drug release because the polymeric membrane coat acts as a barrier. Different types of nanoparticles exist at different sizes, shapes and different materials such as fluorescence nanoparticles, lipid nanoparticles, super paramagnetic nanoparticles and dendrimers.[22, 23] Nanogels are composed of a mesh network. When the nanogels are injected to the body, they disperse immediately in a specific tissue.[24]

Table 2. 1. The types of some targeted cancer therapies and their drugs.

Targeted Therapy	Drugs
Vascular endothelial growth factor (VEGF)	Bevacizumab (Avastin®), Cyramza™
Epidermal growth factor receptor (EGFR)	Tarceva®, Afatinib, Iressa®, Erbitux®
HER2	Herceptin®,Perjeta™,Kadcyla®, Tykerb®
Anaplastic lymphoma kinase (ALK)	Xalkori™
Mechanistic target of rapamycin (mTOR)	Afinitor®
Cyclin-dependent kinase (CDK4 and CDK6)	Ibrance™
Polymeric nanoparticles (polymer-drug conjugates)	Albumin-Taxol (Abraxane®), PGA-Taxol (Xyotax™), PGA-Camptothecin (CT-2106), HPMA-DOX (PK1), HPMA-DOX- galactosamine (PK2)
Polymeric micelles	PEG-Pluronic®-DOX, PEG-PAA-DOX (NK911), PEG-PLA-Taxol (Genexol-PM)
Dendrimers	PAMAM-MTX, PAMAM-platine
Liposomes	Pegylated liposomal DOX (Doxil®), Non-pegylated liposomal DOX (Myocet®), Liposomal daunorubicin (DaunoXome®)
Viral nanoparticles	HSP-DOX, CPMV-DOX
Carbon nanotubes	CNT-MTX, CNT-amphotericin B

Anthracyclines have been used for drug delivery systems for long time. The research of anti-cancer compounds was begun with soil-based microorganisms in the 1950s. Firstly, *Streptomyces peucetius* bacteria were isolated, and it was obtained an antibiotic that have bright red pigment. This was called as 'daunorubicin', and it gave good activity for acute leukemia and lymphoma treatments. However, this antibiotic was producing fatal cardiac toxicity, and this problem was noticed in 1967. Thereupon,

researchers began to study with *Streptomyces peucetius* var. *caesius* bacteria and this was called 'doxorubicin' whose other name was 'Adriamycin'. Afterwards, DOX has been accepted one of the first oncology agent, and it has been most widely used molecule for encapsulation technology with liposomes. DOX has been used for leukemia, breast, bladder, stomach, lung, ovarian, Hodgkin's lymphoma, thyroid, soft tissue sarcoma, multiple myelomas and another types of cancer treatments.[2, 25, 26]

2.2. Doxorubicin

Doxorubicin (DOX) is an anthracycline antibiotic, and it is used as hydrochloride form of doxorubicin (DOX-HCl) to increase its aqueous solubility in drug delivery. The amino group of the sugar can be protonated-unprotonated, as shown in Figure 2.2 and charged-uncharged form of DOX is formed. Also, DOX is an amphiphilic and amphoteric molecule due to carrying acidic and basic functions at its structure. The phenolic group shows acidic property where water-insoluble aglycone (adriamycinone: $C_{21}H_{18}O_9$) has two different pK_a values at C_6 (pK_3=13.2) and C_{11} (pK_2=10.16). The sugar amino group shows basic property where water-soluble region (daunosamine: $C_6H_{13}NO_3$) has another pK_a value as pK_1=8.15. Totally, a DOX molecule has three different pK_a values.[2, 25]
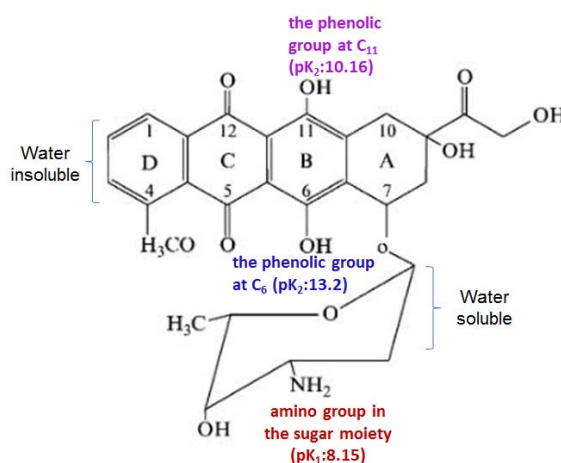
Figure 2.2. The chemical structure of DOX-HCl.[2, 25]

DOX-HCl has dihydroxyanthraquinone chromophore and their physical properties can change depending on any changes in pH, solvent type, ionic strength, drug concentrations, binding ions, and its own concentration. Also, these changes can affect its absorption spectrum. Deprotonation of chromophore gives red shift, and DOX seems orange at pH=7, violet at pH=11, and blue at pH=13. Moreover, the amount of alkali affects the UV spectrum shifts due to the quinone that has indicator-like properties.[2, 27]

DOX has self-association property due to its aromatic dye. Aromatic dyes undergo aggregation and light absorbance variance. A DOX molecule has four aromatic and one planar ring. In aqueous solution, DOX shows different physicochemical properties from monomers to dimers because of electrostatic interactions. For example, DOX exists as monomer at concentrations below 10^{-5} M (37°C, pH=7.3, ionic strength=0.15). DOX's lipid/water partition is constant at lower concentrations. In clinical usage, the activity coefficient of DOX is approximately 0.15 (no unit, the ratio between activity and concentration) at 37°C and pH=7.3. Thus, 85% of DOX is bound to plasma components. This activity coefficient would be different in different experimental conditions, pH, and buffer compositions. The fluorescence spectrum of DOX may change in the presence of liposomes, and cell membranes due to low dielectric medium. On the other hand, DOX is a very toxic molecule due to intercalate with DNA and inhibits the macromolecular biosynthesis as shown in Figure 2.3. When DNA is denatured for replication, DOX stabilizes the topoisomerase II which is responsible for relaxation supercoils in replication. Besides, DOX-HCl generates the free radicals which cause DNA and cell membrane damage. Thus, it results in inhibition of DNA and DNA-dependent RNA synthesis.[2, 28]
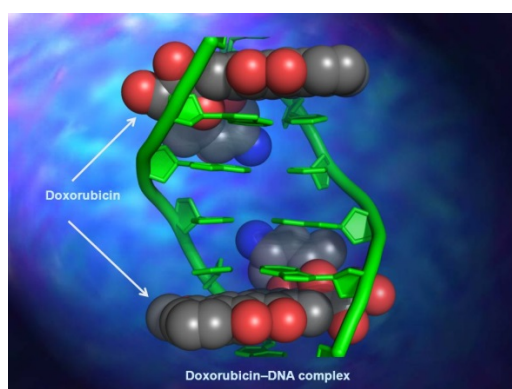
Figure 2.3. DOX-DNA complex.[29]

Additionally, DOX and DOX-HCl cause many side effects such as hair loss, nausea, vomiting, and diarrhea. If the typical acute dose limiting is passed over 550 mg/m^2, then it occurs high incidence of myelosuppression, leukopenia, and thrombocytopenia. Therefore, encapsulation of DOX in drug delivery systems has been studied to decrease the side effects of doxorubicin.[2]

There are many types of drug vehicles but liposomes are more convenient for drug delivery systems by encapsulation due to their biocompatible and biodegradable nature, displaying similarities with biological membrane, easily formed in the laboratory conditions, protecting drug from degradation, transporting drug safely to desired organ, and increasing curative effect. Additionally, the side effects of anti-cancer agents are reduced by liposome.[30]

Liposomes have transportation property of lipid-soluble and water-soluble molecules at the same time because of their both hydrophilic and hydrophobic regions. For this reason, liposomes are used for encapsulation drug delivery vehicles. Unilamellar liposome vesicles are generally used for encapsulation of water-soluble drugs because of the fact that they have an aqueous core. The most important features of determining liposome's efficiency are ingredients, sizes, encapsulation efficiency, stability and biological interaction. Adsorption and endocytosis are most frequently seen in biological interaction. Liposomes can affect to the cells whereby liposome surfaces are prepared to carry on different molecules. The most important problem for liposome technology is liposome clearance by phagocytic system. Scientists encapsulated the liposome surfaces with non-active molecules for immune system. However, the desired results have not been achieved for solid tumors yet. The reason of this problem is accepted as inefficient blood circulation into the solid tumors.[30-34]

2.3. Liposomes

Liposomes were discovered as closed bilayer structures by A. D. Bangham in 1965, and they have accepted the oldest nanocarrier system. Then, liposome term was substituted instead of closed bilayer structure by Sessa and Weissmann in 1968. Liposome term comprises two Greek words which are lipos (fat) and soma (structure). A liposome is formed by lipid bilayers containing aqueous media inside and outside. Liposomes have been used for drug delivery systems in 1970s. In these years, the first

study results were caused disappointment because of instability and low encapsulation efficiency of liposomes. Afterwards, these problems were solved in time, and the many commercial drugs such as Doxil® were produced in 1980s and 1990s.[30, 31, 33, 34]

Liposomes are small artificial lipid vesicles, and their compositions are formed of phospholipid bilayers and other molecules such as protein and cholesterol. A phospholipid composes of one head group that includes choline, phosphate and glycerol, and two tails that include fatty acids as shown in Figure 2.4. A head group has polar and hydrophilic properties when the tails have non-polar and hydrophobic properties. By these properties, lipids form vesicles if they placed in an aqueous medium.[30, 31, 34]
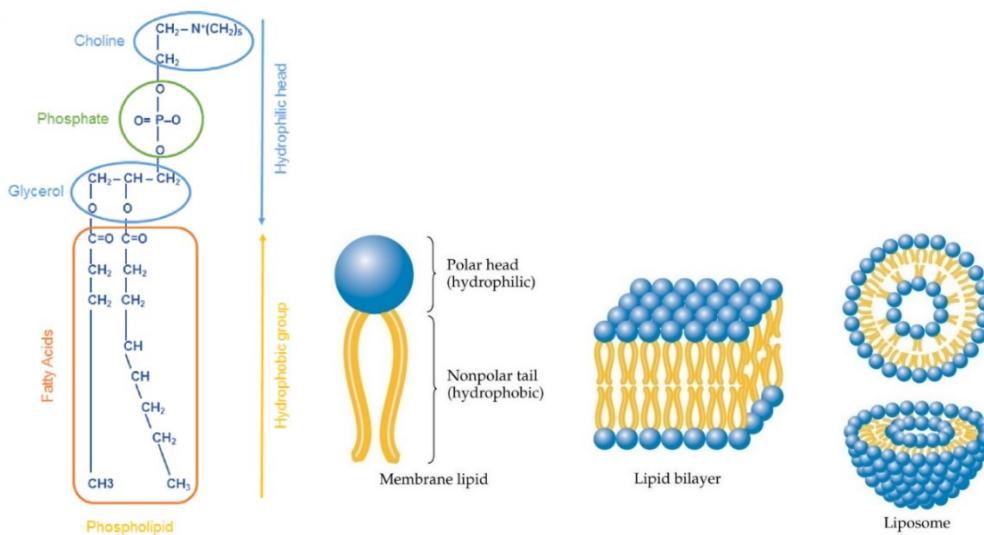
Figure 2.4. Liposome structure.[35]

Liposome classification is made according to its number of bilayers and sizes. They are separated unilamellar vesicles (ULVs, 25 nm to 1 μm), multilamellar vesicles (MLVs, 0.1 μm to 15 μm), and multivesicular vesicles (MVVs, 1.6 μm to 10.5 μm) as illustrated in Figure 2.5. ULVs are separate into two classes as large unilamellar vesicles (LUVs, 100 nm to 1 μm) and small unilamellar vesicles (SUVs, 25 nm to 50 nm). 150-200 nm of liposomes are important for drug delivery systems, and this type of liposomes are called large unilamellar vesicles (LUVs). For obtaining this type of liposomes, there are several methods but the extrusion method is the most popular method. Extrusion process provides the liposome sizes to be the desired levels by using

polycarbonate membranes having different pore sizes. Also, it ensures a homogeneous distribution which is an important property for drug delivery systems. Thus, the pass number of extrusion should be made at least 11 times to obtain a more homogeneous sample and reduce the contamination by leaving the extrusion pass number at an odd number.[36, 37]
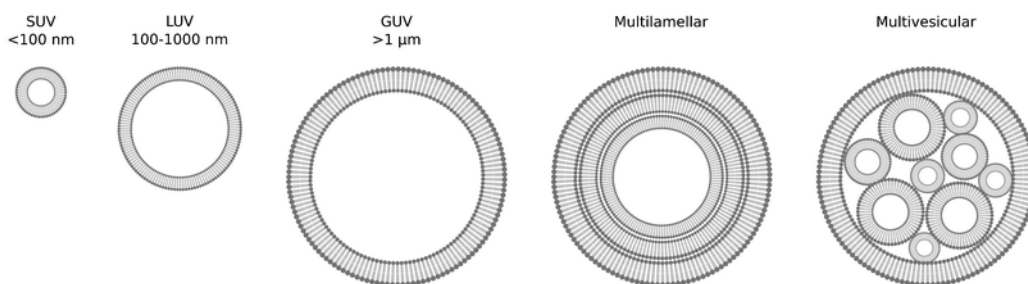
Figure 2.5. Liposome classification.[38]

Liposomes are different with respect to the type of lipid used in their structures such as phosphatidylglycerol (PG), phosphatidylserine (PS), phosphatidylinositol (PI), phosphatidylcholine (PC), 1,2-dioleoyl-3-dimethylammonium-propane (DODAP), 1,2-dioleoyl-3-trimethylammonium-propane (DOTAP). These differences are based on length of the fatty acid chains or the number of carbon atoms and degree of unsaturation. The fatty acids are named according to the number of their carbon atoms. For instance, lauric has 12 carbon atoms, myristic has 14 carbon atoms, palmitic has 16 carbon atoms, and stearic has 18 carbon atoms. Natural phospholipids include unsaturated fatty acids such as PC. The most common artificial phospholipids are DPPC, DMPC, DSPC, HSPC. Also, gel liquid-crystalline phase transition temperature (T_m) affects from the length of lipid chain. Some phospholipids' T_m values were given in Table 2. 2.[33]

Table 2. 2. Gel liquid-crystalline phase transition temperature (T_m) for different phospholipids.

Phospholipid	Acyl chain length, # unsaturation	T_m (°C)
DSPA	18:0, 18:0	58
DSPC	18:0, 18:0	55
DSPG	18:0, 18:0	53
HSPC	16 – 18 (mixture)	52
DPPC	16:0, 16:0	42
DPPG	16:0, 16:0	41,1
POPC	16:0, 18:1	-7
SLPC	18:0, 18:2	-16,7
DOPC	18:1, 18:1	-21

Liposome molecules have fluidity and mobility features, and these properties provide selective permeability which is the main characteristic of cells. Selective permeability ensures that the internal environment is kept different from the external environment for passing through of a given substance. As shown in Figure 2.6, small non-polar molecules have high permeability and pass through the lipid bilayers quickly when large molecules and charged substances cannot pass through the membrane or pass through slowly because of their low permeability.[33, 39]
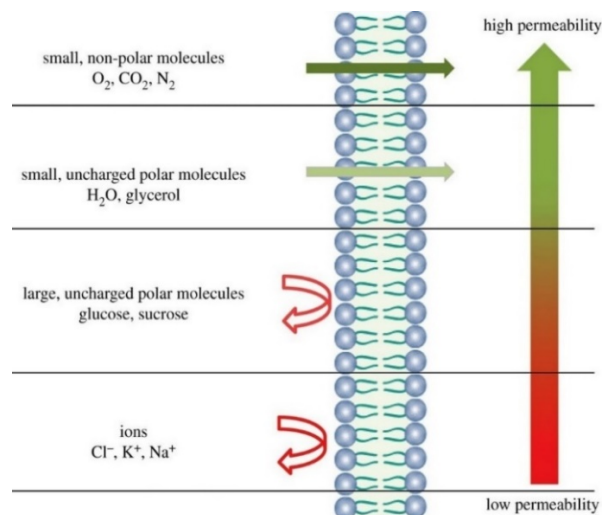
Figure 2.6. Selective permeability of lipids bilayers.[33]

The type of lipid affects the membrane permeability depending on the degree of fatty acid saturation. If carbon atoms have two bonds between each other (C=C), it is called unsaturated hydrocarbons. On the other hand, if the carbon atoms have one bond (C-H), then it is called saturated hydrocarbons. As illustrated in Figure 2.7, double bonds create a gap between hydrophobic tails and become more permeable than saturated hydrocarbons. Also, tail length affects the permeability. Briefly, long and saturated tails are less permeable than shorter and unsaturated tails.[33, 39]
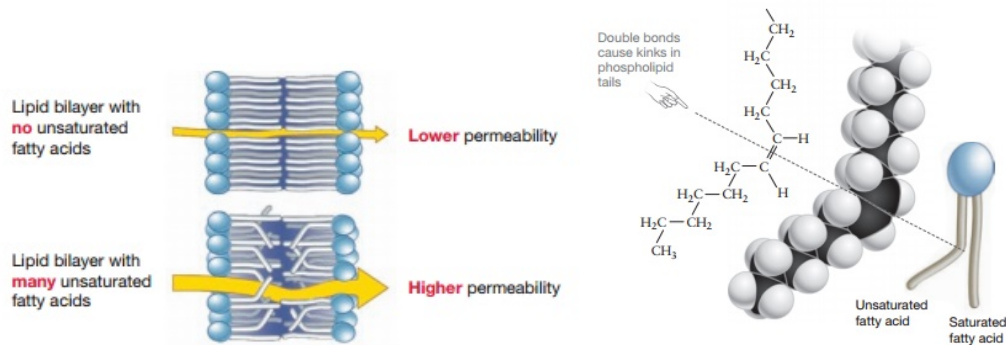
Figure 2.7. Saturated and unsaturated fatty acids.[39]

Temperature affects the membrane permeability and fluidity. If the temperature decreases, the molecules move slowly inside the bilayer, and hydrophobic tails pack together more tightly. As a result of this, membrane permeability decreases. As shown in Figure 2.8, phospholipids are in the gel phase at temperature below the T_m value, and they also show low permeability at temperature above the T_m value. Therefore, the temperature can be adjusted correctly according to phospholipid phase diagram before the formation of liposomes. Additionally, different lipid structures show different permeability at the same temperature due to their different T_m values. For drug delivery systems, the temperature is raised to alter phospholipid permeability because of entrapped lipid vesicles having low permeability. Moreover, T_m values affect the encapsulated drugs such as DOX. For this reason, it has been suggested that temperature should be 10°C higher than T_m value during liposome preparation to ensure that all phospholipids are dissolved homogeneously. The annealing and stabilization period for liposomes is about 30-60 minutes at above its T_m value.[31, 33, 39]
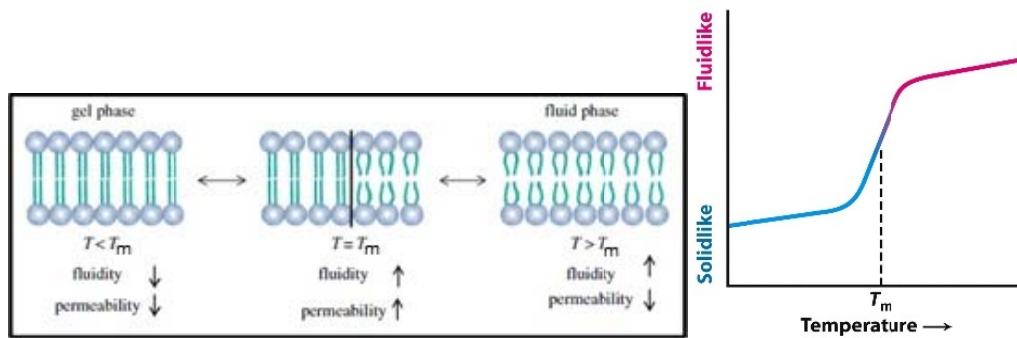
Figure 2.8. Membrane permeability changes with the temperature.[33]

There are other molecules in liposome structure such as sterols. Cholesterol is a sterol, and it also affects the permeability of phospholipids. Cholesterol also provides vesicle stability by adjusting the lipid bilayer fluidity. As illustrated in Figure 2.9, cholesterol fills the gaps between the phospholipids, and it ensures to increase the permeability in gel phase and decrease the permeability in the fluid phase. Cholesterol has dense steroid rings, and so it increases the hydrophobic density of phospholipids. This increasing causes the flexibility reduction in the environment of the lipid chain, mechanical rigidity elevation of the fluid bilayers and lateral diffusion reduction. For drug delivery systems, lipid composition and cholesterol are important parameters. If the amount of cholesterol is higher than 40% of liposome composition, then the liposomes become unable to interact with the model membranes. It means that it is not suitable for drug delivery applications.[31, 33]
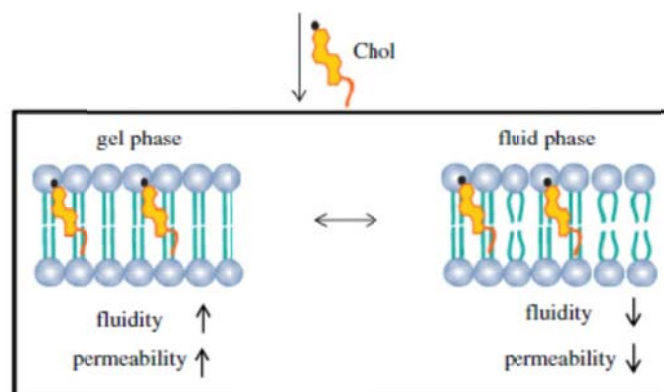
Figure 2.9. Cholesterol in a lipid bilayer structure. [33]

In 1990, hydrophilic polymers were discovered. Hydrophilic polymers provide the steric stabilization of liposomes. For example, polyethylene glycol (PEG) was mixed with phospholipids and cholesterol to change liposome surface property. If liposome formulation is composed of phospholipids and cholesterol, it is called 'conventional liposome' which depends on the size, surface charge and membrane packing density. On the other hand, if liposome formulation is composed of phospholipids, cholesterol and PEG (Figure 2.10), then it is called 'sterically stabilized liposomes (SSLs)' or 'stealth liposomes' or 'PEGylated liposomes' which depends on the increasing surface density by acting like a polymeric chain. Also, PEGylated liposomes have unsaturated, non-immunogenic, dose-independent, high bioavailability properties, and it shows long remaining in the blood circulation (for example, $t_{1/2}$>40h). Moreover, 10-15% of the drug is delivered to the liver in PEGylated liposomes on the contrary 80-90% of the drug is delivered to the liver in conventional liposomes. However, PEGylated liposomes have a disadvantage which is called 'accelerated blood clearance (ABC)' after the dose injection. In spite of PEGylated liposomes are non-immunogenic, the immune system reacts as blood clearance. Therefore, different methods are used such as extrusion to minimize the liposomes. The polycarbonate membranes whose sizes change between 400 nm and less than 70 nm were experimented, and it was seen that ~400 nm was cleared 7,5 times faster than ~200 nm liposomes and 5 times faster than small unilamellar vesicles (SUVs). In briefly, larger liposomes (more than 300 nm) and smaller liposomes (less than 70 nm) were more cleared than the sizes change between 150-200 nm liposomes.[31, 33]
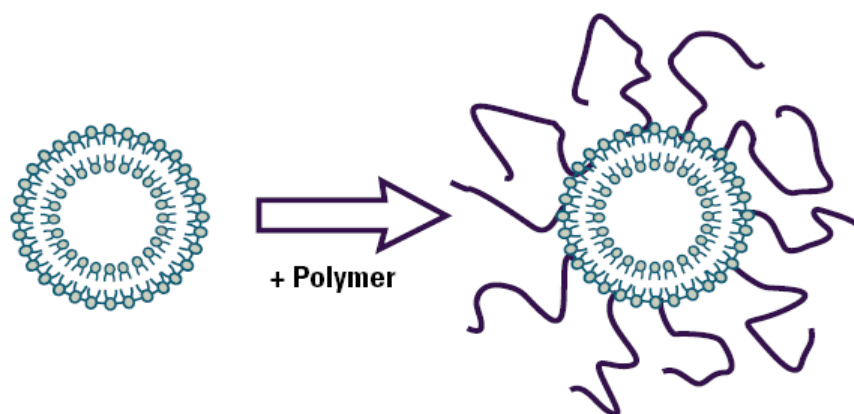
Figure 2.10. PEGylated liposome.[40]

2.4. Detergent Triton X-100

The most commonly used method for lipid destruction in biology is to use a detergent. Detergents are amphipathic molecules, and they have one hydrophilic polar head group and one hydrophobic chain as shown in Figure 2.11.[41]
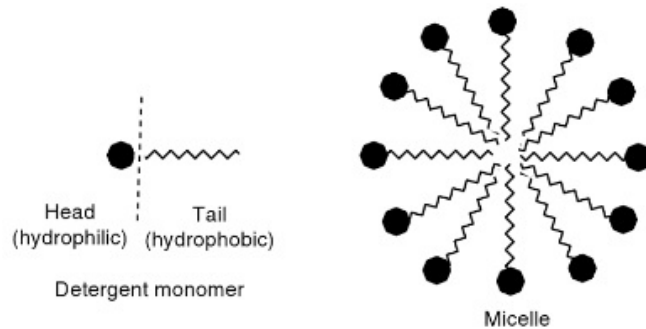
Figure 2.11. Detergent monomer and micelle forms.[42]

Concentration affects the detergent forms. As shown in Figure 2.12, monomer forms exist at low concentration when micelle forms exist at higher than critical micelle concentration (CMC). Micelle form is self-association of monomers above CMC. When detergent is added to solution, monomer concentration increases until the CMC value. Then, it stays constant whereas micelle concentration increases above the CMC due to monomer molecules are in equilibrium with micelles.[42, 43] Detergents have limited size clusters in water, and their micelle size is approximately 5 nm.[44] However, a micelle size and shape show an alteration with regard to type, size, and stereochemistry of monomer surfactant.[42]
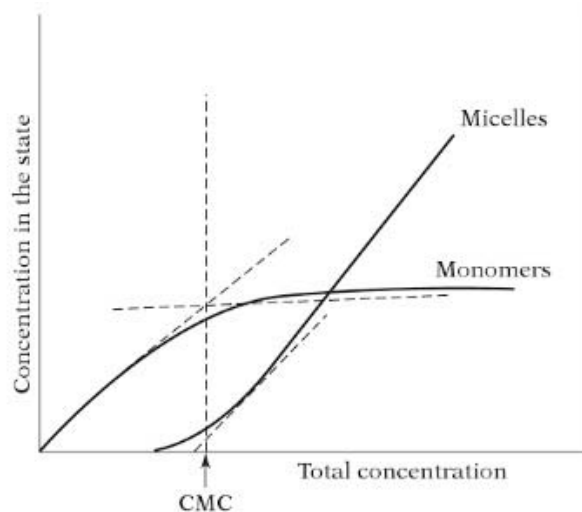
Figure 2.12. Critical micelle concentration.[43]

Aggregation number (N) and hydrophile-lipophile balance (HLP) number determine the detergent behavior. The average number of monomers per micelle is referred to as N, and it depends on the detergent molecular mass. Detergent hydrophilicity index is referred to as HLP number. The concentration of micelles in moles per liter can be calculated with Eq.(2. 1). Here, C_s is the bulk molar concentration of detergent. Ionic strength is affected by aggregation number. The aggregation number can be calculated with Eq.(2. 2). The micellar molecular weight can be obtained by several methods such as gel filtration and light scattering.[45]

$$[\text{micelles}] = (C_s - CMC) \div N \qquad (2.\ 1)$$

$$\text{Aggregation number} = \frac{\textit{micellar molecular weight}}{\textit{monomeric molecular weight}} \qquad (2.\ 2)$$

Also, the critical micelle temperature (CMT) affects the detergent forms as shown in Figure 2.13. The monomer concentration reaches the CMC point when temperature is increasing. This point is called the "Kraft point" or "cloud point". Below the Kraft point, detergents exist as monomer form at low concentration and crystal form at high concentration. When temperature increases, monomer concentration increases until the CMT value. After CMT value, micelles occur, and the solution turbidity clears away because of two phases (micelles and monomers) present in the medium.[43, 45]
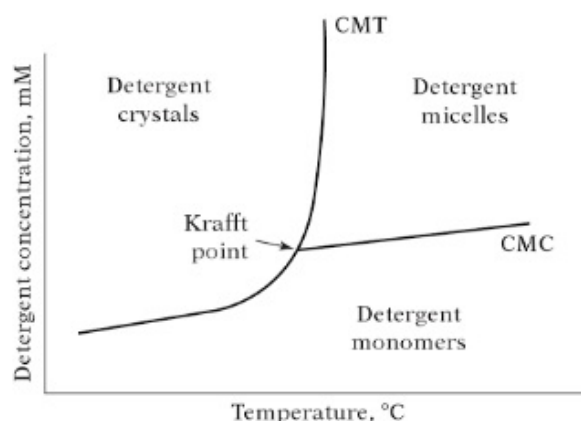
Figure 2.13. Critical micelle temperature.[43, 45]

Low concentration of detergent intercalates into the lipid bilayers as shown in Figure 2.14. At high concentration, detergent disrupts the lipid bilayer and forms mixed micelles which are lipids, micelles, and monomers. There are three stages in detergent-

lipid interaction. In first stage, detergents distribute equally between lipids and water. In second stage, all lipid bilayers are filled with detergents. Mixed bilayers and mixed micelles are formed, and these transformations continue until all of the lipid bilayers disappear. In third stage, there are a lot of micelles in the medium, and the particle sizes decrease.[43, 46]
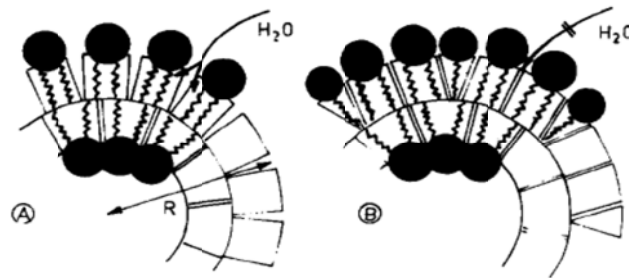
Figure 2.14. Detergent intercalation with lipid molecules.[46]

A phase transition from liposomes to micelles is shown in Figure 2.15. This representation depends on the three stages of detergent-lipid interaction. The first stage continues until the saturation point. The curve represents the turbidity, and it has two breakpoints as line 1 and line2. In line 1, the detergents begin to disrupt the liposomes. In line 2, the liposomes are broken down into mixed micelles. The detergent-to-lipid ratio can be determined with light scattering measurement.[47]
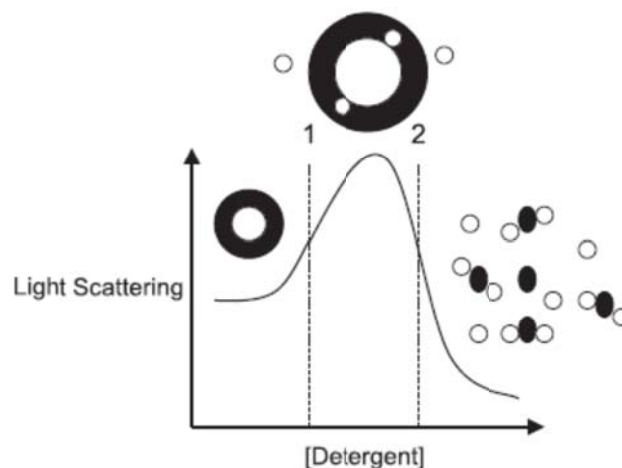
Figure 2.15. Phase transition diagram from liposomes to micelles (black: lipids or liposomes, white: detergent molecules).[47]

As shown in Figure 2.16, detergents are classified according to their chemical structure as ionic, non-ionic, zwitterionic, and bile acid salts. Ionic and zwitterionic

detergents have either positive or negative charge head groups. Non-ionic detergents have uncharged head group. Bile acid salts are a kind of ionic detergent.[45, 47]
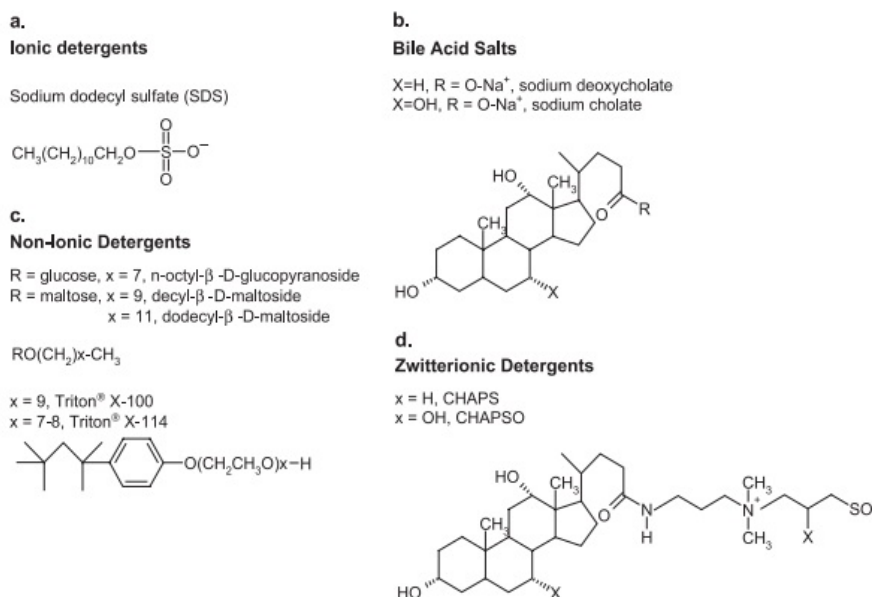
Figure 2.16. Detergent types.[47]

Triton X-100 (T_{x-100}) is one of the widely used non-ionic detergents in the biological research studies for the destruction of liposomes and releasing the DOX trapped in their interiors. T_{x-100} is a polyoxyethylene detergent. Its CMC value changes between 0.2 and 0.9 mM depending on temperature, but generally it is assumed as 0.24 mM.[48] The salt concentration is less sensitive on micelle size.[45] The L_{α} state lipids are easily solubilized by excess T_{x-100} whereas the L_o state lipids are insoluble. Also, cholesterol effects the solubilization of lipids. It provides tightly packed liquid ordered state of lipids, and lipids begin to become insoluble in T_{x-100}according to the amount of cholesterol. There isa very weak interaction between uncharged polymers (PEG) and nonionic surfactants (T_{x-100}).[49]

2.5.DOX Loading within the Liposomes

For cancer treatment, it has been developed an efficient alternative treatment such as PEGylated liposomal doxorubicin (PLD), non-PEGylated liposomal doxorubicin (NPLD), liposomal daunorubicin (DNX), liposome encapsulation of

platinum (Pt) complexes and immunoliposomes. Additionally, it was used contrast agents such as microbubbles to obtain images for the liposomes applications towards medical diagnosis. The advantage of liposomes is transporting more than one contrast agents at the same time according to traditional methods. The most favorite system is PEGylated liposomal doxorubicin systems as shown in Figure 2.17. This system provides to make DOX more tumors targetable and reduce the side effects such as cardiotoxicity, neutropenia, alopecia. But at the same time, it was realized that a new toxicity problem called hand-foot syndrome arose from DOX encapsulation liposomes.[2, 25]
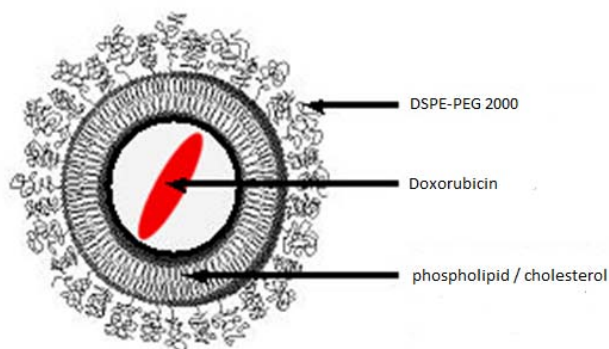
Figure 2.17. PEGylated liposomal doxorubicin.[50]

The parent drugs of anthracycline liposomal formulations are liposomal daunorubicin (DaunoXome), non-PEGylated liposomal doxorubicin (Myocet), and PEGylated liposomal doxorubicin (Doxil). There are four main classes for liposome formulation as Class I, II, III and IV in accordance with these drugs. Liposomes physical properties, composition, drug loading and retention mechanism effect the classification of these groups. Class I is formed by cardiolipin, and it has two sub-classes as Class IA and Class IB. Stearylamine is a positively charged surfactant, and it exists in Class IA with cardiolipin. Thus, it provides positive surface potential for liposomes. Class IB is enhanced version of Class IA. However, there is no stearylamine in this class. It has been reformulated with synthetic cardiolipin, and it has been become a negatively charged surfactant. Class II is formed by PS or PG, and it provides negative surface potential for liposomes. These class liposomes are generally used in gene delivery systems. The Class I and Class II lipo-DOX ensure the carrying drug into the liposomes aqueous region with the help of ion gradient, and they trap the drug inside the liposomes. Thus, electrostatic binding of DOX can be achieved with negatively charged

phospholipids. Class III is neutral form of liposomes, and drug Myocet belongs to this class. It is composed of PC and cholesterol. It is demonstrated that this class lipo-DOX delivers the drug effectively to the tumors. Class IV has negatively charged surfactant, and drug Doxil and Caelyx belongs to this class. This class is successful for decreasing the cardiotoxicity of DOX.[51] According to the researchers, the negatively charged liposomes are more stable than positively charged liposomes, and the drug release has an order of negatively charged > neutral > positively charged liposomes. In addition, PEGylated liposomes are more negatively charged than the bare liposomes.[52]

In addition, the pH of buffer affects the loading efficiency. DOX is positively charged when its primary amino group is partially protonated, but it binds both positive and negative inner and outer membranes of liposome. If the total mass of phospholipid is higher than 4-10 mol%, DOX molecules adhered to the bilayers. This adhesion continues until it stays in a period of storage. It is proposed an acidic medium for liposome association at pH 4 and 6.3 to obtain low release rate on storage. Also, it can be used low amount of DOX under the maximum amount of lipo-DOX. The ratio of DOX to phospholipid is 60-75 mmol dox/mol-phospholipid for negatively charged liposomes and 55 mmol dox/mol-phospholipid for positively charged liposomes. Moreover, the empty liposomes have similar ζ-potential with lipo-DOX. If DOX presents in the organic phase during lipid film formation, there will be no an electrostatic interaction. The binding capacity of negatively charged liposomes does not change when the drug is added in the hydration medium, but the binding capacity of positively charged liposomes dropped dramatically.[51, 53-55]

In cells, liposome uptake such as endocytosis or fusion depends on the liposome, liposome charge, and cell characteristics. It was known that the binding efficiency of positively charged liposomes (cationic liposomes) to the cells is higher than the negatively charged liposomes (anionic liposomes) due to their opposite charge. PEGylated liposomes have steric repulsion and van der Waals interactions between the surface and lipid bilayer as shown in Figure 2.18. For targeted delivery, it requires selective uptake and suppression of nonselective adhesion; however cationic liposomes bind nonselective to all cell types.[56]
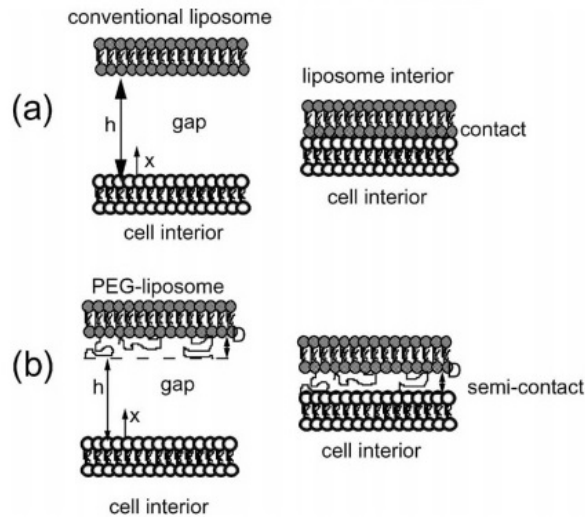
Figure 2.18. The interaction of PEG coated liposomes with cells.[56]

2.6. Microbubbles

Microbubbles are tiny gas-filled contrast agent molecules which sizes change between 0.5 to 10 μm as illustrated in Figure 2.19. They are non-toxic, mechanically oscillate, and enhancing the signal-to-noise ratio (SNR) during imaging. There is an important property of MBs that is cellular and vascular permeability to more effective localized drug uptake in cancer tissue. Microbubbles have different shell structures that are lipid, protein, or polymer. The thicknesses of shell materials are ~3 nm in lipids, 15-20 nm in proteins, and 100-200 nm in polymers. The interactions between the shell structures are hydrophobic and Van der Waals in lipid molecules, covalent disulfide bonds in proteins, and covalently cross-linked in polymer chains. A microbubble size must be less than a red blood cell size in order to pass capillaries in the body.[57, 58]
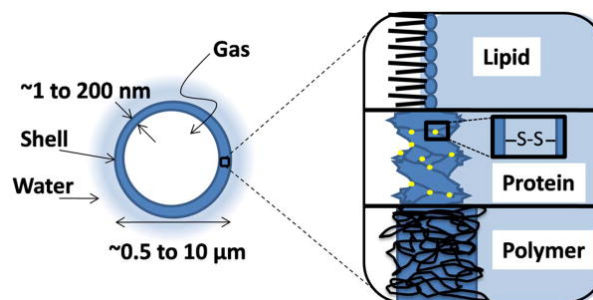
Figure 2.19. Different structures of microbubbles.[57]

The shell structures show differences according to stability, drug payload, compliance, and ultrasound effect. As shown in Table 2. 3, lipid shell has high compliance, and it gives high echogenicity under ultrasound. In addition, microbubbles gain extra property with liposomes which are the best candidates for drug delivery systems due to its structural similarities with biological membranes. Liposomes also provide long circulation times and carry both hydrophilic and hydrophobic drugs due to its amphiphilic structure.[57, 59]

Table 2. 3. The properties of microbubble shell structures.

Shell Type	Thickness	Compliance	Stability	Drug Payload	Ultrasound Effects
Protein	15 - 20 nm	Medium	Medium	Medium	• High echogenicity • Shell does not reseal after rupture
Lipid Surfactant	3 nm	High	Low to Medium	Low to Medium	• High echogenicity • Shell reseals after rupture
Polymer	100 – 200 nm	Low	High	High	• Low echogenicity • Shell does not reseal after rupture
PEM hybrid	10 – 200 nm	High	High	High	• Unknown

2.7. Lipo-DOX and Microbubble Coupling

Streptavidin is a protein which is isolated from the *Streptomyces avidinii*, and streptavidin molecule has four subunits which were bind to the biotin molecule. Biotin

is a water-soluble vitamin, and it can be bound with proteins and nucleic acids. The biotin-streptavidin system is based on the strong binding property between streptavidin and biotin.[60] The schematic representation of biotinylated liposomes was shown in Figure 2.20. In here, fluorescent probe was doxorubicin hydrochloride (DOX-HCl) and antibody was epidermal growth factor biotin-xx conjugate (biotin EGF).
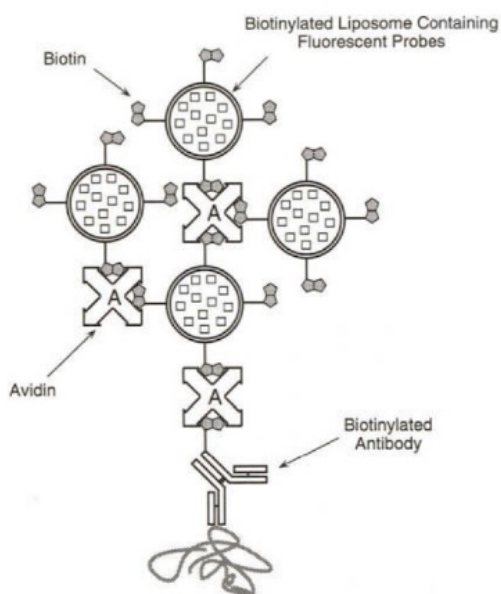
Figure 2.20. The schematic representation of biotinylated liposomes.[60]

A DOX loaded liposome coupled with microbubbles was illustrated in Figure 2.21. This technique is demonstrated as an effective technique for encapsulation targeted therapy. According to this illustration, microbubble's inside have a perfluorocarbon (C_4F_{10}) gas which is sufficiently stable for circulating in the vasculature. Microbubbles carry the drug to the specific area, and they have been burst by ultrasound to cause localized release of the drug.[61]
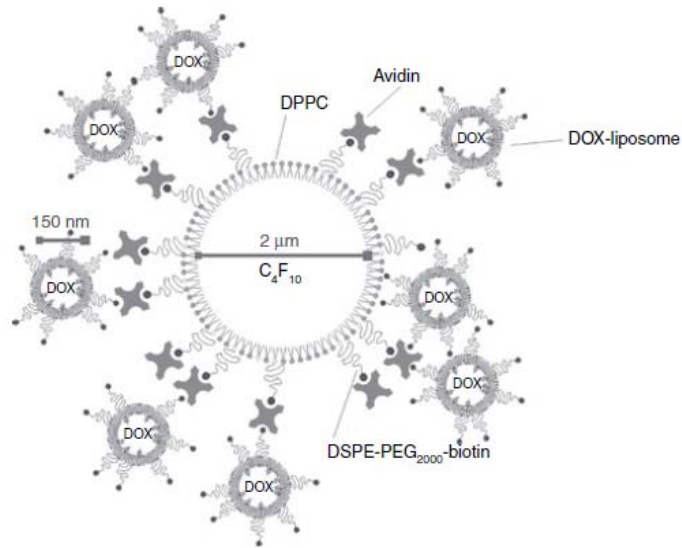
Figure 2.21. DOX-liposome-loaded-microbubbles.[61]

The cancer treatment can be effectively done by the microbubble-liposome conjugates under ultrasound. The encapsulated liposomal drug can be coupled with microbubbles. When the conjugated lipo-DOX was injected into the blood stream, they expected to accumulate in the targeted area. When the microbubbles were burst under high ultrasound, the drugs were expected to release in the targeted area. As a result, the tumor was expected to shrink and cancer cells to die.
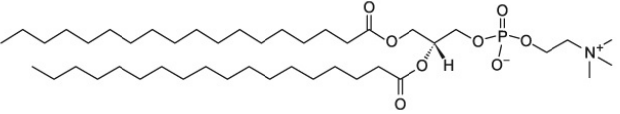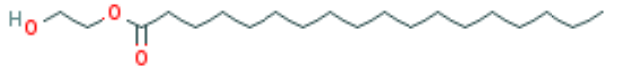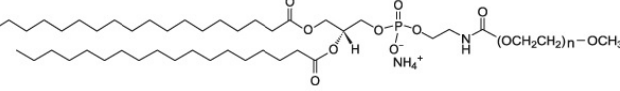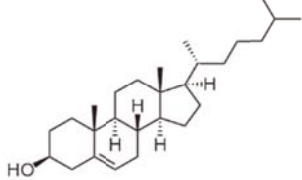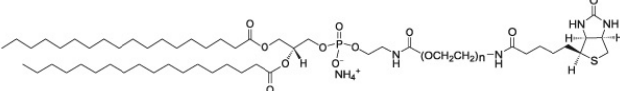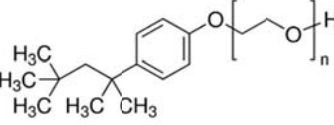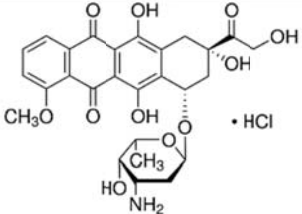
CHAPTER 3

MATERIALS AND METHODS

3.1. Materials

Some of the chemicals and their chemical formula used in the studies were shown in Table 3.1. The lipids 1,2-distearoyl-sn-glycero-3-phosphocholine (DSPC), 1,2-distearoyl-sn-glycero-3-phosphoethanolamine-N-[methoxy(polyethylene glycol)-2000] (DSPE-PEG$_{2000}$), and 1,2-disteoryl-*sn*-glycero-3-phosphoethanolamine-N-[biotinyl(polyethylene glycol)2000] (ammonium salt) (DSPE-PEG$_{2000}$-Biotin) were purchased from Avanti Polar Lipids, Inc. (Alabaster, AL, USA). PEG$_{40}$Stearate (PEG$_{40}$St), DOX-HCl, and chloroform were purchased from Sigma-Aldrich$^{®}$, Inc. (St. Louis, MO, USA).Epidermal growth factor (EGF)-biotin conjugate (biotin-EGF) and streptavidin-PE were purchased from Life Technologies. Cholesterol was purchased from Fluka; the dialysis membrane RC tubing (MWCO: 10 kD, Spectra/Por$^{®}$ 6 Dialysis Membrane) and Sephadex™ G-75 for chromatography column were purchased from GE Healthcare Life Sciences.

Table 3.1. Some of the chemicals and their chemical structures used in the study.

Chemical	Chemical Formula
1,2-distearoyl-sn-glycero-3-phosphocholine (DSPC)	
PEG$_{40}$-Stearate (PEG$_{40}$St)	
1,2-distearoyl-sn-glycero-3-phosphoethanolamine-N-[methoxy(polyethylene glycol)-2000] (DSPE-PEG$_{2000}$)	
Cholesterol	
1,2-disteoryl-*sn*-glycero-3-phosphoethanolamine-N-[biotinyl(polyethylene glycol)2000] (ammonium salt) (DSPE-PEG$_{2000}$-Biotin)	
Triton X-100	
DOX-HCl	

3.2. Methods

3.2.1. Liposome Making

The first step in liposome making was the preparation of thin lipid film formation as shown in Figure 3.1.The liposomes were formed with a mixture of DSPC, cholesterol, DSPE-PEG$_{2000}$ and DSPE-PEG$_{2000}$-Biotin with a composition of 57-38-4.9-0.1 mole%, respectively. Each component was weighted in a 20 ml vial and added 2 ml of chloroform to dissolve and make a homogenous mixture. A stream of nitrogen gas was used to evaporate the chloroform while rotating on a spinning table at a rate of 200 rpm. After evaporation of chloroform and formation of the thin film, the vial was put into the vacuum oven for 3 hours to ensure a complete removal of the chloroform within the thin film. If the film was not used at the same day of preparation, it was stored in the fridge at -20°C.
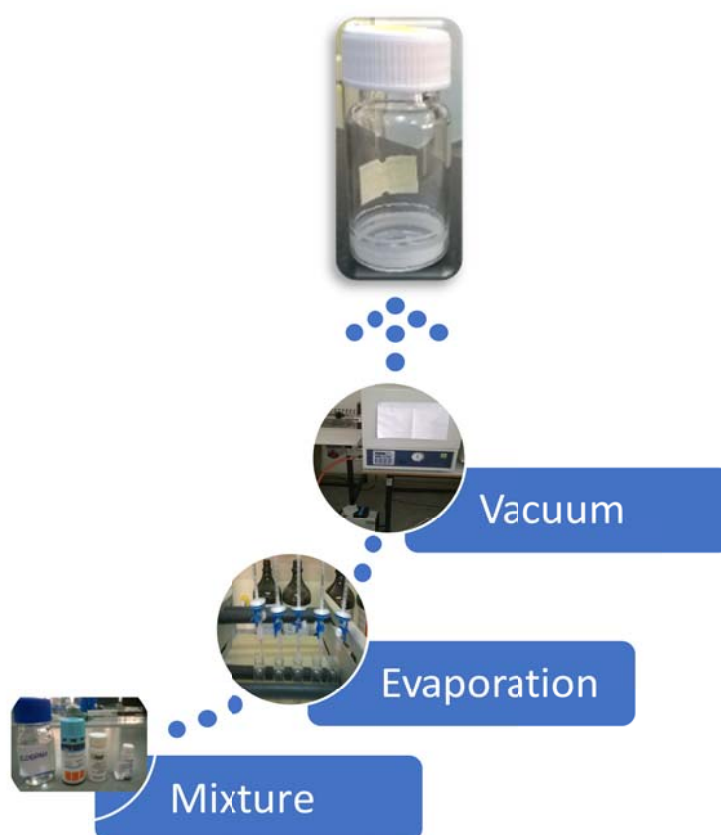
Figure 3.1. The formation steps of thin lipid film.

The second step in liposome making was the hydration of the thin lipid film as shown in Figure 3.2. The lipid film was mixed with 1 ml of ammonium sulfate $[(NH_4)_2SO_4]$ (250 mM, pH=5,4) buffer solution for DOX loading, and hydrated for about 1 hour at a temperature of 65°C in a shaking water bath.
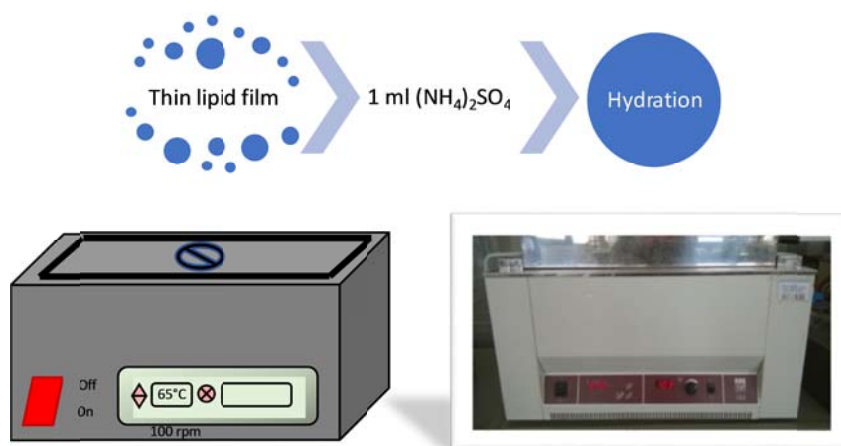
Figure 3.2. The hydration step of thin lipid film.

The third step in liposome making was the thin lipid film extrusion as shown in Figure 3.3. The mini-extruder consisted of a polycarbonate membrane (Whatman Nucleopore Track-Etch filtration product) with a pore size of 400 nm, 200 nm, and 100 nm, a filter supports made of polytetrafloroethylene (PTFE), O-rings, and a Swagelok connector assembly for holding the filter system, which were all purchased from Avanti Polar Lipids, Inc. (Alabaster, AL, ABD). Extrusion was conducted on a hot plate at 65°C. Firstly, the parts of the mini-extrusion device were assembled. Primarily, white round PTFE was put into the retainer nut and the other internal membrane support was put into the longer extruder outer casing. Then, two filter supports and one polycarbonate membrane were wetted in the buffer, specifically in $[(NH_4)_2SO_4]$ buffer for DOX loading, by holding a tweezer. The 200 nm polycarbonate membrane was placed in between the membrane supports and put onto the black round O-ring. The retainer nut was assembled with another O-ring and sealed together properly. The Hamilton syringe was filled with buffer and passed several times through the filter to replace air and fill the gaps and discarded for lipid extrusion. Then, the lipid solution was filled in a Hamilton syringe and placed into the filter assembly. The ensemble mini-extruder with lipids was put on the hot plate and 10 minutes were allowed to adjust its

temperature to 65 $^{\circ}$C. The lipids were injected for extrusion through the filter with a Longer Syringe Pump (LSP02-1B).
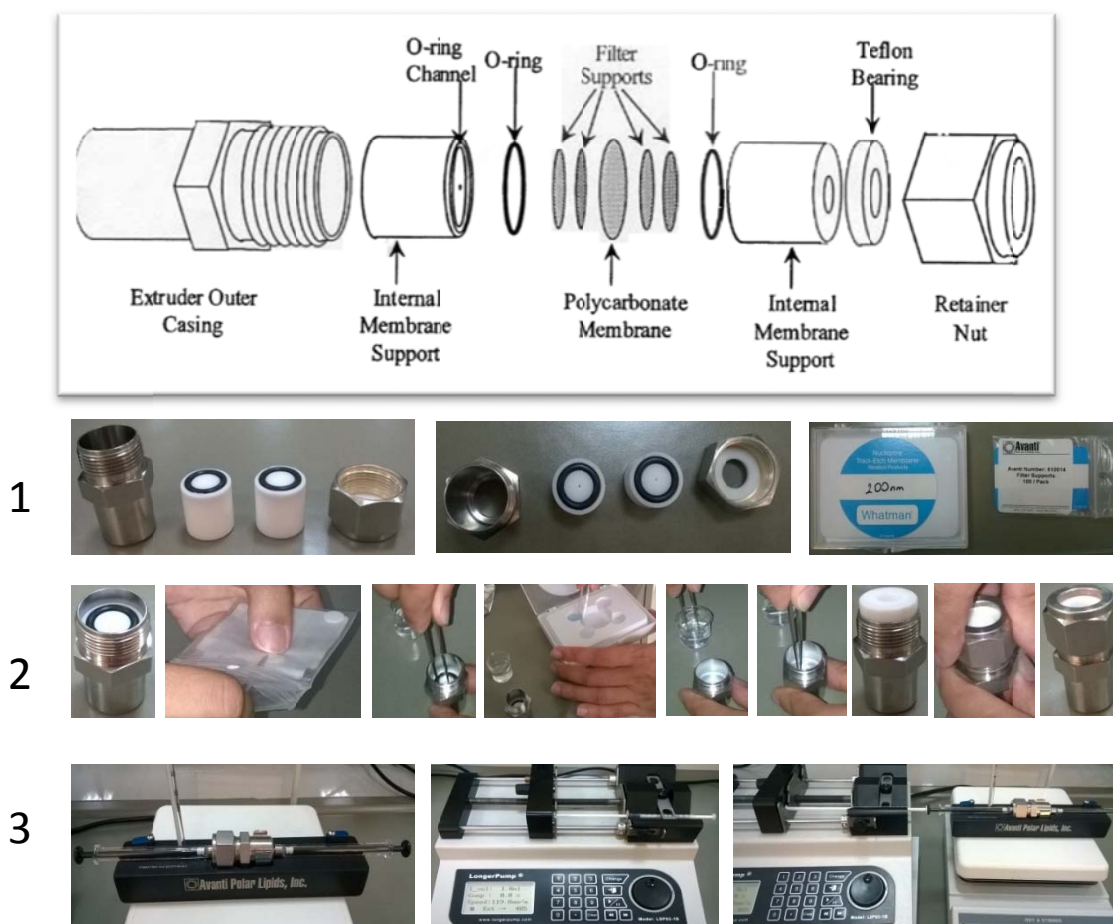
Figure 3.3. The steps of mini-extruder process.[36]

About 1.0 ml of hydrated lipid mixture was extruded through a 200 nm polycarbonate filter at a constant flow rate of 120 mm/min adjusted by the Longer pump. The hydrated lipid film was passed 11 times with an odd number through the membrane to obtain a more homogeneous sample as shown in Figure 3.4. Finally, the liposome sample was put in a clean vial and stored in the fridge at +**4**°C for further use.

Figure 3.4. Extrusion process and liposome making.[62]

Samples were taken before extrusion and after extrusion to estimate the size distribution and average sizes of the liposomes.

3.2.4. DOX Loading within Liposomes

Ammonium sulfate loaded liposomes were used for DOX loading within liposomes. The liposomes were dialyzed in order to remove extra ammonium sulfate from the exterior environment of the liposomes against 0.9% sodium chloride (NaCl) salt solution as shown in Figure 3.5. A piece of dialysis membrane (Spectra/Por[®] 6, Spectrum Laboratories, Inc.) was cut and washed with fresh ultra-pure water to get rid of the sodium azide which was the protecting chemical for the membrane. The dialysis membrane properties were shown in Table 3.2. One end of the membrane was tied with a clip, and liposomes were put into the dialysis membrane with a pipette. The other end of the membrane was also tied with clips, and inserted into about 1.0lt of 0.9 % NaCl solution in a beaker. The NaCl solution created an osmatic pressure across the membrane; otherwise, the dialysis membrane may swell and ruptures. The dialysis was conducted overnight at room temperature on a magnetic stirrer.

Table 3.2. Dialysis membrane properties.

Standard RC Membrane (Spectra/Por[®] 6 Pre-wetted Dialysis Tubing)			
MWCO	Nominal Flat Width	Diameter	Volume/Length
10 kD	24 mm	15 mm	1.8 ml/cm
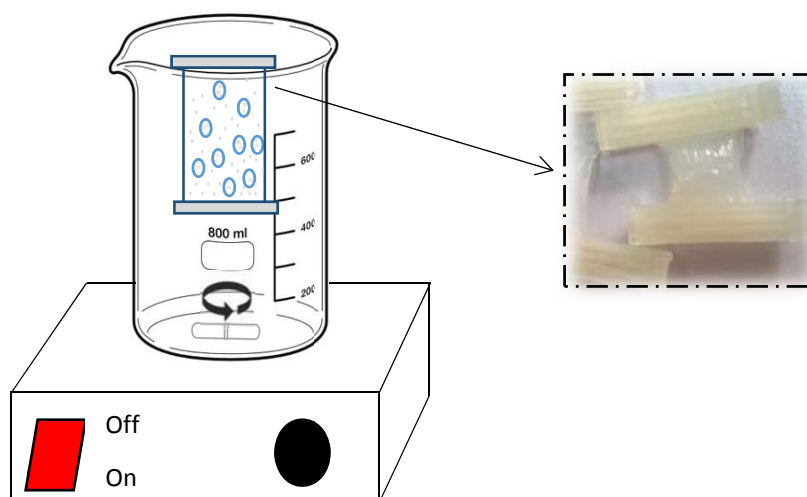
Figure 3.5. An illustration for liposome dialysis against 0.9% sodium chloride (NaCl) salt solution to remove external ammonium sulfate buffer.

Following the dialysis, about 1.0 ml of DOX solution at different concentrations were added into about 1.0 ml of dialyzed liposomes in a 20 ml vial and incubated at 65°C for 4 hours in a water bath shaking at a rate of 140 rpm. As shown in Figure 3.6, DOX-HCl is red in color when it was diluted with ultrapure water and, this color became almost pink after the drug loading due to $[(NH_4)_2SO_4]$ buffer in the liposomes.

Before   After

Figure 3.6. DOX loading within liposomes.

3.2.5. Separation of Unencapsulated DOX from Lipo-DOX

The free-DOX which did not enter into the liposomes was separated from the lipo-DOX by mainly two methods; one is the membrane dialysis method, and the other

is the separation by column chromatography as shown in Figure 3.7. In membrane dialysis method, the free-DOX molecules were dialyzed against 0.9% NaCl solution by using dialysis membranes with a molecular weight cut-off (MWCO) of 10 kDa in sizes. During the dialysis, DOX containing liposomes were trapped within the membrane while the free-DOX molecules pass through the membrane pores to the 0.9% NaCl solution at infinite dilution. In the separation of column chromatography method, a fixed-bed column was prepared with polymeric Sephadex particles as shown in Figure 3.7b. The Sephadex particles were initially soaked in the DI water for 24 hours at room temperature, by which the particles swelled and their pores opened. When the lipo-DOX sample was added on the surface of the column along with the free-DOX molecules, it was expected that the small molecules, i.e. free-DOX, diffused into the pores of the polymeric particles and the liposomes passed along the particles and flowed through the column. Therefore, liposomes first appeared at the exit of the column while free-DOX molecules were retarded by the porous Sephadex particles and eluted at a later time. The exit stream was collected in a vial 20 drops each and analyzed for liposomes in DLS as a photon counts and free-DOX by the Fluorescence spectroscopy, respectively.
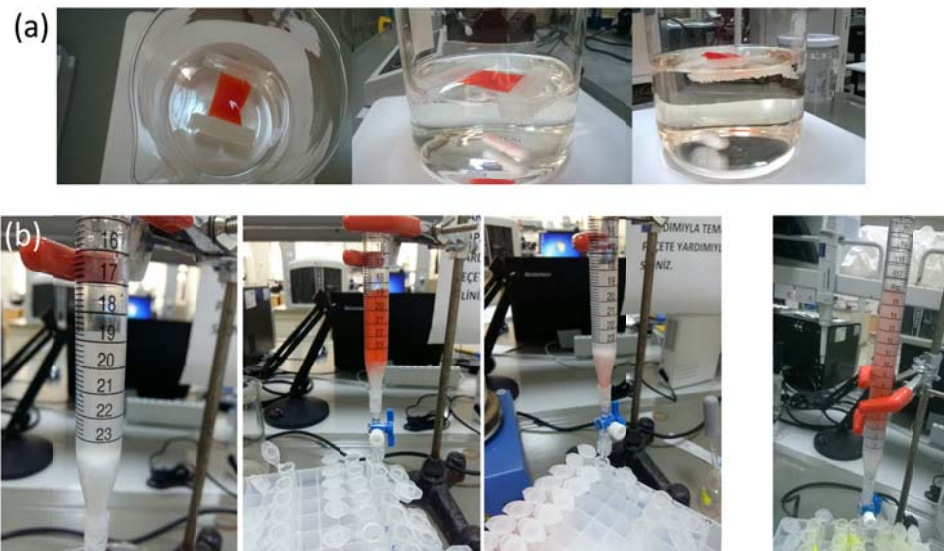
Figure 3.7. Two main methods for separation of free-DOX from lipo-DOX (a) membrane dialysis method (b) Column chromatography method.

3.2.6. Microbubble Making

Microbubbles were formed from a mixture of DSPC and $PEG_{40}St$ with a mole ratio of 5:5. For coupling, $DSPE\text{-}PEG_{2000}$ and $DSPE\text{-}PEG_{2000}\text{-}Biotin$ were also added to the formulations. In order to make a lipid film, each component were weighted in a 20 ml vial and added 5 ml of chloroform to solve and mix them homogenously as shown in Figure 3.8. The chloroform then evaporated by a flowing stream of N_2 on an orbital shaker rotating at 200 rpm. The vial was put in a vacuum oven for 3 hours to ensure the complete removal of the chloroform. The film was capped and stored at the freezer at -20°C if the film was not used on the same day.
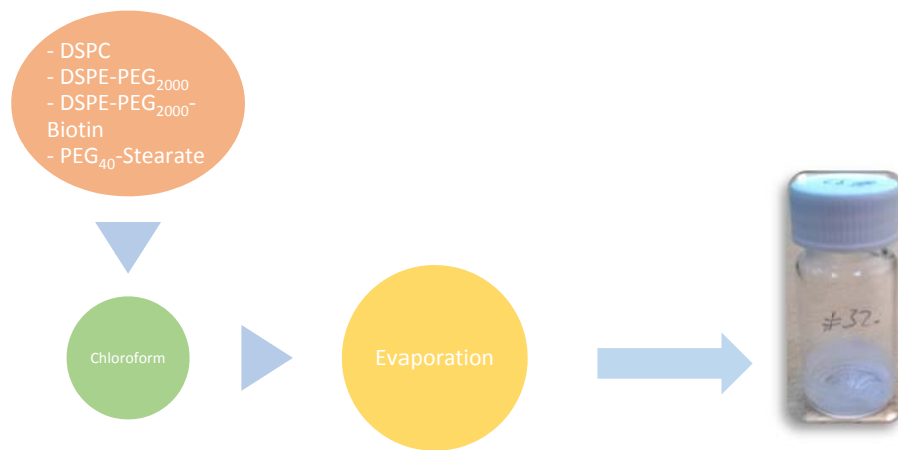
Figure 3.8. The formation steps of MB thin film.

Before microbubble making, as shown in Figure 3. 9, the lipid film was hydrated with 4 ml of phosphate buffer saline (PBS, 50 mM, pH=7.2) in a water bath at 65°C for 2 hours shaking at a rate of 140 rpm.
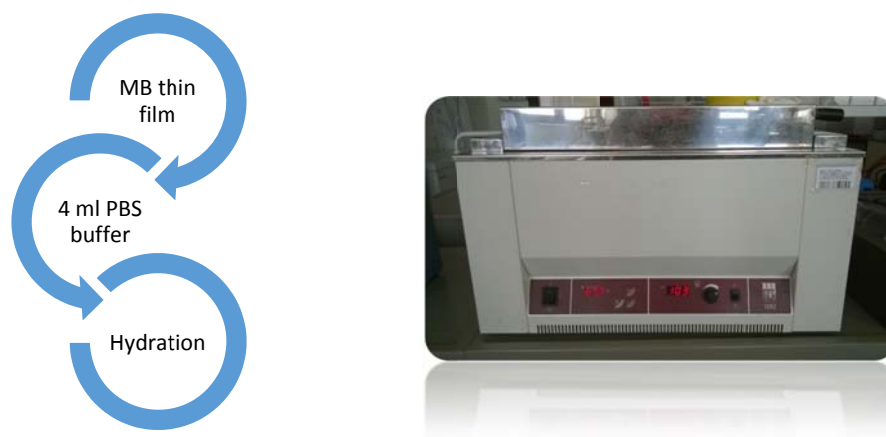
Figure 3. 9. The hydration step of MB thin film.

Microbubbles were produced by sonication method as illustrated in Figure 3. 10. This sonicator is a transducer transforming the electric energy to the mechanical vibration with a piezoelectric crystal. The sonicator has a touch-screen which enables to program the amplitude, pulse time on/off, and energy delivery values, etc. Before the sonication process, the sonicator probe (Misonix Touch-Screen Sonicator-4000 with Probe) was cleaned with ethanol and then with the distilled water. The vial containing the lipid mixture was placed in a plastic bag and added the gas of interest, i.e. perfluorocarbon gas, when other gases were used different than air. The sonicator amplitude was set to 50 kV. The lipid mixture was heated up when the sonicator probe was fully immersed into the lipid suspension, at which the pale white suspension turn into a clear solution. Then, the sonicator probe was moved to the top of the solution, which yielded an intrusion of gas bubbles into the solution making microbubbles in 10-20 s. After sonication, 7 ml cold PBS buffer at +4°C was added into the microbubble suspension to reduce the temperature. Centrifugation at 1750 rpm for 3 min yielded two phases. The bottom phase contained free-lipids and liposomes and were discarded by a needle syringe. The top phase was suspended by about 7 ml of cold PBS+PG buffer at the ratio of 4:1 at +4°C and waited about 15 sec. PG is a viscous and hygroscopic liquid, and it has low toxicity, antibacterial and antifungal properties. [63] Therefore, the larger bubbles were separated by flowing to the top by buoyancy. Then, the microbubbles were obtained from the bottom of the suspension.
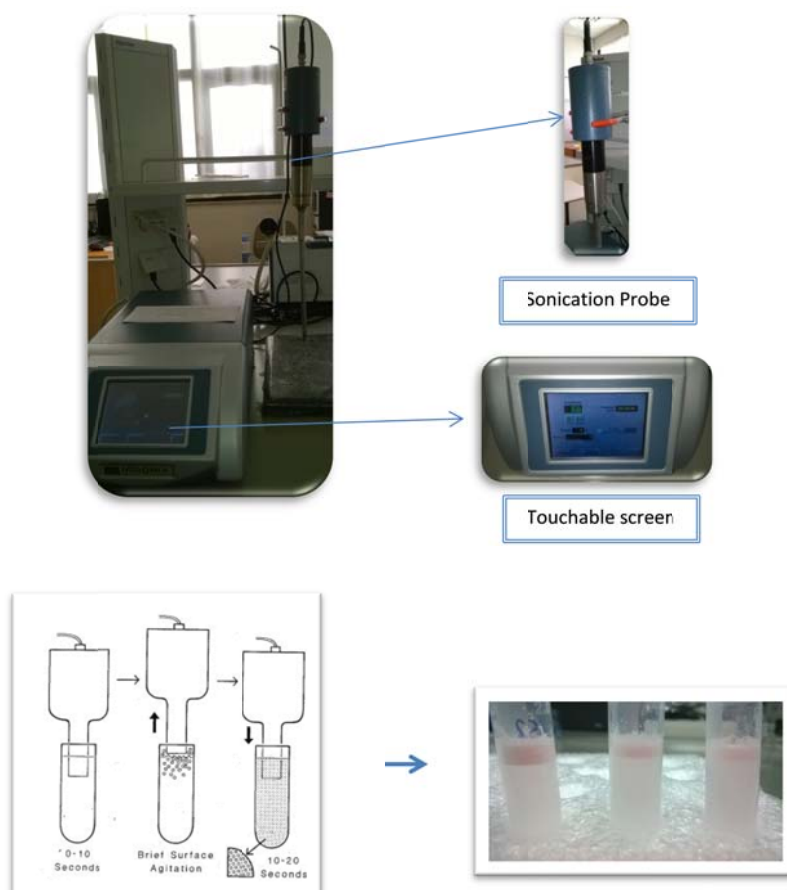
Figure 3. 10. Microbubble formation by the sonication method.[64]

3.2.9. Coupling of Lipo-DOX with Microbubbles

Coupling of lipo-DOX with microbubbles were achieved on microbubbles. Different concentrations of streptavidin solutions were prepared by dissolving streptavidin in ultrapure water and it was diluted at different concentrations. 1 ml of microbubbles was aliquoted in Eppendorf tubes and added 0.1 ml of streptavidin solution each. The attachment of streptavidin to the biotins on the microbubbles was achieved by mixing of the suspension up-and-down for about 30 sec to 60 sec. Then, the unbound streptavidin were separated by centrifugation at 2200 rpm for 2 min. The microbubbles resuspended in a 1 ml of PBS+PG buffer and added 0.2 ml of lipo-DOX. The conjugation was achieved by mixing up-and-down for about 30 sec to 60 sec. Then, the unbound lipo-DOX was separated by centrifugation at 2200 rpm for 2 min. The Microbubble-(Lipo-DOX) conjugate was suspended in a 1 ml of PBS-PG buffer and

visualized by the light and fluorescence microscope and determined for its DOX content.

3.2.10. Characterizations

The size distribution and average size of liposomes were measured by the Dynamic Light Scattering (DLS) method. This method is also known as Photon Correlation Spectroscopy (PCS) or Quasi-Elastic Light Scattering (QELS), and it depends on the Brownian motion of particles, which is based on size, viscosity and temperature using the Stokes-Einstein relationship. The size or hydrodynamic radius (R_H) of particles was determined by Zetasizer Nano Series (ZS, Malvern Instruments) as shown in Figure 3. 11. The random motion of particles is size dependent. The small particles move more rapidly than the larger particles. Also, higher temperatures cause more rapid Brownian motion.[65]Therefore, the size and size distribution of particles were estimated using Malvern Zetasizer with triplicate measurements at room temperature by using disposable cuvettes.
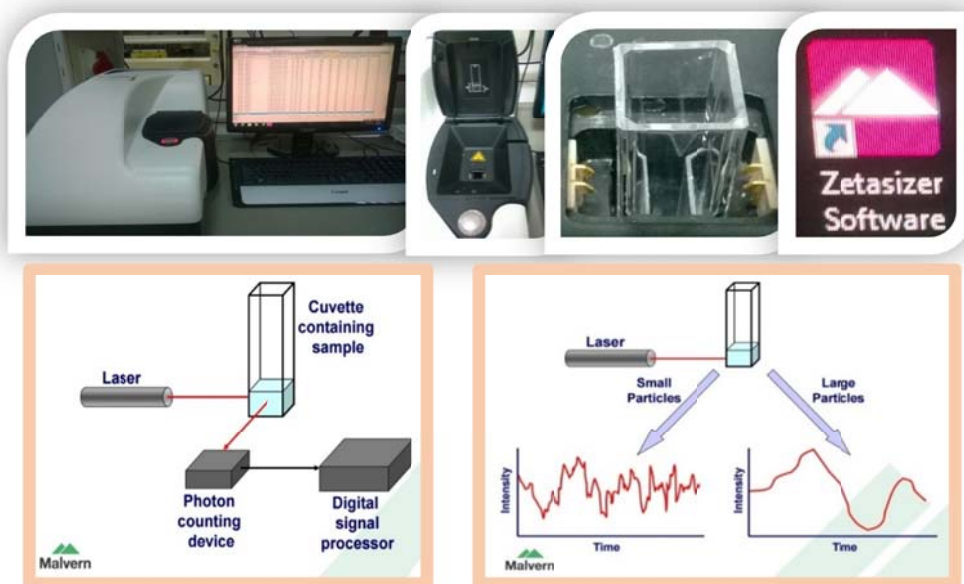
Figure 3. 11. Malvern Zetasizer device and software which were used for the DLS method, DLS instruments (left) and Brownian motion (right).[40]

The concentration of DOX was estimated with the absorbance and fluorescence spectrophotometer (BioTek®, Synergy HTX Multi-Mode Reader) as shown in Figure

3.12. The main principle of spectrophotometer is that the light is passed through the prepared solution at specific wavelength and the transmitted light reaches to the photodetector after passing through the sample in the cuvette. The difference between monochromatic incident light (I_0) and transmitted light (I) gives the amount of absorbance, and this absorbance is calculated with Beer-Lambert law. [66] The absorbance wavelength for DOX was 480 nm and the fluorescence wavelengths were excitation 480 nm and emission 590 nm. It was shown that liposomes scatter light and result in an absorbance reading while they do not have fluorescence property. Therefore, the DOX amount was estimated by the florescence measurements since the florescence intensity is proportional to the concentration.
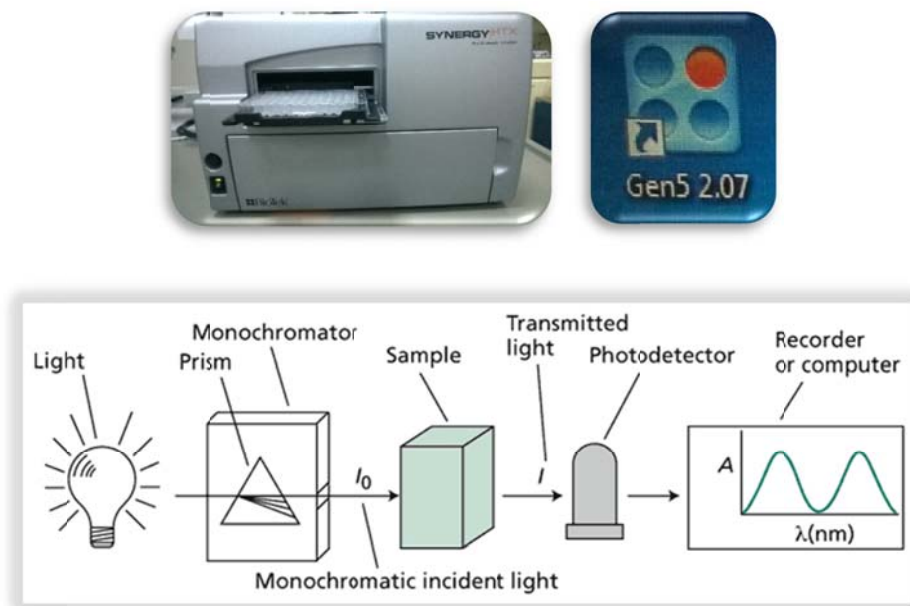
Figure 3.12. The device and software which were used for absorbance and fluorescence detection the principle of spectrophotometer.[66]

The microbubbles and the conjugated lipo-DOX were visualized by light microscopy and florescence microscopy (Carl Zeiss Microscopy, Germany). The microscope's camera was Axiocam 506 Mono (sensor pixel count: 6 megapixel, digitization: 14 bit/pixel, max full well capacity (typical): 15.000 electrons). The microscope has two extra devices. One is Zeiss HXP 120 V unit with 120-watt metal halide bulb (2000+h) which is responsible for the reflected light (Zeiss HXP power in GFP/FITC: 58.3 milliwatts/cm^2). The other device was TempController 2000-2 (PeCon

GmbH, Erbach, Germany) which is responsible for temperature adjustment. The temperature solution is 0.1°C, resolution of internal loop control was 0.01°C, and range for set point values are between 0.0 and 60.0°C. The drug loaded liposomes were visualized by fluorescence microscopy with higher magnification and high resolution. The principle of fluorescence microscopy was shown in Figure 3. 13. DOX absorbs the light as short wavelength of 480 nm and emit light at long wavelengths of 590 nm. The florescence image of DOX was therefore obtained with the fluorescence microscopy by using specific filters for viewing the emitted wavelengths.
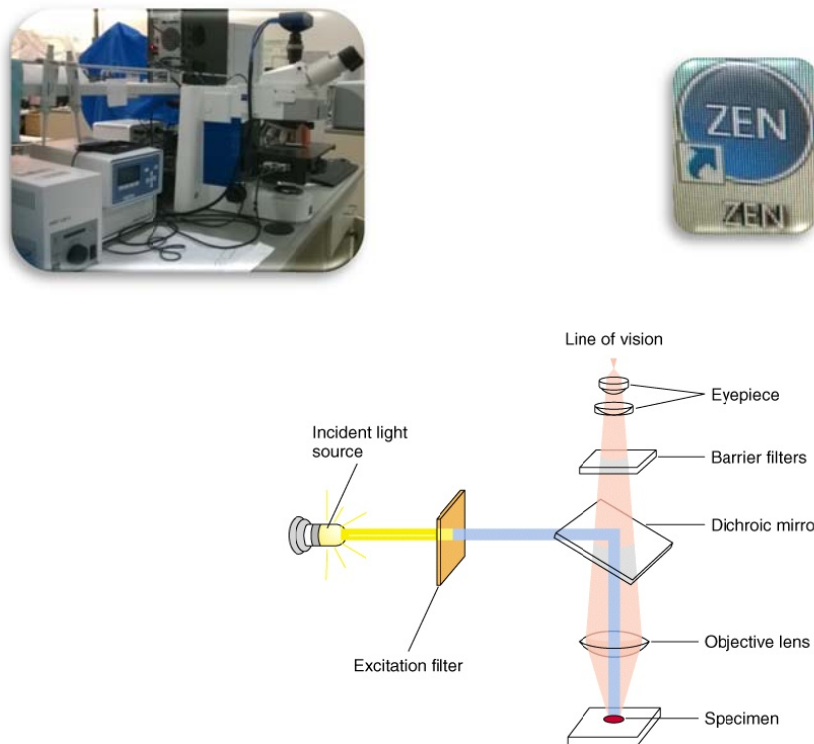
Figure 3. 13. The device and software which were used for imaging the principle of fluorescence microscopes.[64]

The encapsulation efficiency of DOX within liposomes was estimated using Eq.(3. 1).

$$EncapsulationEfficiency(\%) = \frac{F_T}{F_{T_0}} * 100 \qquad (3. 1)$$

where F_{T_0} is the fluorescence intensity value before dialysis, F_T is fluorescence intensity value after dialysis.

The release rate of DOX from the liposomes were estimated by using Eq.(3. 2)

$$Release\ Rate(\%) = \frac{F_T - F_0}{F_{T_{x-100}} - F_0} * 100 \qquad\qquad (3.2)$$

where F_0 is the initial fluorescence intensity value, F_T is the fluorescence intensity value at time t, and $F_{T_{x-100}}$ is the fluorescence intensity after addition of Triton X-100.

CHAPTER 4

RESULTS AND DISCUSSION

4.1. Liposome Production and Characterization

Liposomes were produced by extrusion using polycarbonate membranes with different pore sizes. The pore sizes and distribution of pores on a polycarbonate membrane were shown in Figure 4. 1. As can be seen in the figure, pore sizes are almost even on each size however the pores are not evenly distributed throughout the membranes. Since the pores are extended across the membrane, the larger vesicles were expected pass through these pores and decrease in size at the outlet. Therefore, liposomes with the desired sizes could be obtained by multiple passes through the membrane.
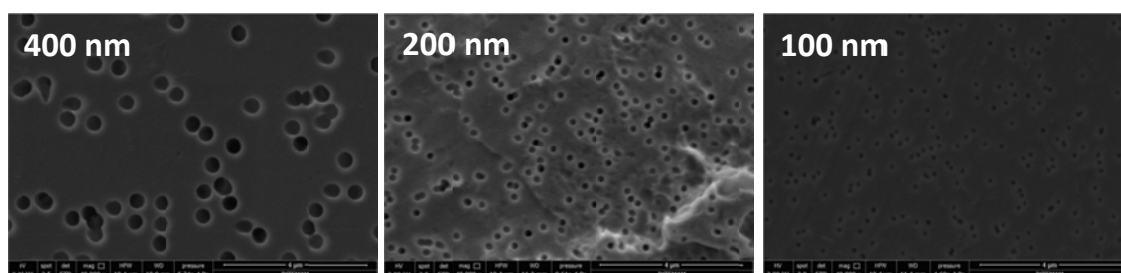
Figure 4. 1. Devices which were used for extrusion polycarbonate membrane sizes.

For drug delivery systems, liposome sizes must be between 150-200 nm.[31, 33] The liposome size distributions before and after the liposome extrusion were measured with the DLS method as shown in Figure 4. 2. There were giant multi-lamellar vesicles (MLV) after hydration and before extrusion with an average size of 3817 nm and small amount of micelles with a size of 42 nm. After the extrusion process with 11 times passage through the membrane, the size distribution reduced to from 90 nm to 330 nm with an average size of about 167 nm. These liposomes therefore became low unilamellar vesicles (LUV) with a bilayer membrane structure.
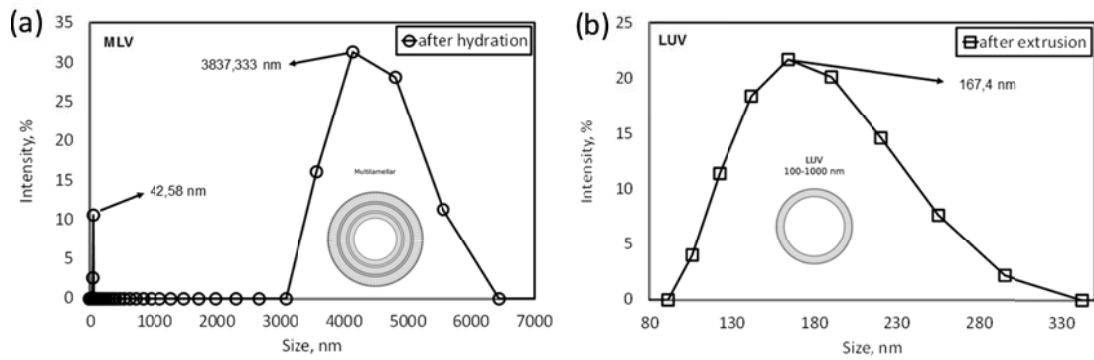
Figure 4. 2. Extrusion process result A. MLV form before extrusion process, B. LUV form after extrusion process.

Figure 4. 3 show the repeatability of the size distribution of the liposomes produced. Although the size distribution is from 90 nm to 300 nm, the difference in size distribution comes from the distribution of the pores on the membrane. It was reported that the smaller and larger liposomes were destroyed by the macrophages in the blood which is called as accelerated blood clearance (ABC). The retention time for 150-200 nm liposomes, smaller than 70 nm and large than 300 nm, was higher in the blood. As a consequence, the size distribution of the liposomes produced was appropriate for the drug delivery.
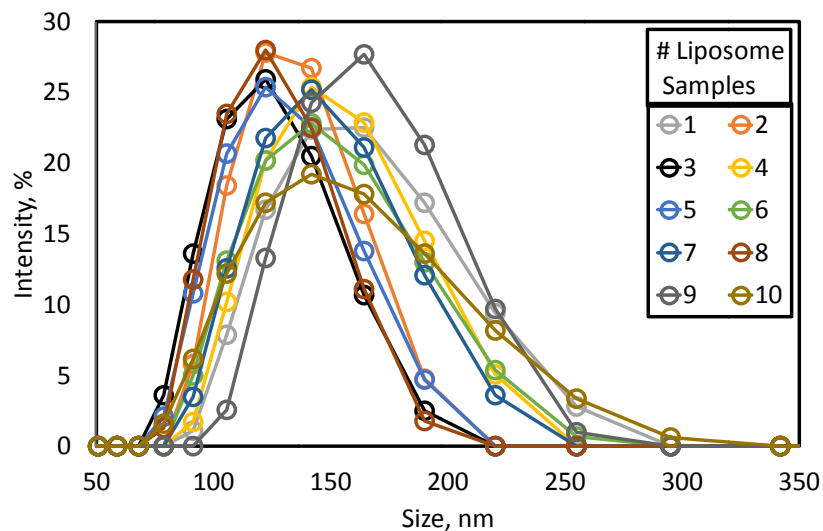
Figure 4. 3. Size distribution A. DLS results for different liposome samples B. 200 nm polycarbonate membrane.

4.2. Effect of Temperature on Liposomes

The temperature effect is a key parameter for drug delivery systems. Temperature affects the bending elasticity modulus of liposome sizes. If the lipids present below the phase transition temperature, then the bending elasticity is two to five times higher. That means that a higher elastic modulus has a more rigid membrane and large liposome size. Also, cholesterol and PEG affect the bending elasticity. The entropy of most materials depends on the temperature, and it is known that the entropy rises with the elevation of temperature. Also, line tension decreases when the temperature increases.[67] On the other hand, leakage is a big problem for drug delivery systems. Leakage affects the shelf-life and encapsulation efficiency of the drug. Temperature is one of the key parameters for leakage. If temperature is above the phase transition temperature of the phospholipid, the drug begins to leak from the liposomes.[68] The phase transition temperature of DSPC is 55°C. It was expected that the leakage is minimal at body temperature at about 37 °C. Here, the effect of temperature on the liposome size was studied.

Samples were withdrawn from the same vial of liposome stored at 4 °C in the fridge and incubated at 25, 37, and 50 °C in a water bath. Samples were taken from each vial at certain time intervals and their size distribution and average sizes were measured by the DLS instrument. As shown in Figure 4.4(a), the size distribution of liposomes measured initially were almost similar, however, as shown in Figure 4.4(b), the size distribution measured after 450 minutes showed a significant variation, where narrower size distribution was observer at higher temperatures and wider size distribution was observed at lower temperatures. Figure 4.4(c) shows the average sizes obtained for each temperature. As can be seen in the figure, the average size increased at 4 °C and decreased at 50 °C in half an hour and did not wary afterwards up to 1200 minutes or 20 hours. Compared to the average size of about 190 nm of the liposomes at 25 °C, as shown in Figure 4.4(d), the average size of liposomes increased by 10% at 4 °C and shrank approximately 15% at 50 °C. It was understood that the average size of liposomes increases approximately 10% when stored at 4 °C in the refrigerator and their sizes shrink by 25% when they were injected in the body at 37 °C.
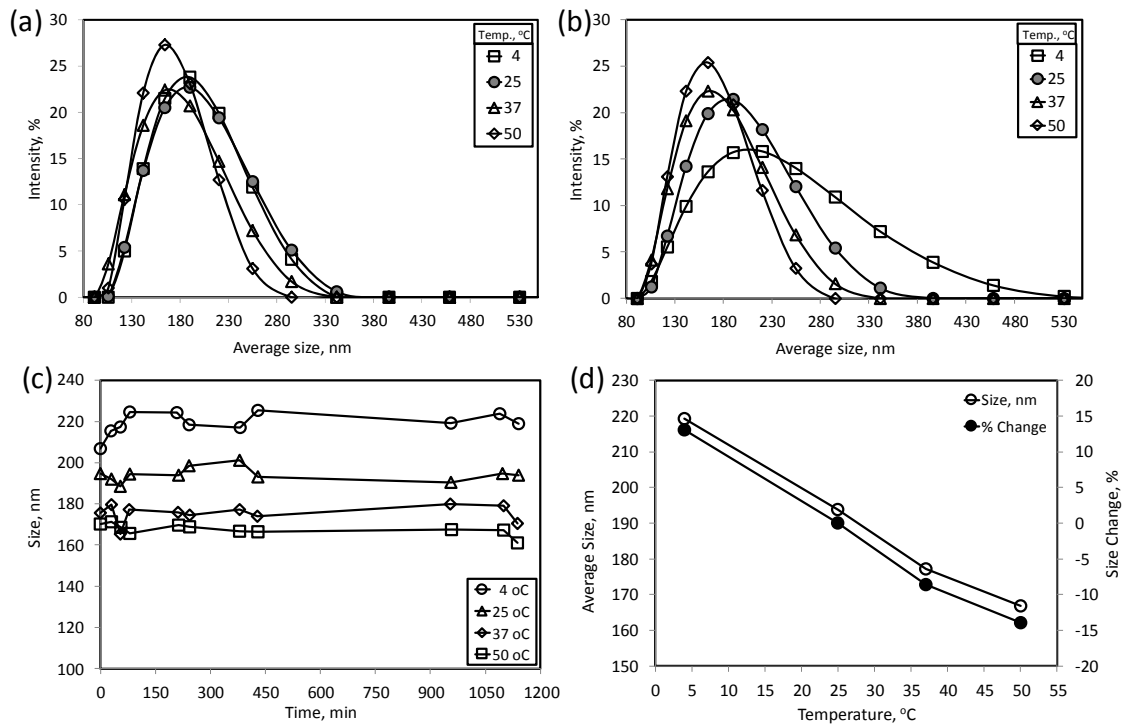
Figure 4.4. Liposome temperature experiment results in the different liposomes A. Size changes according to the different temperatures, B. The proportion of size changes between different temperatures, C. Size distribution changes at initial time (t=0) according to the temperature, D. Size distribution changes at time 450 minutes according to the temperature.

An additional experiment was conducted to observe the volumetric behavior of liposomes at different temperatures. In this case, a liposome solution taken from the refrigerator at 4 ^{o}C was placed in a water bath where its temperature was set to the desired value, i.e. 4 ^{o}C initially. The size distribution and average size were estimated after equilibration. Then, the temperature increased to a higher level and the size distribution and average size of the liposome sample were estimated. After 50 ^{o}C, the same procedure was applied when the set-temperature was decreased. As shown in Figure 4. 5, the average size of the liposomes decreases as the temperature increases. As shown in the figure, compared to the room temperature of 25 ^{o}C, the average size of the liposomes stored in refrigerator at 4 ^{o}C increased approximately 2%, and shrank approximately 6% when their temperature reached to the body temperature of 37 ^{o}C. It was also shown in the figure that this process is reversible.
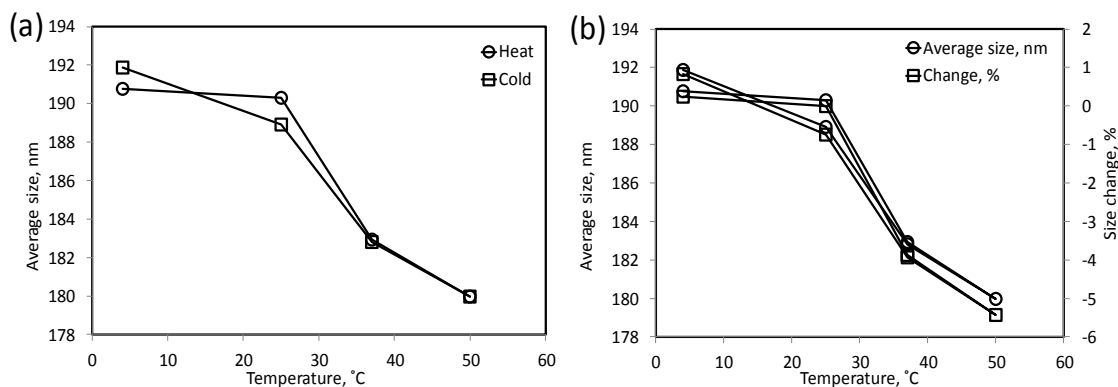
Figure 4. 5. Liposome temperature results for the same liposome. A. Size changes according to the heat and cold processes, B. The proportion of size changes according to the heat and cold processes.

4.3. Liposome Destruction by Triton X-100

Triton X-100 (T_{x-100}) is a detergent and it has been used to destruct the liposomes in order to estimate their drug loading. The working wavelengths for DOX are 480 nm for the absorbance measurement and 480 nm and 590 nm for the excitation and emission wavelengths in the fluorescence measurements, respectively. The absorbance and florescence values were shown in Figure 4. 6(a) and Figure 4. 6(b), respectively, for the lipid amount of the liposomes and different concentrations of T_{x-100}. As shown in Figure 4. 6(a), the absorbance values are linearly proportional to the lipid concentrations of the liposomes, due to probably the light scattering of liposomes in the suspension. There is no florescence intensity detected in the liposome suspension other than the background. As shown in Figure 4. 6(b), T_{x-100} did not absorb nor emit florescence intensity at the specified wavelengths. Because the lipid or the liposomes give an absorbance value, florescence intensity measurements needed to be done in order to quantify the DOX amount in the presence of lipids and/or T_{x-100}.
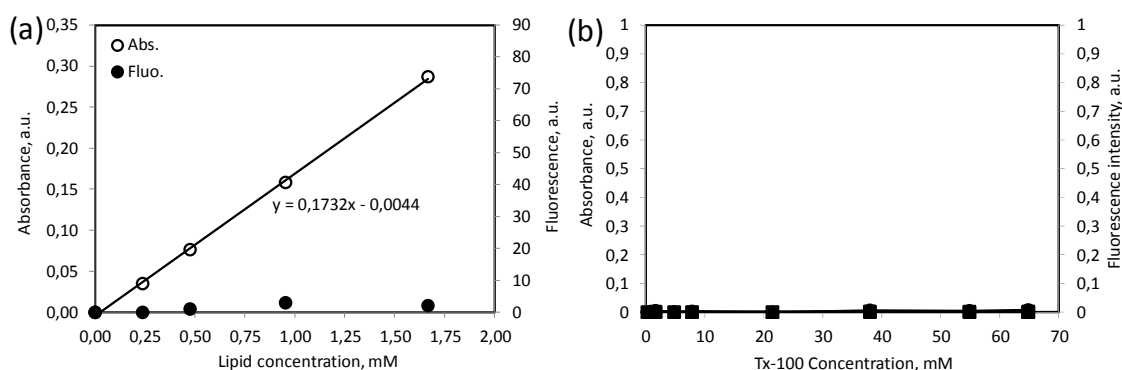
Figure 4. 6. The absorbance and fluorescence values A) the amount of used up lipids during the preparation of liposomes B) T_{x-100}.

The average size and count rate were measured for pure T_{x-100} by the DLS method as shown in Figure 4.7(a) and Figure 4.7(b). The critical micelle concentration (CMC) for T_{x-100} was reported to be between 0.2 and 0.9 mM depending on temperature and it is about 0.24 mM. T_{x-100} exists in monomer form below its CMC and in micelle form above its CMC.[45] In addition, the micelle size for T_{x-100} was reported to be approximately 5 nm.[44] However, the micelle size and shape would vary with the type, size, and stereochemistry of monomer of different surfactants.[42] As shown in Figure 4.7(a), the average size for T_{x-100} was measured to be about 8 nm at lower concentrations and increased slightly to 10 nm as the concentration of T_{x-100} was increased. The increase in intensity up to 50 mM of T_{x-100} shows the number of micelles increases as the concentration of T_{x-100} increased. As shown in Figure 4.7(b), the average count rate is also increased as the micelle size was increased. In all cases, the micelle size of T_{x-100} is about 10 nm and it did not change as its concentration increased.
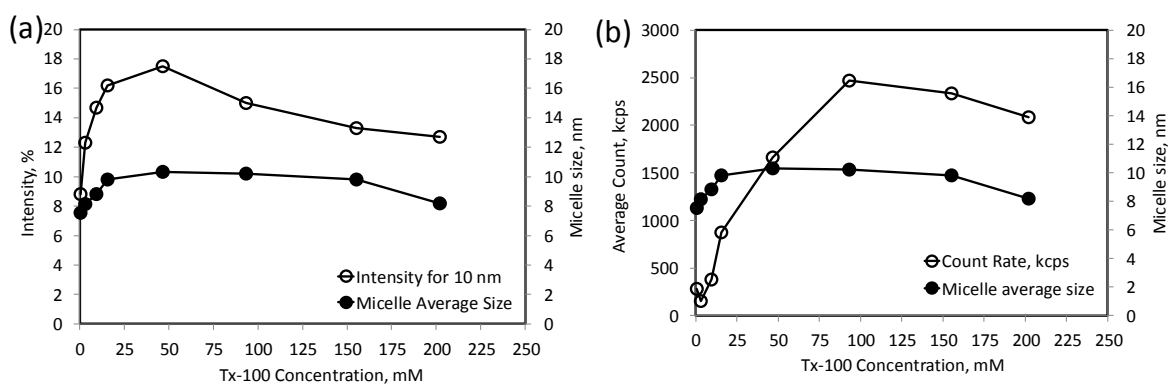
Figure 4.7. The change in (a) average micelle size and DLS intensity, and (b) average micelle size and count rate with T_{x-100} concentration.

The DLS count rate was found to be liposome dependent. As shown in Figure 4.8, the DLS count rate was measured in the presence of different amounts of liposome and T_{x-100}. When only T_{x-100} was present in the solution, the count rate increased slightly, but its value is the lowest as shown in the figure as diamonds. When constant amount of 0.14 mM and 0.98 mM of lipids were included and different amount of T_{x-100} was added, the count rate was higher and did not change at constant temperature as shown in figure as closed circle and square markers. When the amount of lipid was varied, the count rate was also varied. In other words, when the amount of lipid increased, the count rate was also increased as shown in the figure as open circles. When T_{x-100} amount was increased above its CMC, while the monomer concentration was constant, the number of micelles increased.[41, 43] It seems that the count rate is directly related to the number of liposomes which obviously scatter the light. It was understood that the DLS count rate is depended on the number of liposome or the lipid concentration.
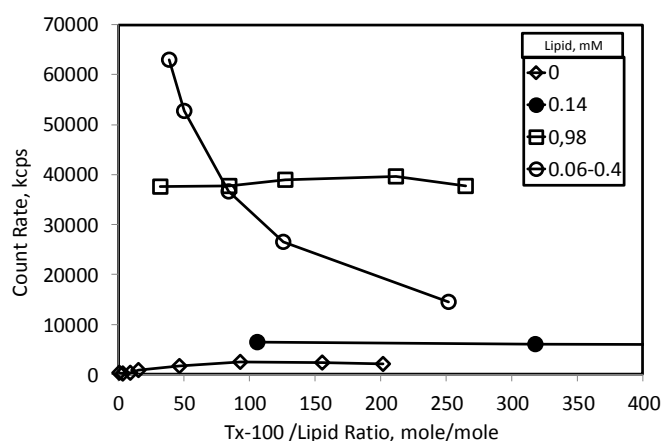
Figure 4.8. DLS count rate in the presence of different amounts of liposome and T_{x-100}.

In order to understand the liposome lyses upon T_{x-100} addition, changes in the size distribution and absorbance were investigated. T_{x-100} was added to a liposome suspension and size distribution was estimated by the DLS and absorbance values were measured by the UV spectrophotometer. As shown in Figure 4.9(a), the average size of the liposomes increased with the addition of T_{x-100}. The average diameter for the liposomes was initially 190 nm and it increased to about 250 nm when the T_{x-100} was added. It seems that T_{x-100} penetrated between the lipids of the liposome membrane and thereby enlarged the size of the liposomes. Figure 4.9(b) shows the absorbance values

measured at each addition of T_{x-100} to the liposome suspension. As shown in the figure, the absorbance value did not change up to T_{x-100}/Lipid ratio of 65 mole/mole after which the absorbance value increased significantly up to T_{x-100}/Lipid ratio of 95 mole/mole and then started to decrease. According to the literature, detergent-lipid interactions occur in three stages.[47] In the first stage, detergent diffuse into the lipid layer of the outer surface of the liposomes, which result in increase the size of the liposomes. In the second stage, the bilayer of the liposomes disintegrates. And, in the third stage, the liposomes are broken down into mixed micelles. As shown in Figure 4.9(a) and Figure 4.9(b), as T_{x-100} was added to the liposome suspension, they penetrated into the lipid outer membrane of the liposomes, their sizes increased, therefore, more light scattered as higher absorbance values observed. Micelles were observed for the first time, as shown in Figure 4.9(c), when the T_{x-100}/Lipid ratio was 212 mole/mole. The sizes of the micelles were about 10 nm indicating that, as shown in Figure 4.9(d), the first stage in liposome lysis was completed and destruction of liposomes has started as more T_{x-100} was added to the liposome suspension. The T_{x-100}/Lipid ratio needed for a complete destruction of liposomes was about 3178 mole/mole and, as shown in Figure 4.9(e), the average size for the liposomes increased considerably and finally destructed.
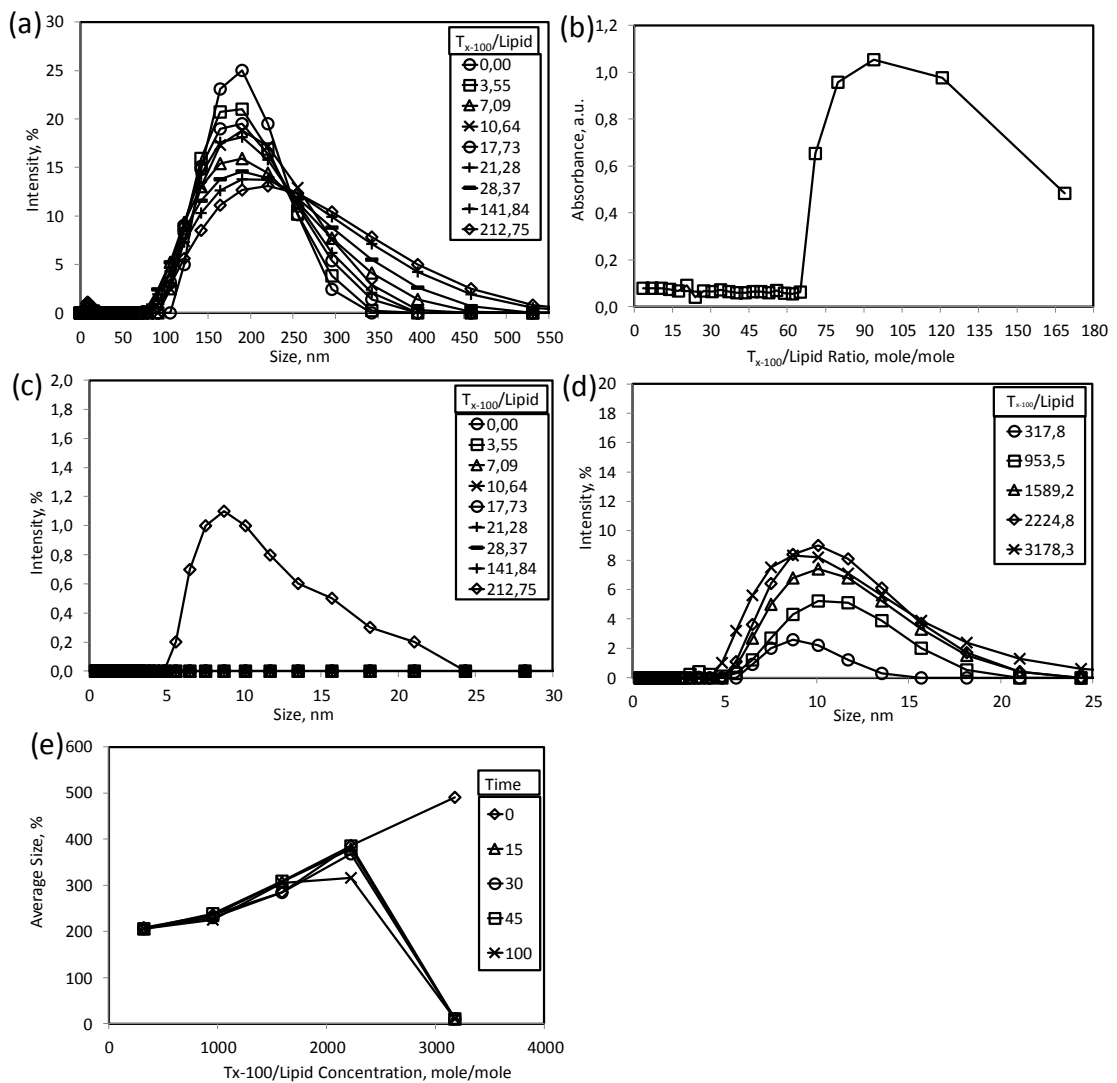
Figure 4.9. Lyses of liposomes by addition of T_{x-100}, (a) size distribution,(b)changes in absorbance by UV spectroscopy, (c) critical concentration for micelle formation,(d) micelle size by T_{x-100}, (e) total disruption of liposomes.

The effect of cholesterol content on liposome destruction by T_{x-100} was investigated and it was shown in Figure 4.10. As shown in the figure, the average liposome size did not change significantly up to T_{x-100}/Lipid ratio of 1000 mole/mole and a sudden decrease in the sizes were observed at different cholesterol contents. Cholesterol provides flexibility in the lipid membranes by its flip-flop motions due to hydrophilic and hydrophobic nature. In overall, cholesterol did not affect significantly the destruction property of liposomes by the T_{x-100}.
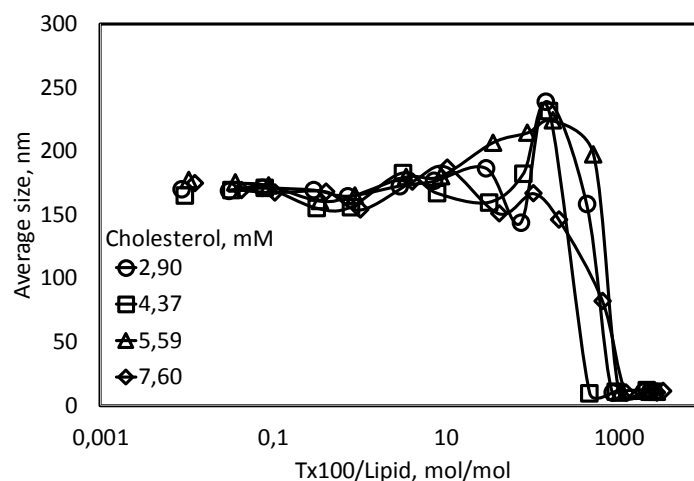
Figure 4.10. Effect of cholesterol on liposome destruction by T_{x-100}.

4.4. Calibration Curve for Doxorubicin

Doxorubicin hydrochloride (DOX-HCl) is an antitumor agent chosen for a model anticancer drug. The absorbance scan and florescence emission scan were conducted to estimate optimum wavelengths for DOX. For this purpose, PBS buffer were prepared at different pH values from pH 5 to 8. Powder DOX was dissolved in ultrapure water, added into each PBS buffer, and scanned for the optimum absorbance and floresence emission wavelegths. As shown in Figure 4.11, the optimum absorbance wavelength for DOX was 480 nm and the excitation wavelength was 480 nm and the emission wavelength was560-590 nm, which are consistent with the literature.[69] As shown in the figure, the absorbance and fluorescence intensities were not affected by the pH between 5 and 8. Because DOX has 3 pKa values, due to quinone characteristic, which are all higher than 8, the pH between 5 and 8 did not affect the absorbance and florescence intensities.[27] Consequently, $[(NH_4)_2SO_4]$ buffer (pH=5.4) and PBS buffer (pH=7.2) were used confidently in the experiments without changing the absorbance and fluorescence excitation/emission values for DOX.
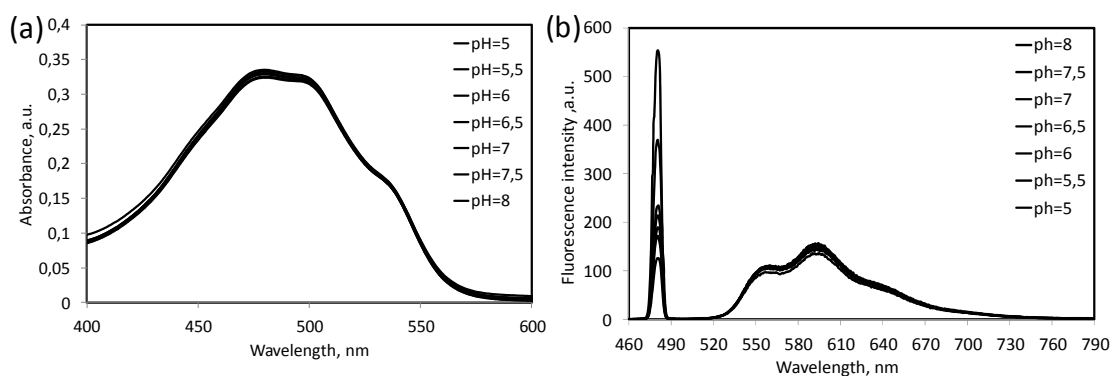
Figure 4.11. Absorbance and fluorescence intensity values for DOX at different pH.

Calibration curves were generated for DOX in order to determine its concentration in the solutions and in the liposomes. 1 mg/ml of DOX solution was prepared in ultra-pure water and diluted to different concentrations. The absorbance at 480 nm and florescence intensities at excitation 480 nm and emission 590 nm were measured and shown in Figure 4.12. As shown in the figures, the absorbance intensity linearly related to the DOX concentration. However, as shown in Figure 4.12(a), the fluorescence intensity values increases linearly at low concentrations and, after a peak value at about 0.1 mg/ml of DOX concentration, decreases as the concentration of DOX further increases. The decrease in florescence intensity was attributed to the aggregation of DOX and therefore quenching the fluorescence intensity at higher concentrations. As shown in Figure 4.12(b), the florescence intensity is still not linear up to 0.045 mg/ml of DOX concentration. As shown in Figure 4.12(c), the linear relationship between the florescence intensity and DOX concentration could be achieved when the DOX concentration was less than 0.012 mg/ml. The solubility of DOX was given as 10^{-5} M (5.79 μg/ml) [2, 28] and the florescence intensity is linearly related to the DOX concentration in these ranges. In our plate reader, the linear relationship could be achieved when the DOX concentration was less than 12 μg/ml, at which the florescence intensity was less than 80 a.u.. It was understood that when higher concentrations of DOX were studied in the experiments, they need to be diluted so that the DOX concentration can be estimated in the linear range.
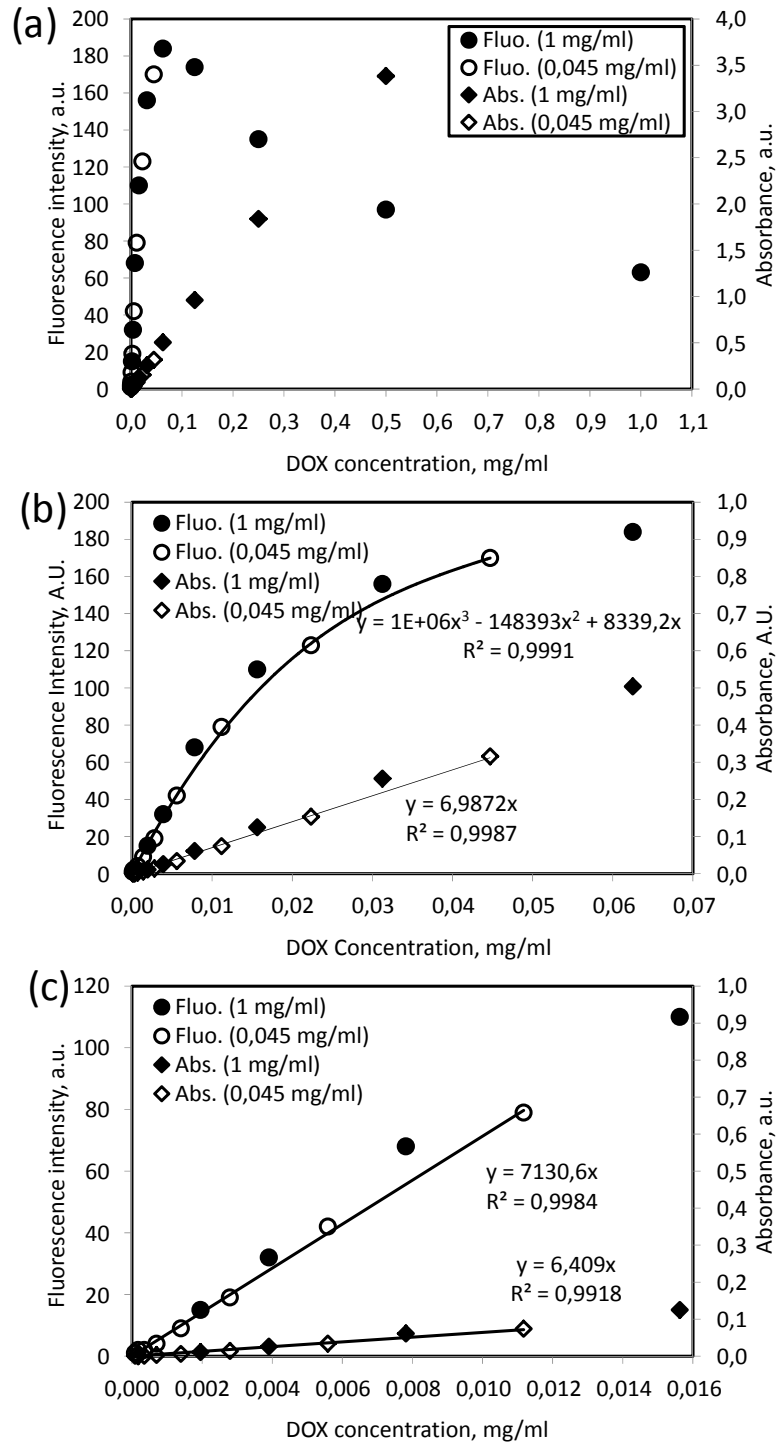
Figure 4.12. Absorbance and florescence calibration curves for DOX. (a) DOX concentration up to 1.0 mg/ml, (b) DOX concentration up to 0.045 mg/ml,(c) DOX concentration up to 0.012 mg/ml.

4.5. DOX Loading within Liposomes

DOX was loaded within liposomes as defined in the experimental methods. The size distributions of liposomes before and after DOX loading were shown in Figure 4.13(a). As shown in the figure, the size distribution of the liposomes is smaller than the DOX loaded liposomes. For instance, the average size of liposomes was 157 nm before the DOX loading and it was 183 nm after the DOX loading. This observation is consistent with 3 different DOX loadings. As shown in Figure 4.13(b), the colors of the DOX were also shown before and after loading within the liposomes. As shown from the images, the color of DOX before loading more likely in a red color while the loaded DOX is a more likely to be a purple color.
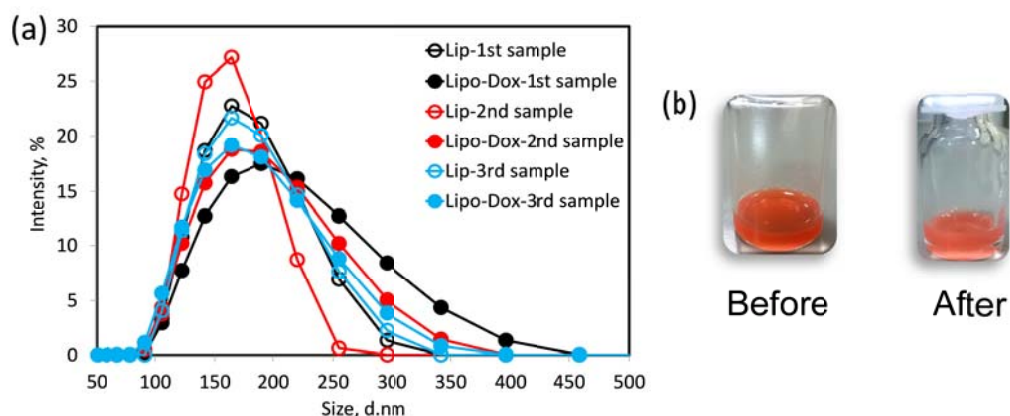
Figure 4.13. (a) Size distribution and (b) color change of liposomes before and after the DOX loading.

4.6. Separation of free-DOX from the Lipo-DOX

The free-DOX need to be separated from the lipo-DOX in order to analyze the amount of DOX loaded within the liposomes. There are basically two methods to separate the free-DOX. One is the column chromatography and the other is membrane dialysis. The column used in column chromatography was filled with pre-soaked Sephadex porous polymeric beads. The column initially washed by passing PBS buffer. When the buffer level was reached to the surface, approximately 1 ml of sample was added on the top of the column and let it drain. Fresh PBS was added on the top of the column when the liquid level of the sample decreased to the surface of the column. 20

drops, about 1 ml, of aliquots were collected from the elution. The liposomes were detected as the count rate in DLS measurements and the free-DOX and loaded-DOX were estimated from the florescence measurements. Figure 4.14 shows the fluorescence intensity values and photon count rate values measured by florescence spectroscopy and DLS methods, respectively at different column heights. Length and diameter (L/D) is deterministic character for column chromatography technique, and the good result occurs at the higher column heights.[70] As shown in the figures, the liposomes eluted from the column in the first 7 to 10 ml as indicated from the DLS count rates. The elution volume peak for the free-DOX was separated from the liposome peaks as the column height was increased. The column L/D ratioof0.77 was satisfactory for the separation of free-DOX from the lipo-DOX. However, the lipo-DOX was highly diluted in the column chromatography method.
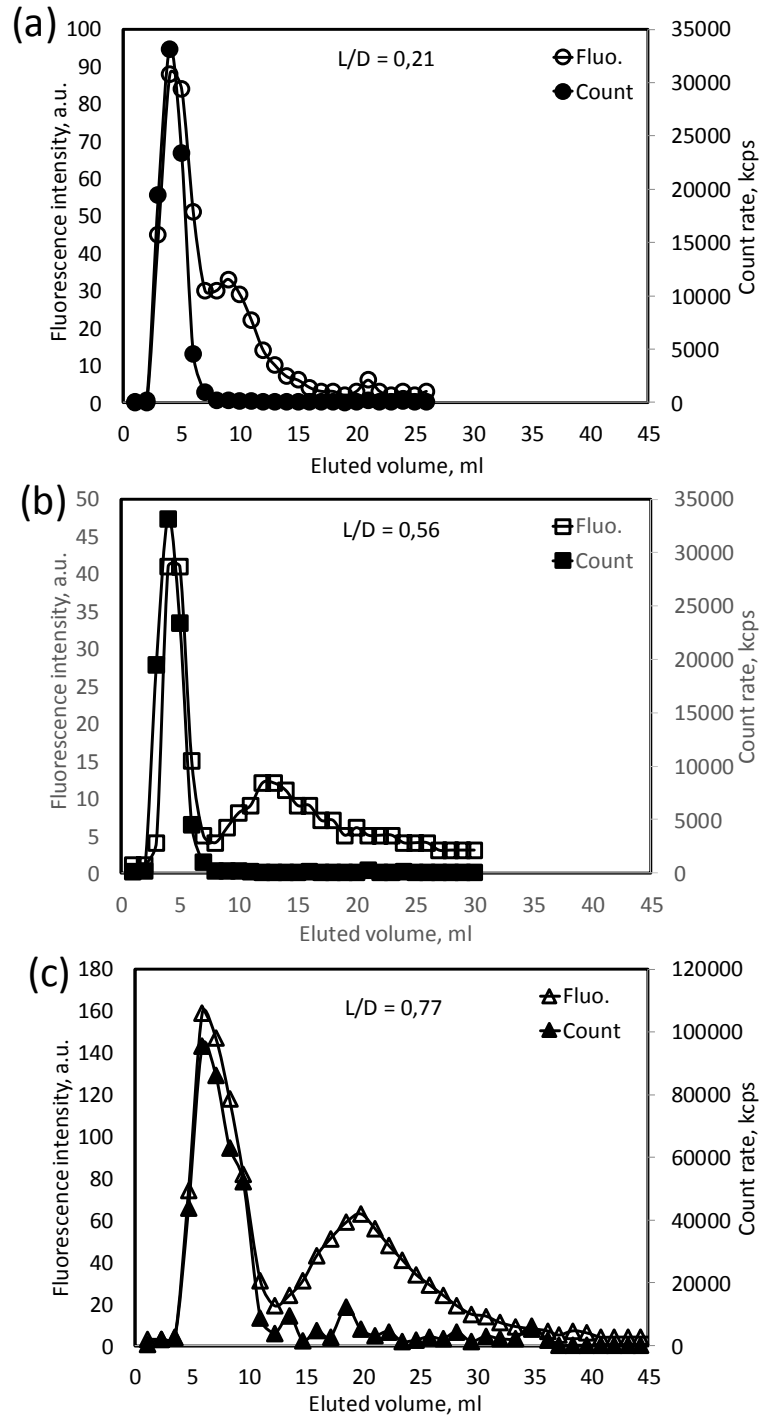
Figure 4.14. The fluorescence intensity values and photon count rate values measured by florescence spectroscopy and DLS methods, respectively at different column heights. (a) 3 cm, (b) 8 cm and (c) 11 cm.

The free-DOX can also be separated by using the membrane dialysis method as shown in Figure 4.15. In the membrane dialysis method, a membrane was used to molecular weight cut-off (MWCO) of 10K which was enough to separate the free-DOX and retain the liposomes. Because the dialysis was conducted against 0.9% NaCl

solution in order to balance the osmatic pressure, minimal liquid volume change was observed preserving the lipo-DOX volume. Therefore, the separation method was selected herein as the membrane dialysis method for the subsequent studies.
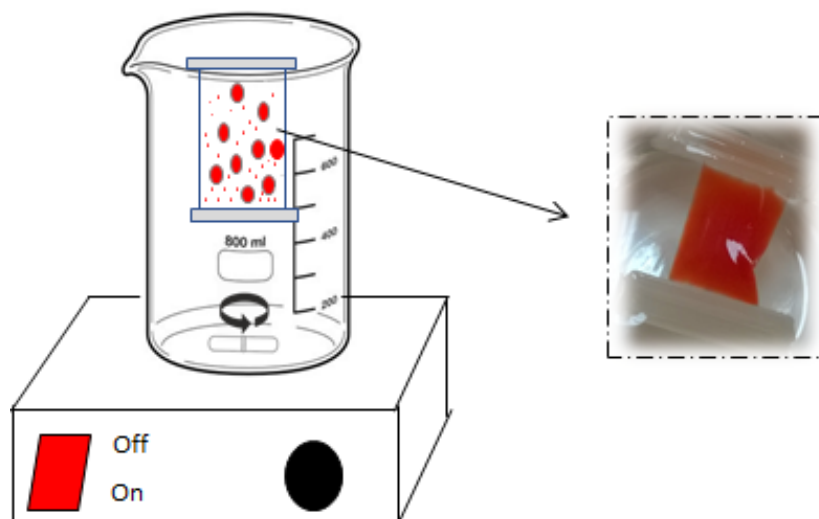
Figure 4.15. Separation of free-DOX from lipo-DOX by membrane dialysis method.

4.7. Percent DOX Release from Liposomes

Release of DOX from the liposomes was studied. Different concentrations of DOX loaded liposomes were prepared by diluting different amount of lipo-DOX in PBS buffer and measured the absorbance and fluorescence intensities at the room temperature as shown in Figure 4.16. As shown in the figure, after 30 min, the absorbance and florescence values did not change while the florescence intensity increased significantly upon addition of T_{x-100} indicating that there is no DOX release from liposomes at room temperature.
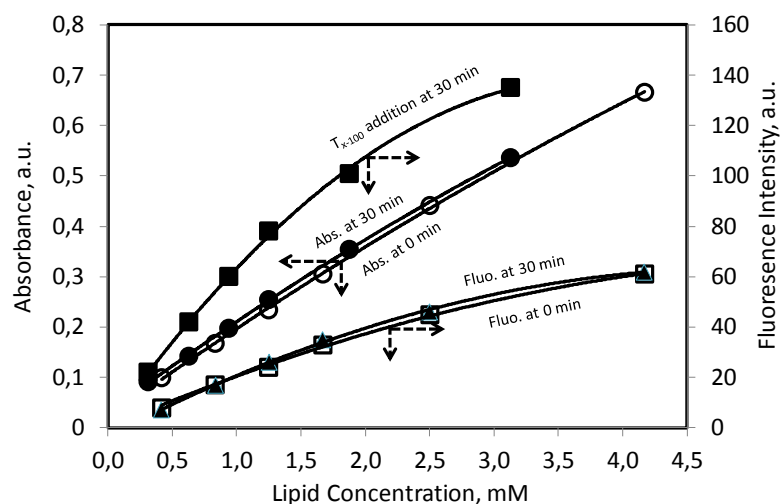
Figure 4.16. DOX release measurements from different concentrations of DOX-loaded liposomes.

Percent DOX release from the liposomes was also studied at different temperatures. Figure 4.17(a) shows percent DOX release by time at different temperatures. As shown in the figure, the DOX release was completed in the first 60 minutes and did not change afterwards indicating that the DOX release is due to the volumetric changes occurring on the liposomes during temperature deviations. As shown in Figure 4.17(b), the DOX release was temperature dependent; almost no release at room temperature, about 10% at body temperature, and about 25% at the transition temperature of DSPC at 55 ^{o}C, and about 45% at 70 ^{o}C. It seems that DSPC liposomes are so rigid in structure that there is limited amount of release from the liposomes due most probably to the volumetric changes of the liposomes.
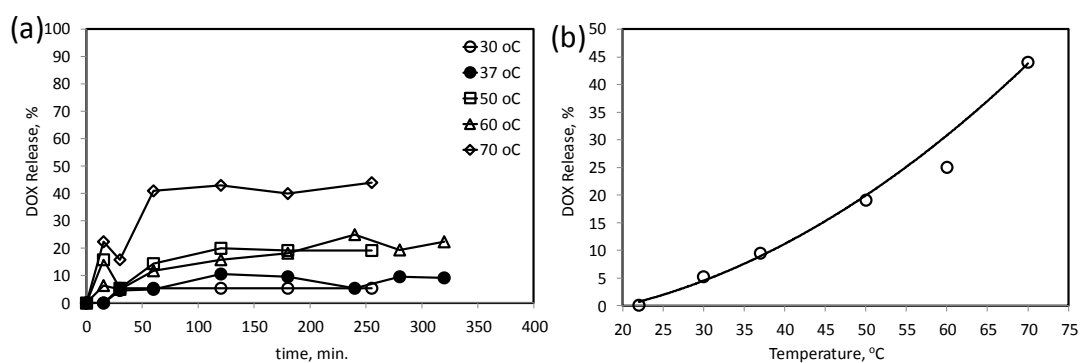
Figure 4.17. (a) Percent DOX release from liposomes at different temperatures by time, (b) Percent DOX release at different temperatures.

4.7. Quantification of DOX

DOX amounts loaded within the liposomes were determined by the florescence method. The free-DOX was initially removed by dialysis and the lipo-DOX was stored in a vial as the stock lipo-DOX suspension. Different volumes of samples from the stock suspension were diluted in DI water and added T_{x-100} to disrupt the liposomes. Then, the DOX amount was determined by the fluorescence intensity measurements. If the DOX concentration of stock suspension is C_T, the sample volume taken is V_i, the final volume of dilution is V_1, and the concentration of diluted solution is C_1 which is the one estimated from the florescence measurement, then the DOX concentration in the stock suspension can be determined from the mass balance as

$$C_T = \left(\frac{V_1}{V_i}\right) C_1 \qquad (4.1)$$

or

$$C_T = (DF_i)^{-1} C_1 \qquad (4.2)$$

where, DF_i is the dilution factor

$$DF_i = \left(\frac{V_i}{V_1}\right) \qquad (4.3)$$

Also, each dilution may be further diluted and its concentration C_n is estimated, therefore, the total DOX concentration can be calculated similarly as

$$C_T = (DF_n)^{-1} C_n \qquad (4.4)$$

where, DF_n is the multiplication of each individual dilution factors

$$DF_n = \prod_{i=1}^{n} DF_i \qquad (4.5)$$

The estimated concentrations of DOX in the lipo-DOX stock suspension at different dilutions and subsequent dilutions were shown in Figure 4.18. As seen in this figure, the amount of the DOX determined in the stock suspension was different for each sample and each dilution. The total amounts of DOX diluted in each sample were not constant and increased exponentially. In order to understand the factors that affect the estimation of the right amount of DOX in the stock lipo-DOX suspension, different parameters involved in the amount of DOX measurements were studied systematically.
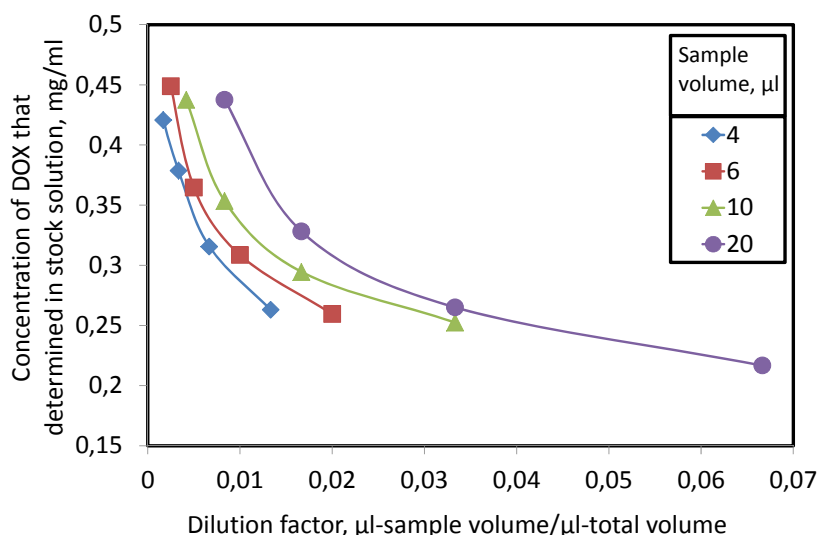
Figure 4.18. The estimated concentrations of DOX in the lipo-DOX stock suspension at different dilutions and subsequent dilutions.

In determination of DOX concentration from the lipo-DOX suspensions, phosphate-buffered saline (PBS) was used as a buffer. Triton X-100 (T_{x-100}) was used to disrupt the liposomes to release the DOX from their interior. The number of liposomes and therefore the amount of lipids would be another parameter in DOX concentration estimation. Finally, ammonium sulphate ((NH_3)$_2SO_4$) was used as buffer inside the liposomes and it could affect the estimation of DOX. Therefore, the main parameters selected to investigate were different concentration of PBS solution, T_{x-100}, lipid (liposome), and (NH_3)$_2SO_4$, respectively.

Figure 4.19 shows the effect of PBS on the florescence intensity of DOX at two concentrations. The low concentration of DOX was 2.68 µg/ml and it was in the linear region of the DOX calibration curve. The high concentration of DOX was 66.8 µg/ml and it was in the non-linear region and almost at the curvature part of the DOX calibration curve. Initially, 50 mM of PBS solution was prepared and diluted in half to lower concentrations. Then, the same volumes of of free-DOX solutions were added to each PBS solutions. As shown in Figure 4.19(a), the absorbance and florescence values did not change significantly at low free-DOX concentration. On the other hand, as shown in Figure 4.19(b), the absorbance and florescence values both decreased exponentially at high free-DOX concentration indicating that the DOX molecules interact with the PBS molecules especially charged form of monovalent (HPO_4^-) and bivalent ($PO_4^=$) phosphate groups.
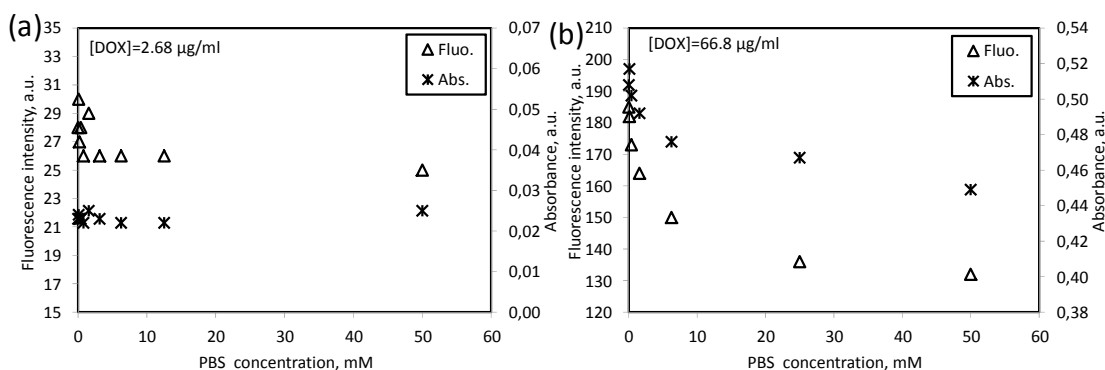
Figure 4.19. The absorbance and fluorescence intensity values of (a) 2.68 µg/ml and (b) 66.8 µg/ml of free-DOX in PBS solutions.

The effect of T_{x-100} on free-DOX florescence intensity was investigated. T_{x-100} solution of 259 mM was prepared and diluted in half with ultra-pure water. Then, two different concentrations of free-DOX solutions were added into each solution and their absorbance and fluorescence intensity values were measured. Figure 4.20 shows a significant effect of T_{x-100} on the absorbance and florescence intensity measurements. As shown in Figure 4.20(a), the absorbance value did not change while the fluorescence intensity decreased exponentially at low free-DOX concentration. The CMC for T_{x-100} is 0.24 mM [36] and T_{x-100} is generally in micelle form above its CMC. It seems that free-DOX molecules diffused into and trapped by the micelles. Therefore, the concentration of DOX increased within the micelles and the fluorescence intensity decreased because of the quenching effect. At higher free-DOX concentration, as shown in Figure 4.20(b), both the absorbance and fluorescence intensities changed. A shown in the figure, there is a significant loss in absorbance intensity decreasing exponentially, indicating that the concentration of DOX decreased along the light path during the absorbance measurements. The fluorescence intensity first increased and the decreased after a maximum as the concentration of T_{x-100} increased. It was understood from the calibration curve of DOX that the fluorescence intensity of free-DOX decreases due to the quenching effect when the concentration of free DOX was 66.8 µg/ml. Due to the fact that when the free-DOX concentration decreased in the solution due to the trapment of DOX within the T_{x-100} micelles, a positive effect was seen in the fluorescence intensity. Further increasing the T_{x-100} concentration resulted in decreasing the fluorescence intensity value due to the quenching effect of the concentrated DOX within the micelles. It was understood that the T_{x-100} concentration is an important factor in estimating the free-DOX concentration in solution.

Figure 4.20. The absorbance and fluorescence intensity values of (a) 2.68 µg/ml and (b) 66.8 µg/ml of free-DOX in different concentrations of T_{x-100} solutions.

The effect of liposomes on the measurement of absorbance and fluorescence intensity values for the free-DOX was investigated. Because the number of liposomes could not be counted, initial lipid concentrations from which liposomes were prepared were accounted for the dilutions of liposomes. The absorbance and florescence intensity values for two set of liposome suspensions at half dilutions each were measured before addition of free-DOX. The florescence intensity values were zero or negligible for different concentrations of liposomes (data not shown). On the other hand, as shown in Figure 4.21, the absorbance is linearly proportional to the liposome or lipid concentrations.
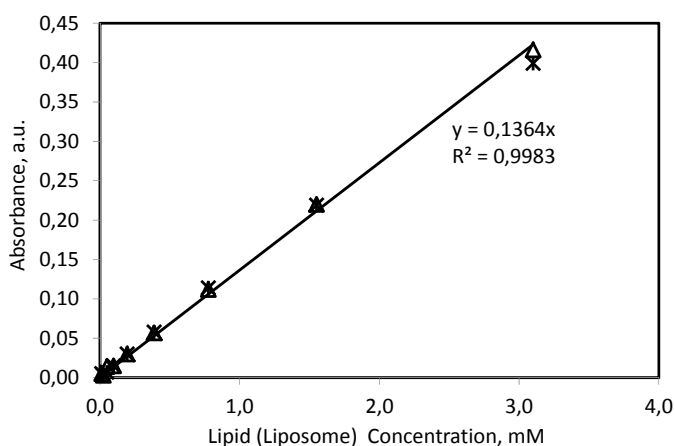
Figure 4.21. The absorbance values for liposomes as lipids at different concentrations.

The absorbance and fluorescence intensity values for free-DOX at concentrations of 2.68 µg/ml and 66.8 µg/ml were measured in the presence of different concentrations of lipid (liposome) suspensions. In order to adjust the required

concentrations, constant volume of free-DOX were added into each liposome solutions. In order to make a background correction, the absorbance value is need to know for the liposome samples. The measurement of the liposome number is practically not possible. Therefore, the measured absorbance values for DOX were subtracted from the absorbance values initially measured for liposomes. Figure 4.22 shows the absorbance and fluorescence intensity values for the two DOX concentrations in different liposome suspensions. As shown in the figures, the absorbance values for the two different DOX concentrations were almost the same whereas the florescence intensity increased as the lipid concentration increased. A steady increase was seen at low DOX concentration as shown in Figure 4.22(a) and a sudden increase has occurred at high DOX concentration and continued to increase with the liposome concentrations as shown in Figure 4.22(b). It seems that the DOX molecules adsorbed on the liposomes and their fluorescence quantum efficiency, which is the florescence intensity per absorbed light, has increased. Therefore, an increase was observed for the free-DOX samples as the amount of liposomes was increased in the solution.
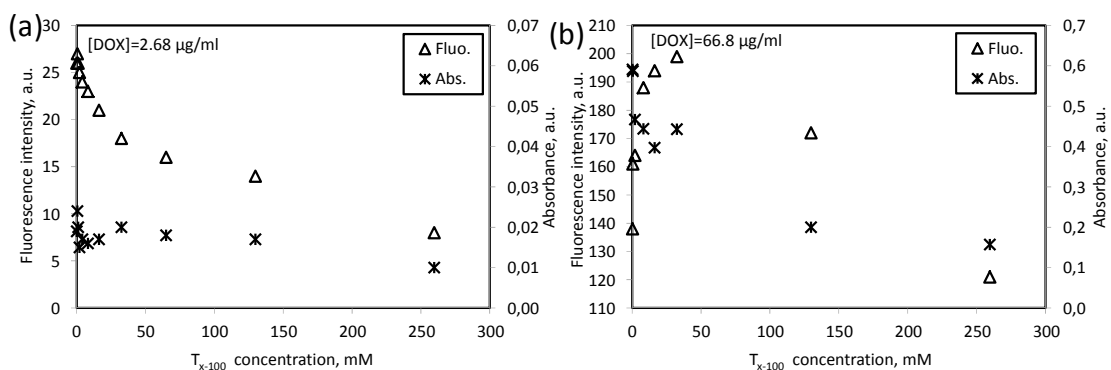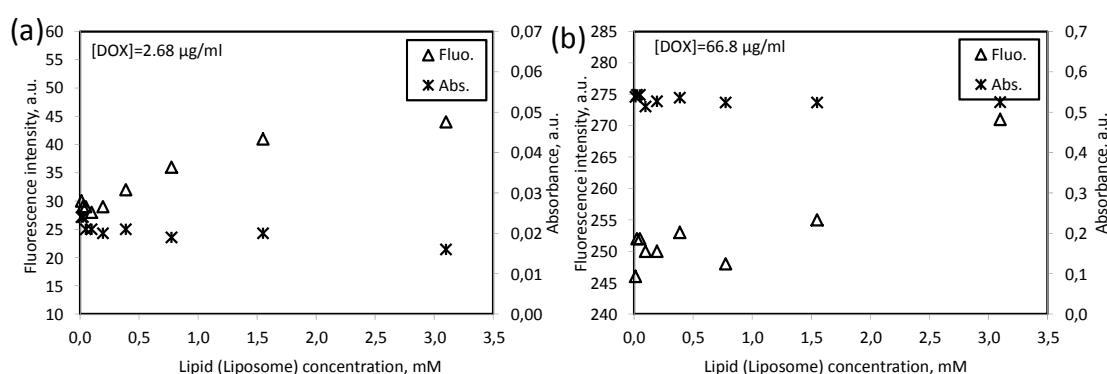

Figure 4.22. The absorbance and fluorescence intensity values of (a) 2.68 µg/ml and (b) 66.8 µg/ml of free-DOX in different concentrations of lipid (liposome) suspensions.

Ammonium sulfate buffer was used during liposome synthesis in order to trap the $(NH_4)_2SO_4$ within the liposomes. When the DOX molecules diffused into the liposomes, they are expected to precipitate with $SO_4^=$ ions with a gel-like structure. Therefore, it was investigated whether the $SO_4^=$ ions have an effect on the absorbance and fluorescence intensity values for the DOX. For this purpose, 250 mM of $(NH_4)_2SO_4$ buffer was diluted to its half with the ultra-pure water to prepare its different concentrations. Then, the absorbance and fluorescence intensity values were measured

after adding the lower and higher concentrations of the two DOX solutions into each dilution. Figure 4.23 shows the absorbance and fluorescence intensity values of 2.68 µg/ml and 66.8 µg/ml of free-DOX in different concentrations of $(NH_4)_2SO_4$ solutions. As shown in the figure, the absorbance values were not affected significantly however, the fluorescence values decreased as the $(NH_4)_2SO_4$ concentration increased. It seems that there is an interaction between $SO_4^=$ ions and $DOXH^+$ ions and both ions form a complex. However, measured solubility product constant (K_{sp}) of $SO_4^=$ and $DOXH^+$ ions complex was under the theoretical K_{sp} as seen in Figure 4.24. In this situation, it was expected a precipitation in the environment. The decline of fluorescence intensity value of $(NH_4)_2SO_4$ concentration was interpreted as fluorescence quenching effect due to interaction of $SO_4^=$ ions with $DOXH^+$ ions.
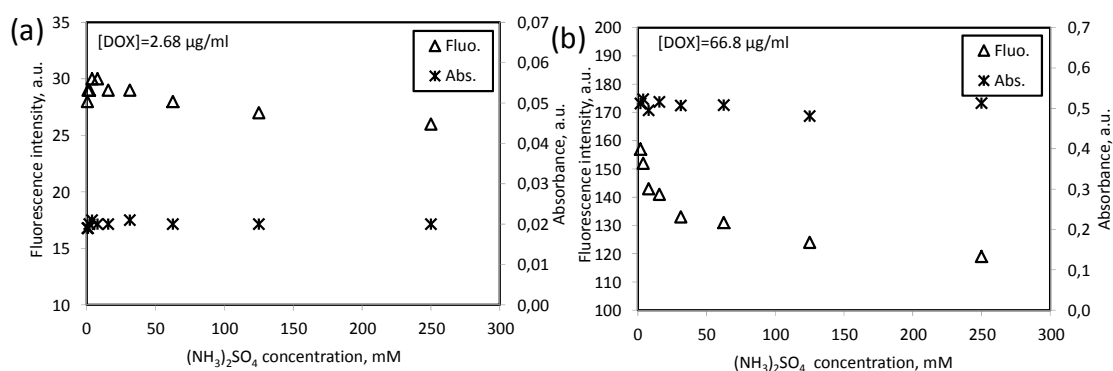
Figure 4.23. The absorbance and fluorescence intensity values of (a) 2.68 µg/ml and (b) 66.8 µg/ml of free-DOX in different concentrations of $(NH_4)_2SO_4$ solutions.

The calculated solubility (K_{sp}) values were calculated for the complex between $SO_4^=$ and $DOXH^+$ ions at different $(NH_4)_2SO_4$ buffer concentrations. As shown in Figure 4.24, the measured solubility constant (K_{sp}) for the $SO_4^=$ and $DOXH^+$ ions was lower than the theoretical K_{sp} value. In this case, any precipitation was not expected, however, the decrease in the florescence intensity could be due to the complexation between the $SO_4^=$ and $DOXH^+$ ions. Therefore, it was understood that the $SO_4^=$ and $DOXH^+$ ions can interact each other and aggregate with complex formation, which can reduce the florescence intensity.
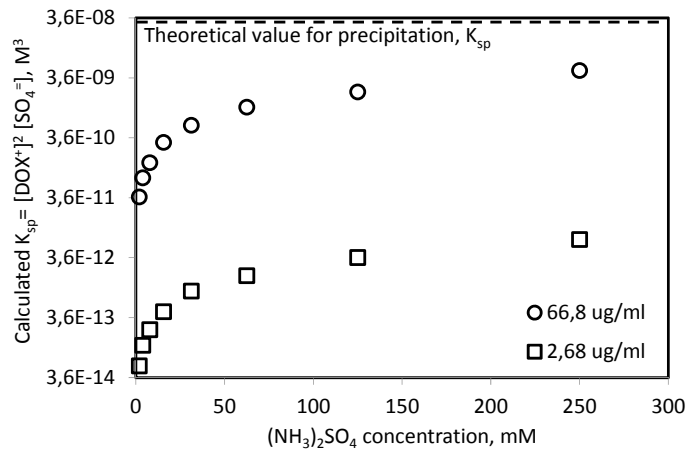
Figure 4.24. The calculated solubility (K_{sp}) values for the complex between $SO_4^=$ and $DOXH^+$ ions at different $(NH_4)_2SO_4$ buffer concentrations.

The calibration curves for the free-DOX were obtained in ultra-pure water, 50 mM of PBS, and 82 mM of T_{x-100} solutions. As shown in Figure 4. 25, the fluorescence intensities for the free-DOX in PBS solutions were relatively lower than those in the ultra-pure water at higher DOX concentrations. The fluorescence intensities for the free-DOX in T_{x-100} solutions were significantly higher than those in the ultra-pure water and PBS at higher DOX concentrations. It seems that DOX molecules form complexes with PBS, especially with the charged phosphates groups in PBS, and isolated within micelles in the T_{x-100} solution so that the florescence intensities were significantly higher in the T_{x-100} solution.
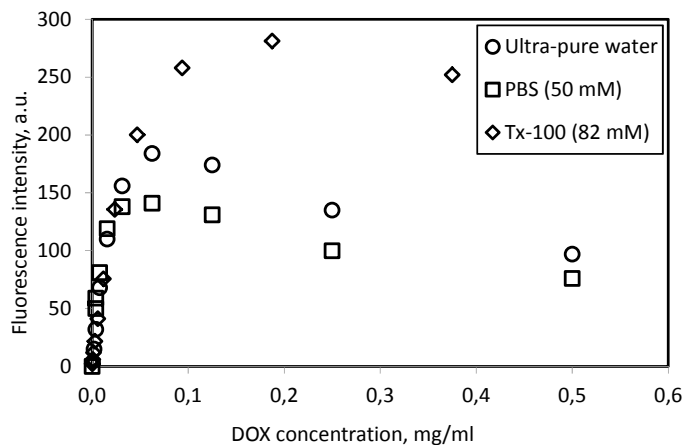
Figure 4. 25. The comparison of the calibration curves for the free-DOX in ultra-pure water, 50 mM of PBS, and 82 mM of T_{x-100} solutions.

At lower DOX concentrations, a linear trend was observed. However, the linearity was different for each solution depending on the initial concentration of DOX

diluted. For instance, when the DOX molecules formed complexes in PBS solution or aggregated among themselves in ultra-pure water, the dilution would have been resulted in relatively higher concentrations than the values theoretically calculated. Therefore, as shown in Figure 4.26, the fluorescence intensity was higher for the diluted free-DOX solutions; indeed, their concentration must be higher if the calibration curve for DOX in the T_{x-100}solution is more realistic. In order to evaluate the DOX concentration especially at higher concentrations, the self-association of DOX need to be analyzed.
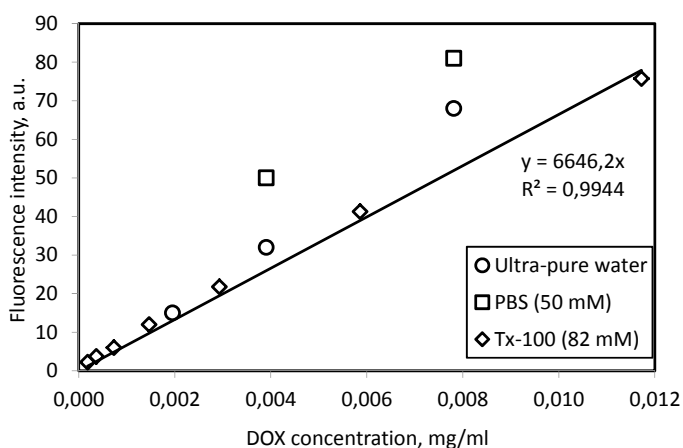
Figure 4.26. The calibration curves for free-DOX in ultra-pure water, PBS, and Tx-100 solutions.

A self-association model, which is called as isodesmic self-association model, was first reported for Daunomycin or Daunodoxorubicin by Chaires et al.[71] in 1982. Recently, Csuhai et al.[72] reported a similar self-association model for DOX in 2015. In this model, the monomer DOX molecules associated to each other and dimers occur. At concentrations higher than 10^{-5} M or 5.75 µg/ml, DOX molecules associated with dimers to form trimers, trimers to tetramer, etc.. These associations are in equilibrium with each other and the equilibrium relationships can also be written with an equilibrium constant as indicated in Eq. (4.6) to Eq. (4.9) below.

$$D_m + D_m \rightleftharpoons D_2 \qquad K_1 = \frac{[D_2]}{[D_m]^2} \qquad\qquad (4.\,6)$$

$$D_2 + D_m \rightleftharpoons D_3 \qquad K_2 = \frac{[D_3]}{[D_2][D_m]} \qquad\qquad (4.\,7)$$

$$D_3 + D_m \rightleftharpoons D_4 \qquad K_3 = \frac{[D_4]}{[D_3][D_m]} \qquad\qquad (4.\,8)$$

$$\begin{array}{ccc} . & & . \\ . & & . \\ . & & . \end{array}$$

$$D_{n\text{-}1} + D_m \rightleftharpoons D_n \qquad K_{n-1} = \frac{[D_n]}{[D_{n-1}][D_m]} \qquad\qquad (4.\,9)$$
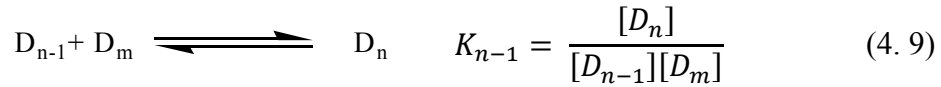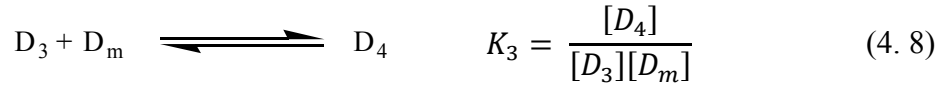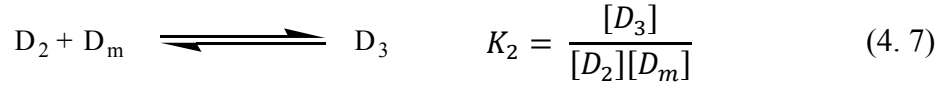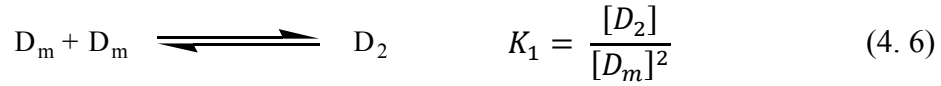
It was assumed that the equilibrium constants from Eq. (4.6) to Eq. (4.9) are equal to each other ($K_1 = K_2 = K_3 = \ldots = K_n$). According to the isodesmic self-association model, the monomer concentration (D_m) is related to the total DOX concentration (D_T) with Eq. (4.10).

$$\frac{D_m}{D_T} = f = \left(\frac{2}{1 + \sqrt{1 + 4K_n D_T}} \right)^2 \qquad\qquad (4.\,10)$$

Here, the equilibrium constant, K_n, was reported to be 7030 ± 920 M^{-1}. According to the isodesmic self-association model, the ratio of the monomer DOX concentration (D_m) to the total DOX concentration (D_T) can be related to the total DOX concentrations (D_T) as shown in Figure 4.27. As shown in the figure, the monomer DOX concentration is related to the total DOX concentration with a non-linear relationship. Because the main source for the fluorescence intensity is originated from the monomer DOX molecules, any aggregates of DOX from dimers, trimers, tetramers,

etc. cause a quenching effect in florescence measurement and decrease the fluorescence intensity values during the measurements. The isodesmic self-association model can be used to correct the quenching effect of DOX at higher concentrations and to obtain more realistic results.
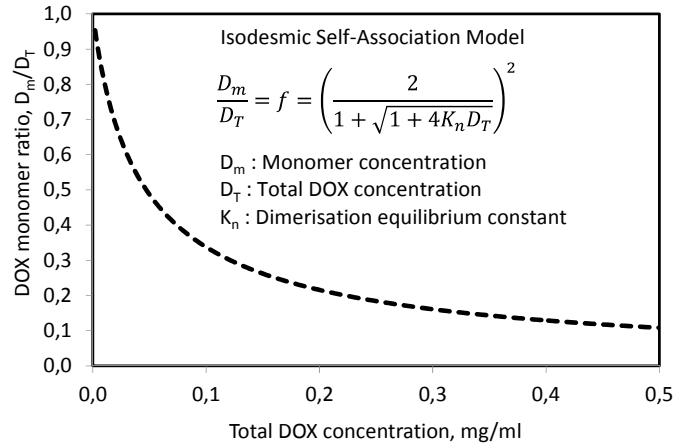
Figure 4.27. According to the isodesmic self-association model, Representation of the monomer DOX concentration (D_m) in the total DOX concentration (D_T) at different total DOX concentrations (D_T).

The fluorescence intensity values were compared with respect to the total DOX concentration (D_T) and the monomer DOX concentration (D_m). A known amount of powder DOX was weighed and diluted with known amount of ultra-pure water to prepare the stock solution of DOX. This concentration was the concentration for the total DOX (D_T). The fraction of monomer concentration of DOX (D_m) was calculated using the isodesmic self-association model as shown in Eq. (4.10). Figure 4.28shows the DOX calibration curves with respect tothe total DOX concentration (D_T) and the monomer DOX concentration (D_m). As shown in the figure, the fluorescence intensity deviated considerably for the total DOX compared to those for the monomer DOX. If the fluorescence intensity is linearly proportional to monomer DOX, the relationship can be represented by Eq. (4.11). The monomer DOX concentration (D_m) is related to the total DOX concentration (D_T) with Eq. (4.12). Therefore, the fluorescence intensity for total DOX (D_T) can be given as shown in Eq. (4.13). As shown in Eq. (4.13), the slope of the calibration curve for the total DOX concentration (D_T) has two components, one is the slope from the monomer concentration and the other is the fraction factor (*f*) which is dependent on the total DOX. Therefore, the slope for the total DOX concentration deviates significantly after the fluorescence intensity value of 80 a.u. as shown in the figure. It was understood that

the slope of the calibration curves is almost linear up to the florescence intensity value of 140 a.u. and 90 a.u.for the monomer (D_m) and total(D_T) DOX concentrations, respectively, and can be used in the calculations.

$$F = \alpha.[D_m]$$
(4. 11)

$$[D_m] = f.[D_T]$$
(4. 12)

$$F = (\alpha.f).[D_T]$$
(4. 13)
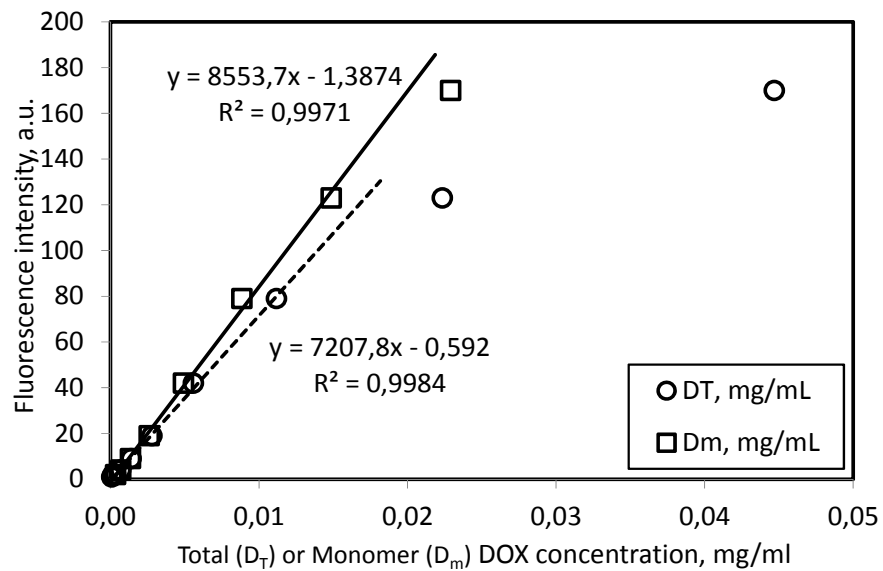
Figure 4.28. The fluorescence intensity values with respect to both the total DOX concentration (D_T) and the monomer DOX concentration (D_m).

When the calibration curve for the fluorescence intensity with respect to the monomer DOX concentration was used, a conversion is needed from the monomer concentration to the total DOX concentration. In this case, the f-factor given in Eq. (4.10) is used. Therefore, a polynomial equation was generated to calculate the total DOX concentration (D_T) from the monomer DOX concentration (D_m) as shown in Figure 4.29. Note that the generated polynomial equation is valid only when the D_m

concentration was smaller than 0.035 mg/ml or the D_T concentration was smaller than 0.11 mg/ml.
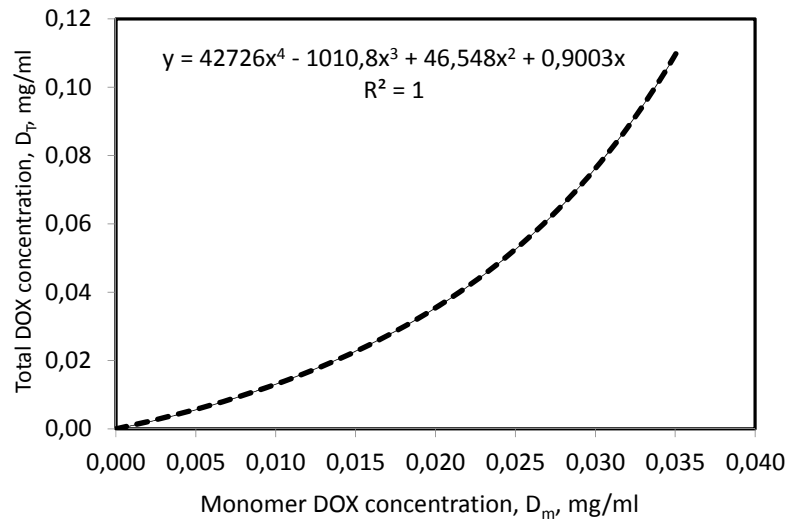
Figure 4.29. The polynomial equation to calculate the total DOX concentration (D_T) from the monomer DOX concentration (D_m).

In the light of the generated information, the DOX contents within the liposomes were reanalyzed. When a sample with a volume of V_i was withdrawn from a stock solution of lipo-DOX with a concentration of C_o and diluted it to a final volume of V_T, its concentration becomes C_1. From the mass balance, Eq. (4.14) can be written and the concentration in the cuvette can be calculated from Eq. (4.15).

$$C_0.V_i = C_1.V_T \qquad (4.14)$$

$$C_1 = \left(\frac{V_i}{V_T}\right).C_0 \qquad (4.15)$$

When the fluorescence intensity exceeds the limit defined in the linear region of the calibration curve, additional dilutions can be made. In this case, the concentration estimated for each cuvette, C_n, is related to the dilution factor, DF_n, and the slope should give the concentration of the stock solution, C_o.

$$C_n = DF_n.C_o \qquad (4.16)$$

Figure 4.30shows the DOX concentrations in each cuvette with respect to different dilution factor using calibration curves for total DOX concentration (D_T) and monomer DOX concentration (D_m). As shown in the figure, there is a linear trend between the dilution factors and the measured concentrations in each cuvette. As shown in the figure, the slope of each line gave the concentration of the stock lipo-DOX solutions

which must be the same for each. However, the general trend show a deviation from linearity when the initial concentration exceeded the limit concentration of about 0.012 mg/ml DOX, especially for the total DOX concentration for which the estimated concentration of the stock lipo-DOX solution is significantly lower.

From the mass balance, Eq. (4.15) or Eq. (4.16) can be used. It was expected a linear curve between the measured concentration versus the dilution factor (V_i/V_T). It can be determined the concentration of stock solution from the slopes of the lines. It was given the D_T and D_m concentration values which were drawn versus the dilution factor in Figure 4.30. As seen in this graph, the calculated DOX concentrations changed linearly for dilution factor of two calculations. According to the evaluation from the calibration curves for the total concentration and monomer concentrations, it was understood from initial volumes of samples that the concentration of the stock lipo-DOX solution was between 0.2 and 0.26 mg/ml. And, most probably, the concentration of the stock lipo-DOX solution was about 0.237 mg/ml.
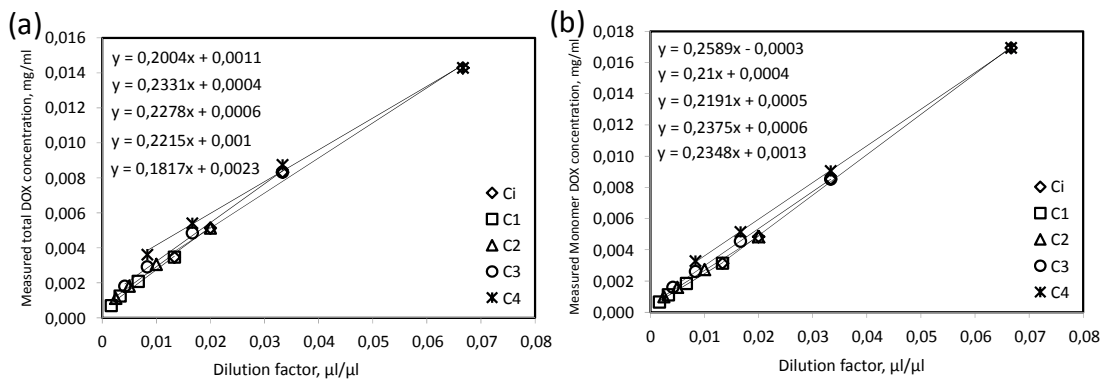
Figure 4.30. The DOX concentrations in each cuvette with respect to different dilution factor using calibration curves for (a) total DOX concentration (D_T) and (b) monomer DOX concentration (D_m).

Figure 4.31 shows the measured concentrations of the stock lipo-DOX solution estimated from its first dilutions and from the subsequent dilutions using the calibration curves for total DOX (D_T) and monomer DOX (D_m) calibration curves. As shown in the figure, the concentrations of stock DOX solution obtained from the first dilutions and subsequent dilutions were approximately 0.26 and 0.23 mg/ml, respectively, using the calibration curve for the total DOX amount. These values for the first and subsequent dilutions were 0.23 and 0.21 mg/ml, respectively, using the calibration curve for the monomer DOX amount. These values were in the range of expected limitations. It

seems that relatively lower DOX concentration was detected by using the calibration curve for the total DOX when the DOX concentration was higher. The opposite is true when the calibration curve was used for the monomer DOX, that is, relatively lower DOX concentration was detected by using the calibration curve for the monomer DOX when the DOX concentration was lower. It was understood that one sample would be satisfactory to estimate the concentration of the stock lipo-DOX solution by estimating the concentration of the subsequent dilutions.
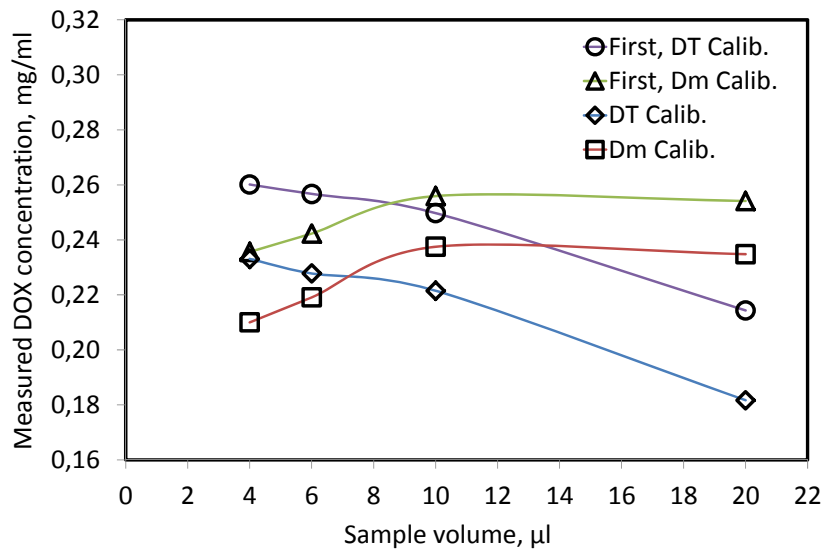
Figure 4.31. The measured concentrations of the stock lipo-DOX solution estimated from its first dilutions and from the subsequent dilutions using the calibration curves for total DOX (D_T) and monomer DOX (D_m) calibration curves.

4.4. Effect of T_{x-100} on Estimation of DOX from Lipo-DOX

An experimental study was conducted to understand the effect of T_{x-100} concentration on the estimation of DOX amount in the lipo-DOX suspensions prepared at different concentrations. Different concentrations of solutions were prepared by diluting the Lipo-DOX suspensions into a series of cuvettes. Samples were withdrawn from each mix and measured their fluorescence intensity values, which was shown in Figure 4.32(a). As shown in the figure, the fluorescence intensity values are significantly lower at T_{x-100} concentration slower than 0.135 mM. Because the critical micelle concentration (CMC) for T_{x-100} is 0.24 mM, any concentration below the CMC did not disrupt the liposomes and release their DOX contents. At higher T_{x-100}

71

concentrations, higher than CMC, the fluorescence intensity showed a linear trend up to 0.5 mM of the lipo-DOX (lipid) concentrations and did not increase at higher concentration due to the quenching effect because the fluorescence intensity was much higher at these concentrations. When the fluorescence intensity value is higher than 80, the calibration curve with respect to the total DOX concentrations (D_T) cannot be used. Therefore, the calibration curve with respect to monomer DOX concentration (D_m) was employed upto the fluorescence intensity vale of 150 a.u.. Figure 4.28(b) shows the DOX concentrations estimated for different concentrations of lipo-DOX suspensions at different T_{x-100} concentrations. As shown in the figure, DOX concentrations could not be detected at T_{x-100} concentrations lower than 0.24 mM. DOX concentrations were obtained for higher T_{x-100} concentrations and they were linear with respect to different concentrations of lipo-DOX suspensions. At higher lipo-DOX concentrations, the linearity was deviated due to quenching effect. The linear increase/decrease of the diluted samples is in good agreement with each other.
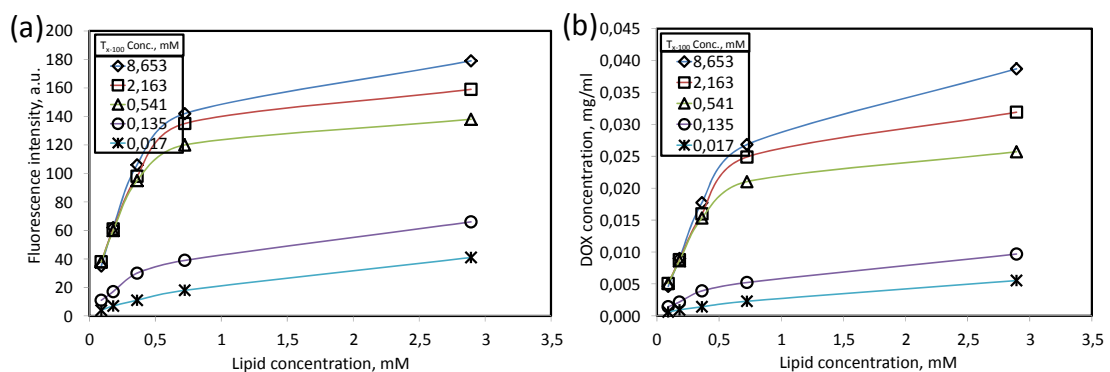
Figure 4.32. (a) Fluorescence intensity values and (b) estimated DOX concentrations for different concentrations of Lipo-DOX suspensions containing different concentrations of T_{x-100} solution.

The DOX concentrations for the stock lipo-DOX samples were estimated using different T_{x-100} concentrations as shown in Figure 4.33. As shown in the figure, the T_{x-100} concentration must be higher than the CMC as mentioned before. The DOX concentrations of the stock lipo-DOX suspensions increased when the lipo-DOX concentration decreased. An important finding of this study is that the lipo-DOX concentrations need to be as low as possible to estimate the DOX amount of the lipo-DOX suspensions as accurate as possible.
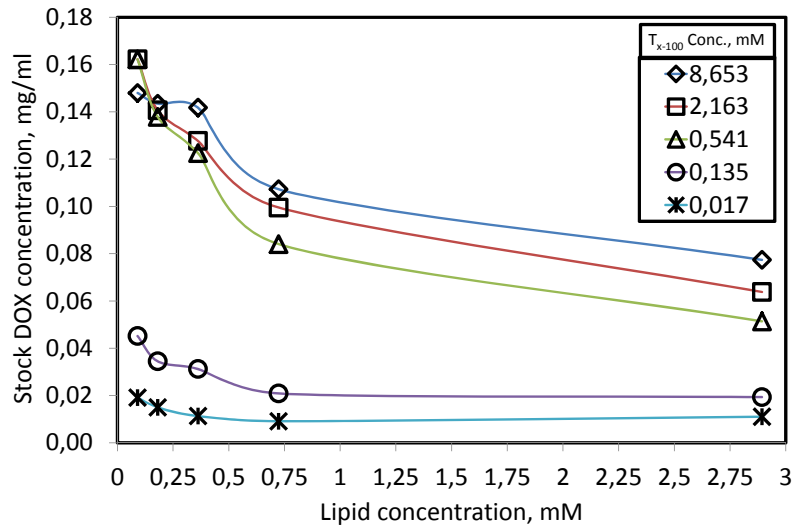
Figure 4.33. Estimated DOX concentration for the stock lipo-DOX solutions at different T_{x-100} concentrations

The estimated stock DOX concentrations were analyzed for each lipo-DOX suspension at different T_{x-100}/Lipid ratios. Figure 4.34 shows the determined stock DOX concentrations with respect to different T_{x-100}/Lipid ratios at different lipo-DOX suspensions. As shown in the figure, T_{x-100}/Lipid ratio must be above 6.0 mol/mol for the determination of DOX concentrations from lipo-DOX samples. Below this ratio, T_{x-100} concentration might not open the pores on the liposomes and release the DOX out of the liposomes.
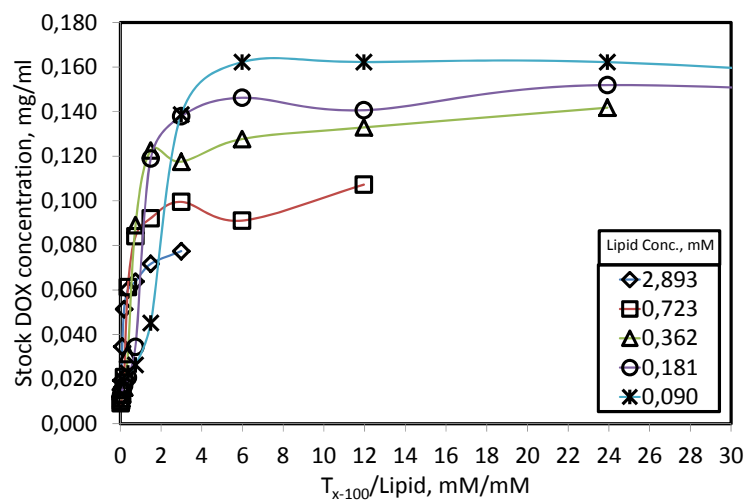
Figure 4.34. The estimated stock DOX concentrations for each lipo-DOX suspension at different T_{x-100}/Lipid ratios

4.4. Langmuir-Type Doxorubicin Loading within Liposomes

Doxorubicin was loaded within liposomes. Different concentrations of liposomes were prepared. Similarly, different concentrations of DOX solutions were prepared. Then, DOX solutions were loaded within different concentrations of liposomes and analyzed. Figure 4.35 shows the loading of DOX within liposomes at different DOX concentrations for each liposome (lipid) amount. As shown in Figure 4.35(a), the loaded-DOX concentrations are Langmuir-like at different liposome concentrations. The dashed lines show the curve fit of the experimental data to the Langmuir equation, Eq. (4.17). As shown in the figure, the Langmuir-like behavior is consistent with each liposome content. Figure 4.35(b) show the Langmuir constants (n_o and K) for different liposome concentrations. As shown in the figure, the Langmuir constants are linearly related to the liposome concentrations. When the liposome concentrations varied, as shown in Figure 4.35(c), similar Langmuir-type relationships were observed for the loaded-DOX concentrations with the liposome (lipid) concentrations at different loading DOX concentrations. Again, the Langmuir constants are linearly related to the loading DOX concentrations.

$$n = \frac{n_o . C}{K + C} \qquad (4.17)$$

The mechanism of the Langmuir equation is related to the number of sites on a surface. There is equilibrium between the adsorbing molecules and adsorbed molecules. When the DOX loading within the liposomes was considered, it was expected that the DOX molecules adsorb on the liposomes, diffuse through their bilayer membrane, and make complex or crystallize with the available $SO_4^=$ ions within the liposomes. Our understanding is primitive at this stage whether the DOX encapsulation is an equilibrium process or not. However, it is clear that there is an encapsulation capacity of liposomes for DOX as shown in the figures as a level-off as the DOX or liposome (lipid) concentration increases. Therefore, the Langmuir-like behavior has a practical importance in DOX loading within the liposomes. The loaded-DOX concentration can be figured-out before conducting an experiment.
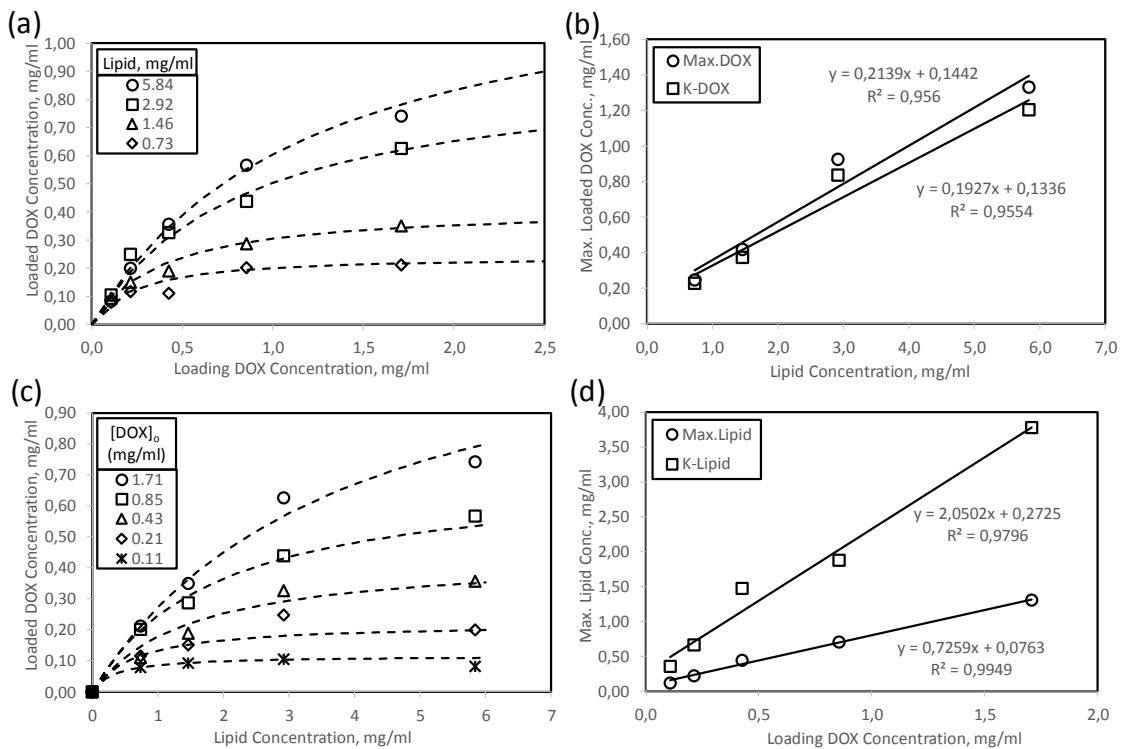
Figure 4.35.Loading of DOX within liposomes; (a) Loading different concentrations of DOX to liposome at different concentrations, (b) Langmuir constants for the model equation, (c) Loading of DOX to different concentrations of liposomes (lipids), (d) Langmuir constants for the model equation.

4.5. Coupling of Lipo-DOX with Microbubbles

The produced liposomes containing DOX molecules (lipo-DOX) were coupled to microbubbles with avidin-biotin chemistry. Liposomes were prepared with 0.1% of biotin in their formulations and DOX was loaded within these liposomes in order to prepare biotinylated-lipo-DOX. Microbubbles were also prepared containing different biotin% in their formulations. Before conjugation, stock solution of avidin was prepared and diluted half into different concentrations. Then, biotinylated-microbubbles were incubated with 0.1 ml of avidin at different concentrations and washed out before loading the lipo-DOX samples. The lipo-DOX samples of 0.2 ml were incubated with the avidin-conjugated microbubbles and washed out in order to eliminate the unbound lipo-DOX from the conjugated microbubbles. Figure 4.36 shows the DOX content of the conjugated microbubbles with respect to avidin/biotin mole ratio on the microbubbles. As shown in the figure, as the biotin% on the microbubbles increased (from right to left of the figure) the conjugated DOX amount increased. As biotin%

further increased, the conjugated DOX amount started to decrease after a maximum at avidin/biotin mole ration of 7.0. As shown in the figure, the conjugated DOX amount on the microbubble is about 3.10^{-8} μg-DOX/MB at the optimum at avidin/biotin mole ration of 7.0 on microbubbles which is in good agreement with the literature.
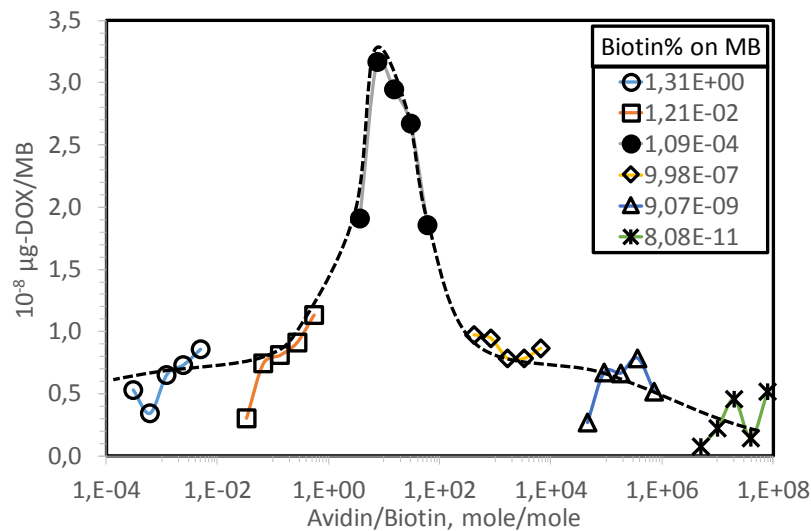
Figure 4.36. Conjugated DOX amount with respect to avidin/biotin mole ratio on the microbubbles prepared at different biotin%.

Figure 4.37 shows the fluorescence images of microbubble-lipo-DOX conjugates. As shown in the figure, the liposomes containing DOX is coupled with the microbubbles. The doxorubicin anti-cancer agent was successfully encapsulated with the liposomes and conjugated with the microbubbles.
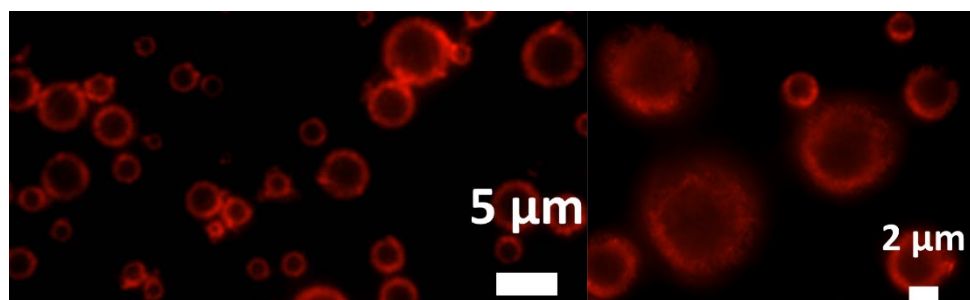
Figure 4.37. The images of microbubble-lipo-DOXconjugates

CHAPTER 5

CONCLUSIONS

Doxorubicin was loaded within liposomes and coupled with microbubbles for an efficient drug delivery vehicle. Liposomes were produced by the extrusion method through polycarbonate membranes with a pore size of 200 nm and a narrow size distribution between 90 nm and 330 nm were obtained. The average size for liposomes was generally between 180-190 nm. The sizes of liposomes were found to be temperature dependent. When temperature increased, liposomes were found to shrink and when the temperature decreased, they found to swell. The shrinkage was about 25% from 4 ^{o}C in the fridge to the body temperature of 37 ^{o}C. The DOX release% was found to be about 0% at room temperature, about 10% at body temperature and about 45% at 70 ^{o}C. The low permeability of DSPC liposomes to DOX at lower temperatures was thought to be due to the volumetric expansion of liposomes. The increase in the DOX release% at higher temperatures was thought to be due to the volumetric shrinkage of liposomes. It was therefore found that DSPC liposomes are very stable and impermeable to DOX release. The micelle size for Triton X-100 solution was found to be between 8 nm and 10 nm. When absorbance measurements were conducted, it was found that liposomes gave absorbance values linearly related to its concentration due probably to the scattering of light from 200 nm of liposomal particles. T_{x-100} solutions were null or negligible in the absorbance measurements. However, neither liposome nor T_{x-100} solutions did not produce a fluorescence intensity. It was understood from the calibration curves of DOX that the sample needed to be diluted up to a DOX concentration lower than 12 μg/ml. Otherwise, the fluorescence values were deviated from the linear line during the measurements. Therefore, a measurement protocol was developed to estimate the DOX concentration of a solution. In the protocol, either different volume of sample needs to be measured or one of the samples needs to be diluted subsequently. The linear range in florescence measurements was found to be 80 florescence units. When the measured fluorescence intensity exceeds the linear range, an isodesmic self-association model was used, where it was shown that the fluorescence intensity is linearly related to the monomeric DOX concentration up to 150 fluorescence

unit. The estimation of concentration from each dilution will give the stock solution of the sample. A T_{x-100}/lipid mole ratio was found to disrupt the liposomes and estimate the concentration of DOX from the liposomes. It was found a Langmuir-like DOX loading equation for the loading of DOX within liposomes. The Langmuir constants were linear with respect to the loading DOX concentration and for the liposome (lipid9 concentrations. By using the model equation, the amount of DOX loadings can be estimated before conducting experiments. DOX-loaded liposomes could be coupled with the biotinylated-microbubbles with avidin-biotin chemistry. The avidin/biotin mole ratio was found to be about 7.0on the microbubbles. A maximum of 3×10^{-8} μg-DOX/MB was conjugated on the microbubbles at the optimum avidin/biotin ratio of 7.0. I was concluded that the conjugated lipo-DOX microbubbles can be used in drug delivery and cancer treatments.

REFERENCES

1. Goyal P, Goyal K, Vijaya Kumar SG, Singh A, Katare OP, Mishra DN. Liposomal Drug Delivery Systems - Clinical Applications. Acta Pharmaceutica. 2005;55: 1-25.

2. Abraham SA, Waterhouse DN, Mayer LD, Cullis PR, Madden TD, Bally MB. The Liposomal Formulation of Doxorubicin. In: Düzgüneş N, editor. Methods in Enzymology: Academic Press, 2005:71-97.

3. Park JW. Liposome-Based Drug Delivery in Breast Cancer Treatment. Breast Cancer Res. 2002;4: 95-99.

4. Ma X, Yu H. Global Burden of Cancer. Yale J Biol Med. 2006;79: 85-94.

5. Cooper GM, Hausman RE. Cancer. In: Cooper GM, Hausman RE, editors. The Cell: A Molecular Approach: Sinauer Associates, 2013:713.

6. Hanahan D, Weinberg RA. Hallmarks of Cancer: The Next Generation. Cell. 2011;144: 646-674.

7. Tu S-M. Origin of Cancers: Clinical Perspectives and Implications of a Stem-Cell Theory of Cancer. Springer, 2010.

8. Bouyet B. Diseases in the Akita. In: Bouyet B, editor. Akita, Treasure of Japan: Magnum 2002:220-280.

9. Alberts B, Johnson A, Lewis J, Raff M, Roberts K, Walter P. The Lipid Bilayer. Molecular Biology of the Cell: Garland Science, 2002:584-593.

10. Nishida N, Yano H, Nishida T, Kamura T, Kojiro M. Angiogenesis in Cancer. Vascular Health and Risk Management. 2006;2: 213-219.

11. Alexander M, Bendas G. The Role of Adhesion Receptors in Melanoma Metastasis and Therapeutic Intervention Thereof. In: Murph M, editor. Research on Melanoma - A Glimpse into Current Directions and Future Trends: InTech, 2011:393-407.

12. Samarasinghe B. The Hallmarks of Cancer 5: Sustained Angiogenesis. Available from URL: https://blogs.scientificamerican.com/guest-blog/the-hallmarks-of-cancer-5-sustained-angiogenesis/.

13. Gerweck LE, Seetharaman K. Cellular pH Gradient in Tumor Versus Normal Tissue: Potential Exploitation for the Treatment of Cancer. Cancer Res. 1996;56: 1194-1198.

14. Damaghi M, Wojtkowiak JW, Gillies RJ. pH Sensing and Regulation in Cancer. Frontiers in Physiology. 2013;4: 370.

15. Baskar R, Dai J, Wenlong N, Yeo R, Yeoh K-W. Biological Response of Cancer Cells to Radiation Treatment. Frontiers in Molecular Biosciences. 2014;1.

16. DiSaia PJ, Creasman WT, Mannell RS, McMeekin DS, Mutch DG. Basic Principles of Chemotherapy. Clinical Gynecologic Oncology: Elsevier Health Sciences, 2017:449-470.

17. Gallagher CJ, Smith M, Shamash J. Malignant Disease. In: Kumar P, Clark ML, editors. Kumar and Clark's Clinical Medicine: Elsevier Health Sciences UK, 2016:583-644.

18. Farkona S, Diamandis EP, Blasutig IM. Cancer Immunotherapy: The Beginning of the End of Cancer. BioMed Central Medicine. 2016;14: 73.

19. Gerber DE. Targeted Therapies: A New Generation of Cancer Treatments. Am Fam Physician. 2008;77: 311-319.

20. Nikalje AP. Nanotechnology and Its Applications in Medicine. Medical Chemistry. 2015;5: 81-89.

21. Lin C, Liu Y, Yan H. Designer DNA Nanoarchitectures. Biochemistry. 2009;48: 1663-1674.

22. Mudshinge SR, Deore AB, Patil S, Bhalgat CM. Nanoparticles: Emerging Carriers for Drug Delivery. Saudi Pharm J. 2011;19: 129-141.

23. Singh R, Lillard JW, Jr. Nanoparticle-Based Targeted Drug Delivery. Exp Mol Pathol. 2009;86: 215-223.

24. Zhang H, Zhai Y, Wang J, Zhai G. New Progress and Prospects: The Application of Nanogel in Drug Delivery. Materials Science and Engineering: C. 2016;60: 560-568.

25. Mohan P, Rapoport N. Doxorubicin as a Molecular Nanotheranostic Agent: Effect of Doxorubicin Encapsulation in Micelles or Nanoemulsions on the Ultrasound-Mediated Intracellular Delivery and Nuclear Trafficking. Molecular pharmaceutics. 2010;7: 1959-1973.

26. Rivankar S. An Overview of Doxorubicin Formulations in Cancer Therapy. Journal of Cancer Research and Therapeutics. 2014;10: 853-858.

27. Zutshi A. Physicochemical Characterization and Stability of Doxorubicin in Aqueous Solutions: PhD Dissertation, University of Florida, 1994.

28. Muggia FM, Young CW, Carter SK. Anthracycline Antibiotics in Cancer Therapy. The International Symposium on Anthracycline Antibiotics in Cancer Therapy. New York: Springer, 16-18 September 1981.

29. Frederick CA, Williams LD, Ughetto G, et al. Structural Comparison of Anticancer Drug-DNA Complexes: Adriamycin and Daunomycin. Biochemistry. 1990;29: 2538-2549.

30. Akbarzadeh A, Rezaei-Sadabady R, Davaran S, et al. Liposome: Classification, Preparation, and Applications. In: Wang ZM, editor. Nanoscale Research Letters: Springer, 2013:102.

31. Elbayoumi TA, Torchilin VP. Current Trends in Liposome Research. In: Weissig V, editor. Liposomes: Methods and Protocols: Springer, 2010:1-27.

32. Hyodo K, Yamamoto E, Suzuki T, Kikuchi H, Asano M, Ishihara H. Development of Liposomal Anticancer Drugs. Biological and Pharmaceutical Bulletin. 2013;36: 703-707.

33. Monteiro N, Martins A, Reis RL, Neves NM. Liposomes in Tissue Engineering and Regenerative Medicine. Journal of The Royal Society Interface. 2014;11.

34. Pandey H, Rani R, Agarwal V. Liposome and Their Applications in Cancer Therapy. Brazilian Archives of Biology and Technology. 2016;59.

35. McMurry J. Lipids. Fundamentals of General, Organic, and Biological Chemistry: Pearson Prentice Hall, 2010.

36. Avanti Polar Lipids I. The Mini Extruder. Available from URL: https://avantilipids.com/divisions/equipment/mini-extruder-extrusion-technique/ [accessed Sept 14, 2016.

37. Morton LA, Saludes JP, Yin H. Constant Pressure-Controlled Extrusion Method for the Preparation of Nano-Sized Lipid Vesicles. J Vis Exp. 2012.

38. van Swaay D, deMello A. Microfluidic Methods for Forming Liposomes. Lab on a Chip. 2013;13: 752-767.

39. Freeman S. Lipids, Membranes, and the First Cells. Biological Science: Pearson, 2011:99-124.

40. Malvern Instruments L. Liposomes and the Use of Zeta Potential Measurements to Study Sterically Stabilized Liposomes Using Malvern Instruments. Available from URL: http://www.azonano.com/article.aspx?ArticleID=1214 [accessed Dec 24, 2016.

41. Morandat S, El Kirat K. Membrane Resistance to Triton X-100 Explored by Real-Time Atomic Force Microscopy. Langmuir: the ACS Journal of Surfaces and Colloids. 2006;22: 5786-5791.

42. Garavito RM, Ferguson-Miller S. Detergents as Tools in Membrane Biochemistry. J Biol Chem. 2001;276: 32403-32406.

43. Luckey M. Detergents and Model Systems. Membrane Structural Biology: With Biochemical and Biophysical Foundations: Cambridge University Press, 2008:42-50.

44. Ackerman DG, Feigenson GW. Lipid Bilayers: Clusters, Domains and Phases. In: Parmryd I, editor. Membrane Nanodomains: Essays in Biochemistry, 2015:33-42.

45. Bhairi SM, Mohan C. Detergents. In: Calbiochem, editor: EMD Biosciences, 2007.

46. Lasch J, Hoffman J, Omelyanenko WG, et al. Interaction of Triton X-100 and Octyl Glucoside with Liposomal Membranes at Sublytic and Lytic Concentrations. Spectroscopic Studies. Biochimica et Biophysica Acta (BBA) - Biomembranes. 1990;1022: 171-180.

47. Seddon AM, Curnow P, Booth PJ. Membrane Proteins, Lipids and Detergents: Not Just a Soap Opera. Biochimica et Biophysica Acta (BBA) - Biomembranes. 2004;1666: 105-117.

48. Johnson M. Detergents: Triton X-100, Tween-20, and More. Available from URL: https://www.labome.com/method/Detergents-Triton-X-100-Tween-20-and-More.html [accessed Nov 15, 2016.

49. Patel U, Dharaiya N, Parikh J, Aswal VK, Bahadur P. Effect of Amphiphilic and Non-Amphiphilic Polymers on Micellar Behaviour of Nonionic Surfactant Triton X-100. Colloids and Surfaces A: Physicochemical and Engineering Aspects. 2015;481: 100-107.

50. Sun Pharma Global F. Doxorubicin Hydrochloride. Available from URL: https://dailymedqa.nlm.nih.gov/dailymed/4/fda/fdaDrugXsl.cfm?setid=fbc48fa5-0bfb-4957-b13c-a56bb7a13b56&type=display [accessed Nov 12, 2016.

51. Ewer MS, Yeh ETH. Anthracycline Cardiotoxicity: Clinical Aspects, Recognition, Monitoring, Treatment, and Prevention. Cancer and the Heart: People's Medical Publishing House-USA, 2013:11-41.

52. Kozak D, Broom M, Vogel R. Accurate Size, Charge and Concentration Analysis of Liposomes Using Tunable Resistive Pulse Sensing. In: IZON, editor. Izon Science White Paper: Izon Science.

53. Crommelin DJA, Slaats N, van Bloois L. Preparation and Characterization of Doxorubicin-Containing Liposomes: I. Influence of Liposome Charge and pH of Hydration Medium on Loading Capacity and Particle Size. International Journal of Pharmaceutics. 1983;16: 79-92.

54. Crommelin DJA, van Bloois L. Preparation and Characterization of Doxorubicin-Containing Liposomes. II. Loading Capacity, Long-Term Stability and

Doxorubicin-Bilayer Interaction Mechanism. International Journal of Pharmaceutics. 1983;17: 135-144.

55. Hathout RM, Mansour S, Mortada ND, Guinedi AS. Liposomes as an Ocular Delivery System for Acetazolamide: in vitro and in vivo Studies. AAPS PharmSciTech. 2007;8: E1-E12.

56. Dan N. Effect of Liposome Charge and PEG Polymer Layer Thickness on Cell–Liposome Electrostatic Interactions. Biochimica et Biophysica Acta (BBA) - Biomembranes. 2002;1564: 343-348.

57. Sirsi S, Borden M. Microbubble Compositions, Properties and Biomedical Applications. Bubble science engineering and technology. 2009;1: 3-17.

58. Sorace A. Ultrasound and Microbubbles: A Role in Cancer. Birmingham, Alabama: The University of Alabama at Birmingham, 2013.

59. Paul S, Nahire R, Mallik S, Sarkar K. Encapsulated Microbubbles and Echogenic Liposomes for Contrast Ultrasound Imaging and Targeted Drug Delivery. Computational Mechanics. 2014;53: 413-435.

60. Hermanson GT. Liposome Conjugates and Derivatives. Bioconjugate Techniques: Academic Press, 2013:921-950.

61. Lentacker I, Geers B, Demeester J, De Smedt SC, Sanders NN. Design and Evaluation of Doxorubicin-Containing Microbubbles for Ultrasound-Triggered Doxorubicin Delivery: Cytotoxicity and Mechanisms Involved. Molecular Therapy. 2010;18: 101-108.

62. Liang R, Wang J, Wu X, et al. Multifunctional Biodegradable Polymer Nanoparticles with Uniform Sizes: Generation and in vitro Anti-Melanoma Activity. Nanotechnology. 2013;24: 455302.

63. Kinnunen T, Koskela M. Antibacterial and Antifungal Properties of Propylene Glycol, Hexylene Glycol, and 1,3-butylene Glycol in vitro. Acta Derm Venereol. 1991;71: 148-150.

64. Lodish H, Berk A, Zipursky SL, Matsudaira P, Baltimore D, Darnell J. Collagen: The Fibrous Proteins of the Matrix. In: Freeman WH, editor. Molecular Cell Biology: Macmillan, 2000.

65. Malvern. Liposomes and The Use of Zeta Potential Measurements to Study Sterically Stabilized Liposomes Using Malvern Instruments. http://wwwazonanocom/articleaspx?ArticleID=1214, 2005.

66. Hardesty JH. Spectrophotometry and the Beer-Lambert Law: An Important Analytical Technique in Chemistry. Available from URL: http://www.collin.edu/chemistry/Handouts/1411/Beer's%20Law%20(One%20Week)%20Aug%202013.pdf [accessed Oct 04, 2016.

67. Zook JM, Vreeland WN. Effects of Temperature, Acyl Chain Length, and Flow-Rate Ratio on Liposome Formation and Size in a Microfluidic Hydrodynamic Focusing Device. Soft Matter. 2010;6: 1352-1360.

68. Crommelin DJA, Talsma H, Grit M, Zuidam NJ. Physical Stability on Long-Term Storage. In: Cevc G, editor. Phospholipids Handbook: CRC Press, 1993:335-348.

69. de Lange JHM, Schipper NW, Schuurhuis GJ, et al. Quantification by Laser Scan Microscopy of Intracellular Doxorubicin Distribution. Cytometry. 1992;13: 571-576.

70. Deyl Z, Macek K, Janák J. Liquid Column Chromatography: A Survey of Modern Techniques and Applications. 3 ed: Elsevier Scientific Publishing Company, 1975.

71. Chaires JB, Dattagupta N, Crothers DM. Self-Association of Daunomycin. Biochemistry. 1982;21: 3927-3932.

72. Csuhai E, Kangarlou S, Xiang T-X, et al. Determination of Key Parameters for a Mechanism-Based Model to Predict Doxorubicin Release from Actively Loaded Liposomes. Journal of Pharmaceutical Sciences. 2015;104: 1087-1098.